

**Aqueous Near Infrared Fluorescent
Composites
based on
Apo ferritin-Encapsulated PbS Quantum
Dots**

Barbara Hennequin

DEA 'Molécules, Matériaux, Milieux Réactifs et Interfaces'

Thesis submitted to the University of Nottingham
for the degree of Doctor of Philosophy

June 2008

Physics is hard and if you say it's not, you are wrong.

Dr. Daivid Fowler

Contents

Abstract	vi
Publications	viii
Acknowledgements	ix
Abbreviations	xi
1 From Physics & Chemistry to Nanobiotechnology	1
1.1 Semiconductor nanocrystals as fluorescent labels	3
1.1.1 Quantum confinement in a nanocrystal	4
1.1.2 Excitons	6
1.1.3 Quantum dots compared to organic fluorophores	8
1.1.4 Synthesis of colloidal quantum dots	11
1.1.5 Modifying quantum dots with biological tags	15
1.2 Ferritin, the iron storage protein	20
1.2.1 Ferritin structure	21
1.2.2 Electrostatic features	26
1.2.3 Dissociation of the protein shell subunits	27
1.3 Apoferritin as a protein cage for quantum dots	29
1.3.1 Entrapment of materials in apoferritin: The nanoreactor route	29
1.3.2 Entrapment of materials in apoferritin: The reassembly route	35
1.4 Applications of apoferritin-encapsulated materials	37

1.5	Project aims	40
2	PbS quantum dots	43
2.1	Introduction	43
2.1.1	Previous syntheses	43
2.1.2	Synthesis of colloidal thiol-capped PbS quantum dots	45
2.2	Objectives	46
2.3	Results & discussion	46
2.3.1	Morphological properties of PbS quantum dots	47
2.3.2	Optical properties of PbS quantum dots	49
2.4	Conclusion	55
3	Preparation and characterization of the protein cage, apoferritin	56
3.1	Introduction	56
3.2	Objectives	57
3.3	Results & discussion	58
3.3.1	Preparation of the protein cage apoferritin from horse spleen ferritin	58
3.3.2	Purification of apoferritin by gel filtration	59
3.3.2.1	Size exclusion chromatography (SEC) principle	59
3.3.2.2	Elution profiles of ferritin and apoferritin	60
3.3.3	Assessment of apoferritin purity by denaturing gel electrophoresis	61
3.3.3.1	SDS-PAGE principle	61
3.3.3.2	Ferritin and apoferritin under denaturing conditions .	62
3.3.4	Determination of apoferritin purity by BCA assay	64
3.3.5	Determination of iron content by ICP-MS analysis	65
3.3.6	Solubility studies of ferritin in organic solvents	66
3.3.7	Preparation of the cationized ferritin	70
3.4	Conclusion	73
4	PbS-apoferritin composites	74
4.1	Introduction	74

4.2	Objectives	74
4.3	Results & discussion	75
4.3.1	Structural study of the PbS-apoferritin composites	76
4.3.2	Optical properties of the PbS-apoferritin composites	80
4.3.3	Native gel electrophoresis of PbS-apoferritin composites	83
4.4	Conclusion	85
5	Bioluminescence resonance energy transfer (BRET) with PbS quantum dots	86
5.1	Introduction	86
5.1.1	Introduction to FRET phenomena	86
5.1.2	PbS as energy acceptors in a BRET process	91
5.2	Objectives	92
5.3	Results & discussion	92
5.4	Conclusion	94
6	Incorporation of un-natural amino acids into human apoferritin	96
6.1	Introduction	96
6.1.1	Introduction to protein bio-synthesis	97
6.1.2	Previous incorporation of un-natural amino acids into proteins.	98
6.2	Objectives	99
6.3	Results & discussion	100
6.3.1	H-human and L-human apoferritin expressions	100
6.3.2	Incorporation of methionine analogues	103
6.4	Conclusion	110
7	Conclusions and future work	111
8	Experimental techniques	114
8.1	Sample preparation	114
8.1.1	Preparation of apoferritin from ferritin	114

8.1.2	Size exclusion chromatography	115
8.1.3	SDS-PAGE of apoferritin	115
8.1.4	BCA assay on ferritin and cationized ferritin	117
8.1.5	ICP-MS analysis	118
8.1.6	Solubility of ferritin and cationized ferritin in organic media . . .	119
8.1.7	Preparation of the cationized ferritin	120
8.1.8	Determination of amine groups in the cationized ferritin	121
8.1.9	Synthesis of PbS quantum dots	121
8.1.10	Synthesis of PbS-apoferritin composites	122
8.1.11	Synthesis of dihydrolipoic acid-capped PbS QDs	123
8.1.12	Bioluminescence of firefly luciferase from <i>L. mingrelica</i>	124
8.1.13	BRET experiments using firefly luciferase as the energy donor and PbS dots as energy acceptors	125
8.2	Measurements techniques	125
8.2.1	Luminescence spectroscopy	125
8.2.2	Atomic force microscopy	126
8.2.3	Transmission electron microscopy	127
8.2.4	High resolution transmission electron microscopy	127
8.2.5	High angle annular dark field scanning transmission electron mi- croscopy	128
8.2.6	Electron energy loss spectroscopy	128
8.2.7	Energy dispersive X-ray spectroscopy	128
8.3	Expression of H and L human apoferritins	129
8.3.1	Transformation of pET-11a and pET-26b(+) into B834(DE3)pLysS competent cells	129
8.3.2	Agarose gel of over-expressed H and L apoferritins	130
8.3.3	Large-scale expression of H and L apoferritins	131
8.3.4	SDS-PAGE of the large-scale expression culture of H and L apo- ferritins	131

8.3.5	Purification of large-scale expression culture of H human apoferritin	132
8.4	Incorporation of methionine analogues into H and L human apoferritins	133
8.4.1	Preparation of M9 media	133
8.4.2	Expression of H and L human apoferritins containing methionine analogues.	135
8.5	Western blot of L human apoferritin containing methionine analogues .	136
References		138

Abstract

Quantum dots offer a number of advantages over standard fluorescent dyes for monitoring biological systems including high luminescence, stability against photobleaching, and a wide range of fluorescence wavelengths from blue to infrared depending on the particle size. In this work, we investigated in using the protein cage apoferritin as a template for the synthesis of colloidal quantum dots.

We obtained apoferritin after reductive dissolution of the ferritin iron core and showed that the protein structure was left intact during this process. We further studied the solubility of ferritin, apoferritin and cationized ferritin in organic and fluorinated solvents by hydrophobic ion pairing methodology in order to expand the possibility of using an apoferritin template for the synthesis of quantum dots in organic media.

We then focused on the synthesis and fluorescence properties of PbS quantum dots in aqueous solution. PbS dots are thermally stable and emit in the range 1,100 to 1,300 nm depending on their size. We demonstrated the encapsulation of these PbS quantum dots within the cavity of the iron storage protein apoferritin using two routes: 1) the disassembly/reassembly of apoferritin subunits trapping previously synthesised PbS quantum dots; and 2) use of the channels present in the protein shell to allow the entrance of Pb^{2+} and S^{2-} ions leading to formation of quantum dots in the apoferritin cavity. We show that PbS-apoferritin composites emit in the near infrared region which make them promising labels for biological applications.

Furthermore, we demonstrated that PbS QDs can be excited *via* a bioluminescence resonance energy transfer (BRET) using luciferin from *Luciola mingrelica* which could be developed into a self-illuminating labelling system.

Finally, in order to make PbS-apoferritin composites selectively attachable to biomolecules during labelling experiments, the apoferritin was modified by the incorporation of analogues of methionine introducing azido groups absent in the proteins. The azido groups can then be selectively modified in complex mixtures e.g. cell lysates using ‘bio-orthogonal’ reactions such as the Cu(I) catalysed Staudinger ligation and Huisgen cycloaddition. This would allow highly selective addition of receptor targeting or cellular permeation of peptides to the outer surface of the apoferritin shell.

Keywords: quantum dots, PbS, apoferritin, photoluminescence, colloidal nanocrystals, template, near infrared, BRET, un-natural amino acid.

Publications

Temperature dependence of the photoluminescence emission from thiol-capped PbS quantum dots. Turyanska, L.; Patanè, A; Henini, M.; Hennequin, B.; Thomas, N. R. *Appl. Phys. Lett.* **2007**, *90*, 101913

Aqueous near infrared fluorescent composites based on apoferritin-encapsulated PbS quantum dots. Hennequin, B.; Turyanska, L.; Ben, T.; Beltrán, A. M.; Molina, S. I.; Li, M.; Mann, S.; Patanè, A. and Thomas, N. R. *accepted in Adv. Mater.* **2008**, adma.200800530.

Acknowledgements

I would like to thank my supervisors Prof. Neil R. Thomas from the School of Chemistry and Prof. Amalia Patanè from the School of Physics & Astronomy for their supervision through my PhD and their useful advice and discussions. I would like to thank them as well for giving me the opportunity to work on a multidisciplinary project which allowed me to learn a lot of new techniques as well as meeting interesting people.

I would like to thank Dr. Lyudmila Turyanska for all the work together on the quantum dots and for teaching me the use of laser, atomic force microscopy and clean rooms.

I would like to thank Dr. Teresa Ben, Ana Beltrán and Prof. Sergio Molina from Cádiz Universidad, Spain and Dr. Mei Li and Prof. Stephen Mann from the University of Bristol, UK for their welcome and their collaboration on the microscopic analyses.

I would like to thank Melike Firat, Dr. Caroline Ajo-Franklin, Dr. Ron Zuckerman and Prof. Carolyn Bertozzi from the Molecular Foundry at Berkeley University, California, USA for their welcome and help on the biological part of this project.

I would like to thank the University of Nottingham, the Interdisciplinary Doctoral Training Centre (IDTC) for funding and the Roberts Money for the travel scholarship to Berkeley University.

Many thanks to all my labmates and friends from the Centre for Biomolecular Sciences namely Betti, Huey-Jen, Juan, Ouannassa, Sarentha, Shalu, Stefanie, Yang, Andrew and from the Wendy House Giles, Olly, Ricky, Spas. I enjoyed every discussion with you all from the intellectual chat to the tea/ice cream break.

Thanks a lot to Dr. Robin Scott (MTFU, I did it!) and Dr. Matt Suddards for

improving my english vocabulary and assisting my writing. Thanks to Robin and Ryan for giving a roof over my head these last months.

Finally, I would like to thank my parents and brothers for leading me there and for being so supportive all these years.

Last but not the least, thanks a lot to Dave who has been extremely heartening every single day. My thanks' list for you is too long, thank you for embellishing so well my english culture and following me to France.

Abbreviations

AA	amino acid
Ab	antibody
AFM	atomic force microscopy
AFP	<i>Aequorea</i> -derived fluorescent protein
AFt	apoferritin
Ala	alanine
Amp	ampicillin
AOT	aerosol-OT (dioctylsulfosuccinate sodium salt)
AP	acceptor peptide
APS	ammonium persulfate
Arg	arginine
Asn	asparagine
Asp	aspartic acid
ATP	adenosine triphosphate
BCA	bicinchoninic assay
BIPS	(1'-3-dihydro-1'-(2-carboxyethyl)-3,3-dimethyl-6-nitrospiro-[2H-1-benzopyran-2,2'-(2H)-indoline])
Bn	benzyl
Boc	tert-butyloxycarbonyl
BRET	bioluminescence resonance energy transfer

BSA	bovin serum albumin
CDI	1,1'-carbonyl diimidazole
CFP	cyan fluorescent protein
Chl	chloramphenicol
CJD	Creutzfeldt-Jacob disease
CMC	carboxymethyl chitosan
CPMV	cowpea mosaic virus
CT	cholera toxin
Cys	cysteine
DABCYL	(4-(dimethylaminoazo)benzene-4-carboxylic acid
DCM	dichloromethane
DEAE	diethylaminoethyl
DFO	desferrioxamine
DHLA	dihydrolipoic acid
DMAP	4-(dimethylamine)-pyridine
DMF	dimethylformamide
DMPA	<i>N,N</i> -dimethyl-1,3-propanediamine
DNA	deoxyribonucleic acid
DPPE	diphosphatidyl ethanolamino
DTG	dithioglycerol
DTT	dithiothreitol
EDC	1-ethyl-3-(3-dimethylaminopropyl) carbodiimide hydrochloride
EDTA	ethylene diamine tetraacetic acid
EDX	energy dispersive X-ray
EELS	electron energy loss spectroscopy
FISH	fluorescence <i>in situ</i> hybridization
FITC	fluorescein isothiocyanate
FP	fluorescent protein
FPLC	fast protein liquid chromatography

FRET	fluorescence resonance energy transfer
FWHM	full width at half maximum
GFP	green fluorescent protein
Gln	glutamine
Glu	glutamic acid
Gly	glycine
GlyR	glycine receptors
H	heavy
HAADF-STEM	high angle annular dark field scanning transmission electron microscopy
HEPES	4-(2-hydroxyethyl)-1-piperazineethanesulfonic acid
HIP	hydrophobic ion pairing
His	histidine
HIV	human immunodeficiency virus
HoSF	horse spleen ferritin
HMD	hexamethylenediamine
HRPO	horseradish peroxidase
HRSEM	high resolution scanning electron microscopy
HRTEM	high resolution transmission electron microscopy
ICP-MS	inductively coupled plasma mass spectrometry
IgG	immunoglobulin G
Ile	isoleucine
IPTG	isopropyl β -D-thiogalactopyranoside
IR	infrared
ITP	inosine triphosphate
Kan	kanamycin
L	light
LB	Luria-Bertani broth, Luria broth or lysogeny broth
Leu	leucine

Lys	lysine
MA	mercaptoacetic acid
MBE	molecular beam epitaxy
MBP	maltose binding protein
Met	methionine
MR	molar ratio
MRI	magnetic resonance imaging
mRNA	messenger RNA
MUA	11-mercaptopundecanoic acid
MWCO	molecular weight cut-off
Ms	mesylate
NC	nanocrystal
NIR	near infrared
NMM	<i>N</i> -methylmaleimide
NMR	nuclear magnetic resonance
NP	nanoparticle
OD	optical density
OPA	<i>o</i> -phthaldialdehyde
PB	prussian blue
PC	phosphatidylcholine
PCR	polymerase chain reaction
PEG	polyethyleneglycol
PEG-PE	<i>n</i> -poly(ethyleneglycol)phosphatidylethanolamine
PEI	poly(ethyleneimine)
PG	protein G
Pgp	<i>p</i> -glycoprotein
Phe	phenylalanine
pI	isoelectronic point
PL	photoluminescence

PM	protein marker
Pro	proline
PVA	poly(vinyl-alcohol)
PVP	poly(vinyl-pyrrolidone)
QD	quantum dot
qdot	quantum dot
QY	quantum yield
R	arginine
RDX	hexahydro-1,3,5-trinitro-1,3,5-triazine
RNA	ribonucleic acid
rpm	revolutions per minute
RT	room temperature
SAED	selected area electron diffraction
SAV	streptavidin
SEB	<i>Staphylococcal enterotoxin B</i>
SEC	size exclusion chromatography
SEM	scanning electron microscopy
Ser	serine
SDS-PAGE	sodium dodecyl sulfate polyacrylamide gel electrophoresis
SLNB	sentinel lymph node biopsy
SLT	shiga-like toxin 1
SMCC	sulfosuccinimidyl 4-[<i>N</i> -maleimidomethyl]cyclohexane-1-carboxylate
SOC	super optimal catobolite
SSA	sheep serum albumin
STEM	scanning transmission electron microscopy
TAE	Tris-Acetate-EDTA
TBA	thrombin-binding aptamer
TBS	Tris-buffered saline

TCS	trichosanthin
TEM	transmission electron microscopy
TEMED	tetramethylethylenediamine
TGL	thioglycerol
Thr	threonine
TMR	tetramethylrhodamine
TNB	2,4,6-trinitrobenzene
TNBS	trinitrobenzene sulfonate
TNT	2,4,6-trinitrotoluene
TOP	trioctyl phosphine
TOPO	trioctyl phosphine oxide
Tris	trihydroxymethylaminomethane
tRNA	transfer RNA
Trp	tryptophan
Tyr	tyrosine
UV	ultraviolet
Val	valine
XRD	X-ray diffraction
YFP	yellow fluorescent protein
ZPL	zero phonon line

Chapter 1

From Physics & Chemistry to Nanobiotechnology

In the past decade, fluorescent proteins and organic fluorophores have been widely used for biological labelling. In addition to these materials, detection of macroscopic molecular targets is now possible using a variety of metal-based nanoparticles.[1–3]

The first nanoparticle was reported in 1570 in the form of aurum potable (potable gold) and luna potable (potable silver).[4] As early as 1971, colloidal gold particles were used as labels for microscopic localization of biomolecules. The ability of nanogold to be covalently attached to antibodies gave them the possibility to be linked specifically to a second biomolecule such as proteins (the prion protein responsible for the Creutzfeldt-Jacob disease (CJD)), peptides (calmodulin - the protein regulating the calcium release), drugs, viruses, carbohydrates, lipids, and nucleic acids (Figure 1.1).[4]

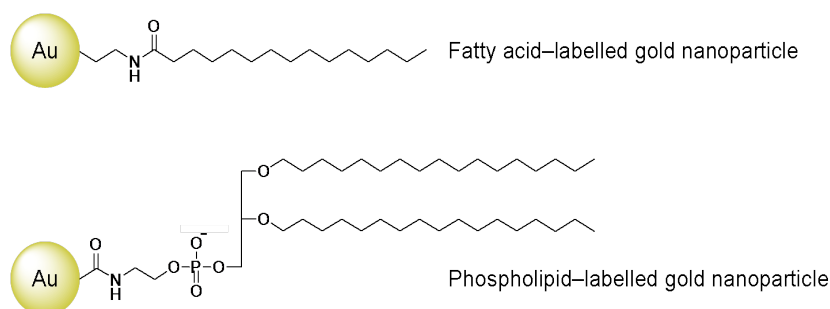


Figure 1.1: Two major lipid classes covalently bound to gold clusters. Commercially available palmitoyl nanogold (fatty acid-gold) and diphosphatidyl ethanolamino (DPPE) nanogold (phospholipid-gold).[5]

The term nanotechnology is employed to describe the creation and exploitation of materials with structural features in between those of atoms and bulk materials, with at least one dimension in the nanometre range (Figure 1.2).[6, 7]

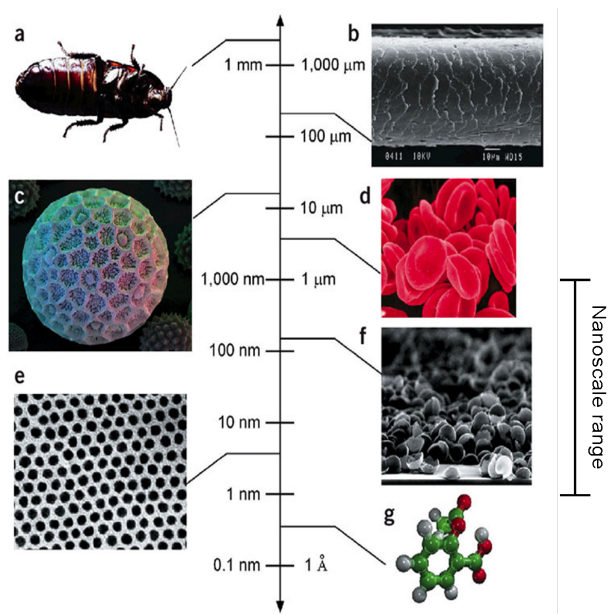


Figure 1.2: Sizes of representative ‘small’ objects. (a) a cockroach; (b) a human hair; (c) polygonum pollen grain; (d) red blood cells; (e) cobalt nanocrystal superlattice; (f) an aggregate of half-shells of palladium; (g) aspirin molecule.[7]

Nanomaterials have led to a massive worldwide investment both in scientific knowl-

edge and in commercial applications (Figure 1.3).[8, 9]

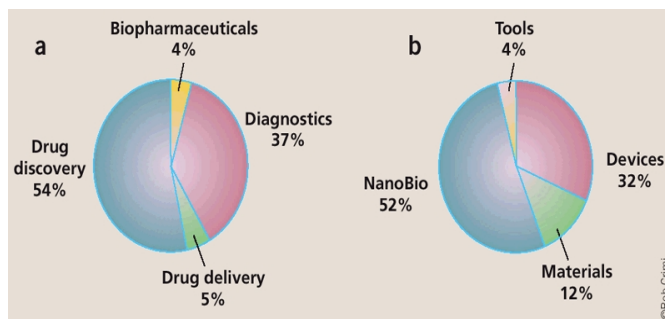


Figure 1.3: Where is the money going? (right): (a) percentage breakdown of nanotechnology venture deals from 1998 to 2003; (b) distribution of venture capital funding in nanotechnology from 1998 to 2003.[8]

In the medical field, pulmonary diseases due to inhalation of inorganic particulate matter such as asbestosis and coal miner's disease, have increased the interest in the nanoscale particle regime for pulmonary toxicologists.[10, 11] They report that nano-scaled materials are more toxic than equivalent micron-sized materials at similar doses per gram of body weight, particle composition and surface chemistry. However, although nanoparticles have been reported to enter the human body through several ports (skin, lungs, intestines), depending on the surface characteristics and the size of the particles, it is thought to be unlikely that exposure to nanomaterials would pose any substantial risk to public health.[11, 12]

1.1 Semiconductor nanocrystals as fluorescent labels

Semiconductor nanocrystals, also called quantum dots (QDs), are nanostructures that confine the motion of an electron in all three spatial dimensions. This gives rise to a set of discrete electronic energy levels, similar to those in atomic physics.

1.1.1 Quantum confinement in a nanocrystal

To describe the energy levels and electronic wavefunctions of a QD, it is necessary to apply the principles of quantum mechanics and solve the Schrödinger equation by taking into account the shape, composition and size of a QD. For a basic understanding of the atomic-like quantization of the electronic states of a dot into discrete energy levels, here we consider a dot of spherical shape (Figure 1.4).

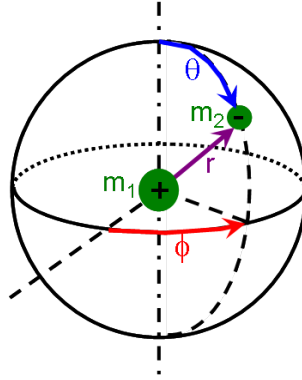


Figure 1.4: Schematic representation of spherical polar coordinates.

The Schrödinger equation for a particle in a spherical potential can be solved by using spherical polar coordinates as shown in Figure 1.4 and can be written as:

$$-\frac{\hbar^2}{2m_e} \nabla^2 \psi(r, \theta, \phi) + U(r) \psi(r, \theta, \phi) = E \psi(r, \theta, \phi) \quad (1.1)$$

where \hbar is the reduced Planck's constant ($\hbar = h/2\pi$), m_e is the effective mass of electron, $U(r)$ is the confinement potential energy and E the total energy. The solution of equation (1.1) can be written as the product of an angular term $Y(\theta, \phi)$ and a radial term $R(r)$:

$$\psi(r, \theta, \phi) = R(r)Y(\theta, \phi) = R(r)\Theta(\theta)\Phi(\phi) \quad (1.2)$$

Using this expression for ψ , equation (1.1) leads to three equations for $R(r)$, $\Theta(\theta)$ and

$\Phi(\phi)$. The solution gives rise to three quantum numbers n , l and m_l :

$$\frac{d}{dr} \left(r^2 \frac{dR}{dr} \right) - \frac{2m_l r^2}{\hbar^2} [U(r) - E] R = l(l+1) R \quad (1.3)$$

$$\sin \Theta \frac{d}{d\Theta} \left(\sin \Theta \frac{d\Phi}{d\Theta} \right) + l(l+1) \sin^2 \Theta \Phi = m_l^2 \Theta \quad (1.4)$$

$$\frac{d^2 \Phi}{d\phi^2} = -m_l^2 \Phi \quad (1.5)$$

The solution of equation (1.3) exists only if the principal quantum number $n = 1, 2, 3, \dots$

The solution of equation (1.4) exists only if the orbital quantum number $l = 0, 1, 2, 3, \dots, n-1$.

The solution of equation (1.5) exists only if the magnetic quantum number $m_l = -l, \dots, +l$.

For an infinite spherical potential well,

$$V(r) = \begin{cases} 0 & \text{if } r \leq a \\ \infty & \text{if } r > a \end{cases}$$

where a is the dot radius. The eigenvalues are given by:

$$E_{n,l} = \frac{\hbar^2}{2m_e a^2} \beta_{nl}^2 \quad (1.6)$$

where β_{nl} is the n^{th} zero of the l^{th} spherical Bessel function.

Figure 1.5 represents the variation of the energy $E_{n,l}$ for $n = 1$ and $l = 0$ upon the dot radius, a , for an electron confined in a spherical PbS QD.

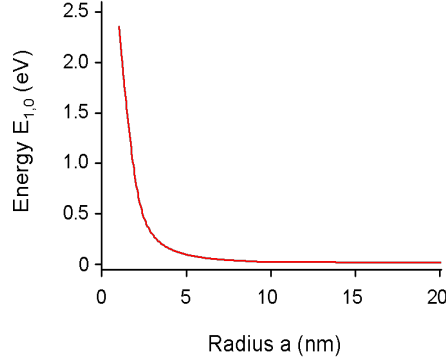


Figure 1.5: Dependence of the energy $E_{n,l}$ on the radius, a , of a spherical PbS QD.

For a PbS spherical dot of radius $a = 5$ nm, we find that the energy of the electron ground state is $E_{1,0} = 0.189$ eV. Here, we have used the effective mass of the electron $m_e = 0.08m_e^0$ where $m_e^0 = 9.11 \times 10^{-31}$ kg and $\beta_{1,0} = 3.15$. A similar confinement energy $H_{1,0}$ can be found for the holes. The electron-hole recombination energy can be expressed as $h\nu = E_{1,0} + H_{1,0} + E_g$ where E_g is the energy gap of bulk PbS ($E_g = 0.41$ eV at 290 K). Using this expression for $h\nu$, we find that $h\nu = 0.788$ eV for $a = 5$ nm.

1.1.2 Excitons

In semiconductors, an exciton is a Coulomb-correlated electron-hole pair. This quasi-particle can be created in a solid crystal by photon excitation: a photon can excite an electron from the valence band into the conduction band leaving behind a hole of positive charge. The Coulomb interaction between the two particles results in a bound electron-hole pair with average distance called the exciton Bohr radius, R_{exc} , in analogy with the Bohr radius for atoms describing the distance between the nucleus and the orbiting electron. An exciton can be described using the same formalism used to describe an hydrogen atom. However, the Bohr radius of an exciton is much larger than that of an H-atom ($a_0 = 0.05$ nm) due to the effect of screening of the atoms in the crystal and the effective mass of the carriers.

To account for these effects, we express R_{exc} as:

$$R_{exc} = \epsilon_r \frac{m_e^0}{\mu} a_0 \quad (1.7)$$

where μ is the reduced mass of the exciton ($\mu^{-1} = m_e^{-1} + m_h^{-1}$, where m_e and m_h are the effective masses for electrons and holes), ϵ_r is the relative permittivity and m_e^0 is the electron mass in a vacuum.

For PbS, $\epsilon_r = 17.2$, $\mu = 0.04m_e^0$ and $R_{exc} = 21$ nm. Table 1.1 reports the Bohr radii of different semiconductor materials. Since the exciton Bohr radius tends to be larger than the size of a QD (< 10 nm), excitons are strongly confined in nanocrystals thus leading to efficient light emission and absorption.

II-VI materials		III-V materials		IV-VI materials	
ZnS	CdSe	GaAs	InAs	PbS	PbSe
3	6	12	34	21	46

Table 1.1: Bohr radii of semiconductor materials in nanometre.

The band gap of a quantum dot is usually tunable as it can be altered by the addition or subtraction of one or more atoms to the semiconductor nanocrystal. Therefore, the exciton emission wavelength can be modified leading to a wide range of coloured nanocrystals. By altering the QD size and its chemical composition, fluorescence emission can be tuned from the near ultraviolet, throughout the visible, and into the near infrared spectrum, spanning a broad wavelength range of 400-2,000 nm (Figure 1.6).[13–18]

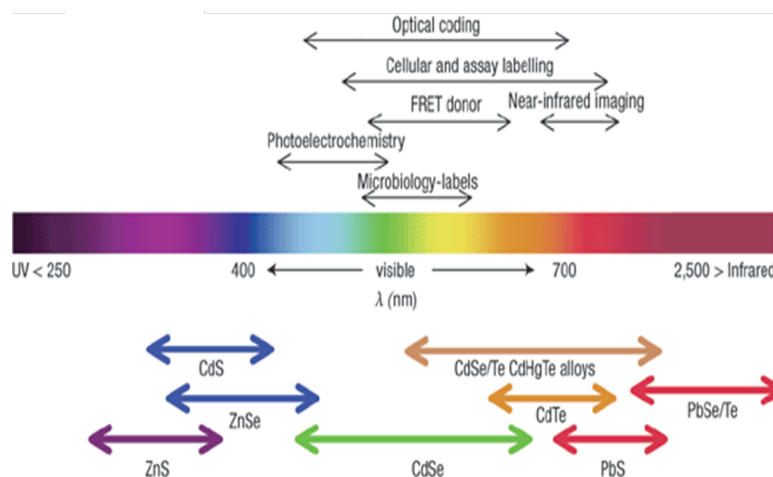


Figure 1.6: Tuning of the quantum dot emission depending on their chemical composition.[19]

1.1.3 Quantum dots compared to organic fluorophores

Conventional organic dyes have been extensively used as bioprobes for labelling and imaging both *in vivo* and *in vitro* for more than three decades.

As an example, a classification-colouring karyotyping of all human chromosomes was established in 1996 by Ried *et al.* using five different organic fluorophores (Cy2, Spectrum Green, Cy3, Texas Red, and Cy5 or combinations of these) to give a multicolour spectral imaging (Figure 1.7).[20]

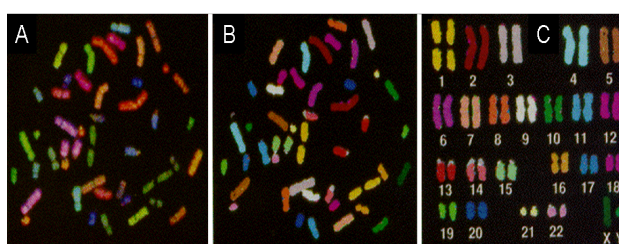


Figure 1.7: Spectral karyotyping of human chromosomes. (A) Presentation of display colours. (B) Presentation of spectra-based classification colours. Regions rich in repetitive sequences. (C) Karyotype of the classification-coloured metaphase chromosomes shown in (B).[20]

More recently, Bradley D. Smith's group reported the use of a near infrared carbocyanine dye to image the bacterial infection by *S. aureus* in a living mouse as shown

in Figure 1.8.[21]

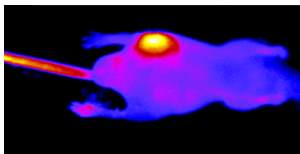


Figure 1.8: Optical images of a mouse with a *S. aureus* infection in the left rear thigh muscle labelled with an organic fluorophore.[21]

Nevertheless, with the emergence of quantum dots, the efficiency of organic chromophores (portion of a molecule that is directly responsible for absorbing photons) has been exceeded. In Table 1.2, the properties of QDs are compared to those of traditional fluorophores.

	Property	Fluorescent probe	Quantum dot probe
1	Broadband excitation	×	✓
2	Narrow bandwidth emission	×	✓
3	Emit light of high intensity	moderate	✓
4	Available in many colours	✓	✓
5	Readily attachable to analytes	✓	moderate
6	Resistant to quenching	×	✓
7	Photochemically stable	×	✓ ^a

^a quantum dots are prone to blinking.

Table 1.2: Comparison of the properties of conventional fluorophores and quantum dots.[22]

Since 2000, the supply of colloidal quantum dots has increased remarkably with the emergence of technological companies. Quantum dots with a variety of conjugates and colours are currently available from Quantum Dot Corporation (Hayward, CA, USA)[23], Evident Technologies (Troy, NY, USA)[24], Invitrogen (Carlsbad, CA, USA)[25] and Nanoco Technologies (Manchester, UK)[26].

It is important to note that QDs permit multiplexed analysis. Broadband excitation and narrow bandwidth emission allow simultaneous excitation of multicolour QDs with

a single light source. In 2002, Chan and Nie quantified a different emission intensity of 20:1, *i.e.*, one quantum dot emits the same amount of light as 20 rhodamine 6G molecules. They established that single dots are ~ 100 -200 times more stable than single organic dye.[27, 28] Figure 1.9 gives an example of the differences observed in the emission and excitation spectra of a quantum dot and an organic dye.

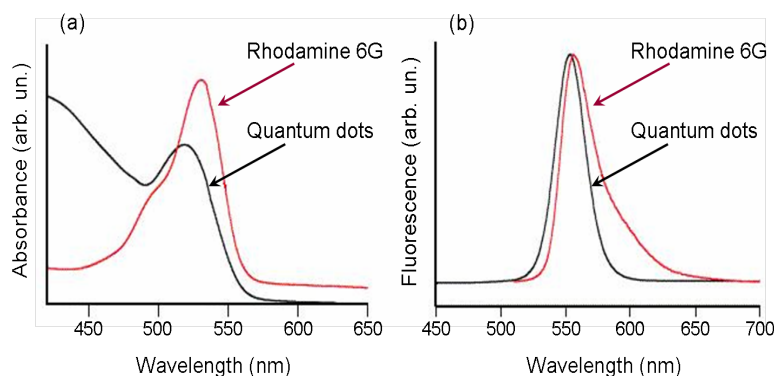


Figure 1.9: Comparison of (a) the excitation and (b) the emission profiles between rhodamine 6G and CdSe quantum dots (adapted from reference [27]).

Concurrently to organic dyes, fluorescent proteins (FPs) were discovered from various marine organisms.[29] For example, the Aequorea-derived fluorescent proteins family has been engineered from the green fluorescent protein (GFP). The GFP, represented in Figure 1.10, is comprised of 238 amino acids (26.9 kDa) and fluoresces green ($\lambda_{em} = 509$ nm) when exposed to blue light.[1, 30, 31]

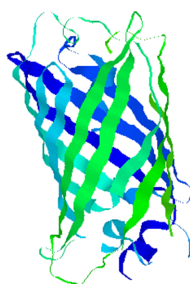
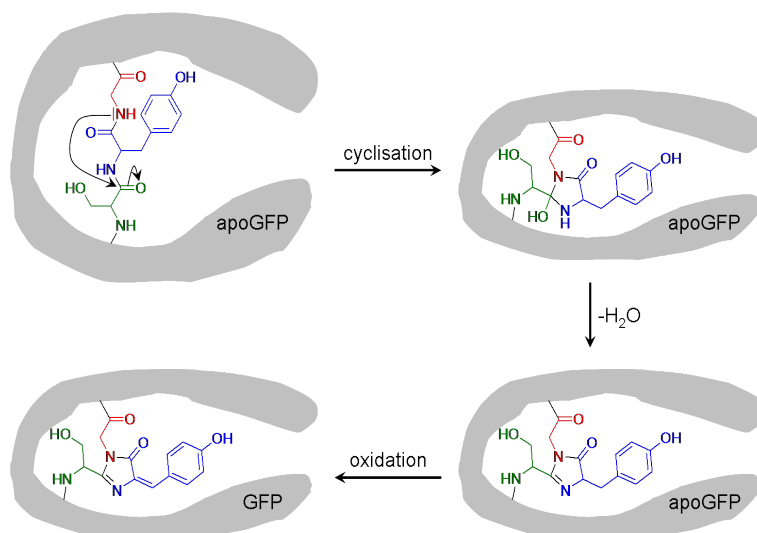


Figure 1.10: Green fluorescent protein ribbon diagram.

However, the main problem with the use of GFP was the excitation and emission spectra of the wild type protein for fluorescence microscopy. Wild type GFP shown in Scheme 1.1 has two excitation peaks: a major one at 395 nm (protonated form of the protein) and a smaller one at 475 nm (unprotonated form).



Scheme 1.1: Cyclization in the tripeptide **Ser65Tyr66Gly67** followed by dehydrogenation and oxidation lead to the formation of the green fluorescent protein.

To alleviate this problem, several mutants of the GFP were constructed into mutants such as cyan (CFP) and yellow (YFP) variants with increased fluorescence and red-shifted major excitation peaks.

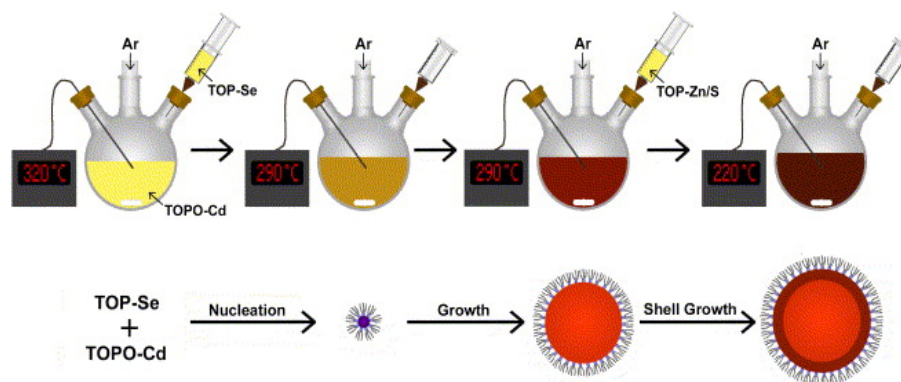
1.1.4 Synthesis of colloidal quantum dots

There are several techniques for nanoparticle synthesis including MBE (molecular beam epitaxy), lithographic patterning and colloidal synthesis. Here, we will focus on colloidal synthesis.

The advantages of the chemical synthesis of nanoparticles are multiple: 1) different sizes of nanocrystals can be obtained with high monodispersity by controlling the reaction conditions and reagent ratios, 2) chemical absorption or surface chemical reactions can be used to passivate the surface states to obtain high quality QDs, 3) the colloidal

method of growth allows the manipulation of the QDs into optically clear solutions or polymer films, as well as the possible attachment to a metal surface or various template structures.[32–34]

For many years, quantum dots have been synthesised in organic media. The ligands TOP (trioctyl phosphine) and TOPO (trioctyl phosphine oxide) are frequently used as stabilizing ligands as they can coordinate both metal and chalcogen elements (S, Se, Te).[35–38] The major drawback of TOPO is its high boiling point (320 °C) and its flammability (Scheme 1.2).



Scheme 1.2: Schematic representation of the synthesis of TOPO-capped CdSe quantum dots.[38]

Nevertheless, the organic ligands are labile for exchange reactions because of their weak bonding to the nanocrystal surface atoms and give imperfect surface passivation. Therefore, the strategy established for increasing both the fluorescence and the stability of QDs in organic media is to grow a shell of higher band gap semiconductor surrounding the core. Currently, the most popular QDs consist of CdSe core, followed by a ZnS shell and one or more organic coats.[39, 40]

During the synthesis of nanocrystals (NCs), two phases of kinetic growth are observed as depicted in Figure 1.11:

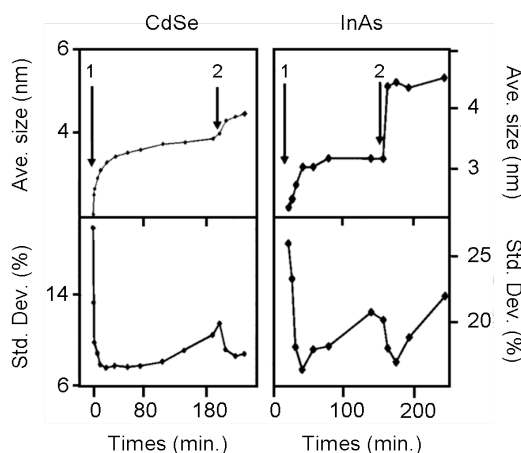


Figure 1.11: Mean size and size distribution of two types of QDs CdSe and InAs (adapted from reference [41]). The arrows 1 represent the first injection of precursors and the arrows 2 represent a second injection of precursors.

Over the first few minutes of the reaction, the average size of the QD increases rapidly and the size distribution decreases, this is called ‘focusing of size distribution’; then, the nanocrystals grow more slowly, the smaller nanocrystals are dissolved and are redeposited on the larger nanocrystals, thus the overall average size of the QDs increases and the size distribution broadens, this is called ‘defocusing’ or ‘Ostwald ripening’.[36, 41]

An important landmark in the development of wet chemical synthetic routes for cadmium chalcogenide nanocrystals was, together with the non-aqueous TOP/TOPO technique, the use of various thiols as capping agents in aqueous solution.[42–44]

A series of thiol-capped CdSe,[44] CdTe,[42, 45] and CdS[43] nanoparticles were synthesized with extremely small sizes (1-3 nm) in aqueous solution. Nanoclusters were obtained through the addition of freshly prepared NaHSe, NaHTe or H₂S solutions to N₂-saturated Cd²⁺ precursor solutions (Cd(ClO₄)₂·6H₂O or CdSO₄) at pH 11.2 in the presence of thioacids or thioalcohols as stabilizing agents. Following this procedure, colloidal HgTe nanocrystals have also been prepared by the passage of hydrogen telluride gas H₂Te through aqueous N₂-saturated mercury(II) perchlorate Hg(ClO₄)₂ solutions at pH 11.2 in the presence of thioglycerol (Figure 1.12).[46]

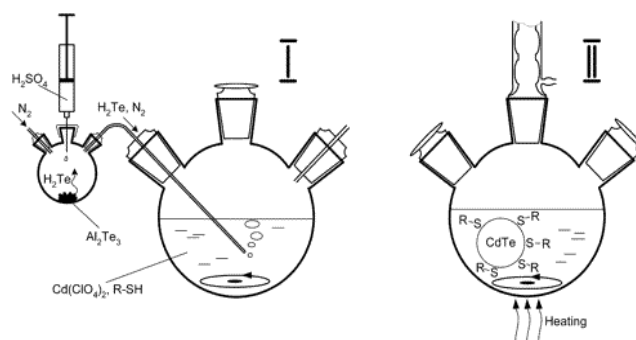


Figure 1.12: Representation of the synthesis of thiol-capped CdTe QDs. I) formation of CdTe precursors by introducing H_2Te gas. II) formation and growth of CdTe nanocrystals promoted by reflux.[45]

The idea to introduce colloidal quantum dots into living cells for biological labelling has emerged from their photophysical properties and from the realisation that QDs are the size of a typical protein (Figure 1.13).[19, 47]

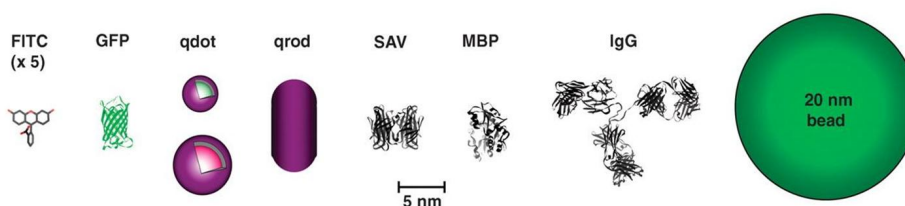


Figure 1.13: Size comparison of QDs and comparable objects, fluorescein isothiocyanate (FITC), quantum dot (qdot), quantum rod (qrod), streptavidin (SAV), maltose-binding protein (MBP), immunoglobulin G (IgG).[18]

Currently, the use of semiconductor nanocrystals for diagnostic applications is a rapidly developing research field of nanotechnology.[48–52] Indeed, quantum dots are the most promising nanostructures for testing technologies that meet the clinical laboratory medicine demands for sensitivity and cost-effectiveness.[53–55] Quantum dot-based diagnostics have the potential to be more cost-effective than existing technologies.[56–59] “Biologists have always had to figure out what they could do in the first 5 or 10 minutes before the dye ran out. Now they can look for much longer” says Paul

Alivisatos, a chemist at the University of California, Berkeley and one of the founders of Quantum Dot Corporation.[23]

1.1.5 Modifying quantum dots with biological tags

The potential of colloidal semiconductor nanocrystals to overcome problems encountered by organic fluorophores make them useful elements/components for optical, electronic and biological applications.[53, 60–70] Scientific interest in interfacing of technology and biology is based on the principle that nanotechnology offers biology new tools, and that biology offers nanotechnology new types of functional scaffolds.[71]

As emphasized by S. Weiss of the University of California, Los Angeles, a founder of Quantum Dot Corporation “We need to protect the quantum dots so that they are not oxidized, are very stable, can withstand salt concentrations in cells, and do not bind to what you do not want them to”.[48] Thus, for successful biological assays, the nanocrystals must be hydrophilic and not interfere with normal physiology, as well as being stable, exhibiting narrow fluorescence peaks, and having a high quantum yield (QY¹). Importantly, they would also be size-tuneable in the near infrared spectral range if they are to be used *in vivo*. [72–76] As shown in Figure 1.14, the range 600-1,100 nm is the ‘optical window’ of biological systems where the main components of the cells (H₂O, melanin and haemoglobin) have their lowest absorption coefficients.[77]

¹Probability of luminescence occurring in given conditions - expressed by the ratio of the number of photons that are emitted by the luminescent species to the number of photons that are absorbed.

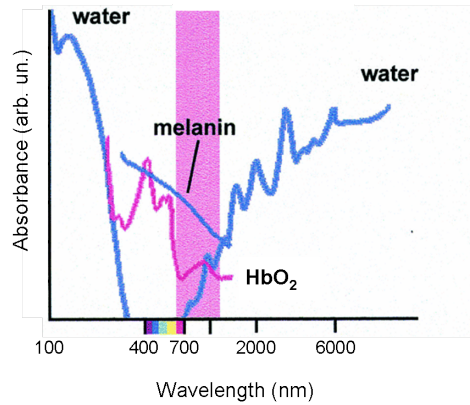
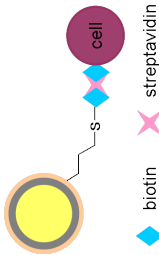
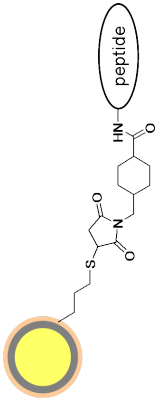
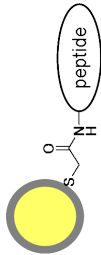
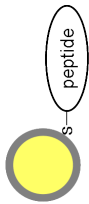
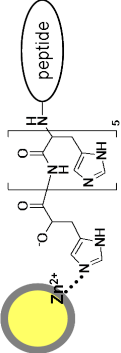
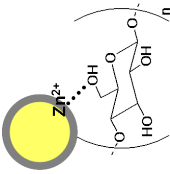
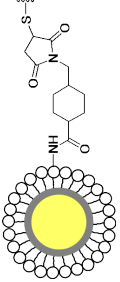
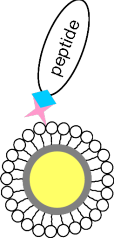


Figure 1.14: Absorption spectra of intracellular absorbers. The molecular extinction coefficients (ϵ) of oxygenated haemoglobin and melanin and the absorption coefficient (α) of water are shown.[77]

One current major drawback of QDs is that they are not easily linked to biomolecules that can be used to target receptor, improve solubility or cell permeability. The use of bioinorganic conjugates - QDs/protein systems - could overcome this problem and therefore represent an attractive tool as a novel method for use as bioactive fluorescent probes in sensing, imaging, immunoassays, and other diagnostics applications.[19, 59, 78–87] In 1998, two research groups, Alivisatos *et al.*[89] and Nie *et al.*[56], reported the first use of quantum dots nanocrystals to label single molecules during living-cell assays and this topic is now being intensively investigated.

Different types of bioconjugated systems are schematically illustrated in Table 1.3:

Method of attachment to QD	Linker	Scheme	Information	References
Silanization	Biotin-avidin		<ul style="list-style-type: none"> • In 1998, Alivisatos <i>et al.</i> were the first group to report the bioconjugation of silica-coated CdSe/CdS core-shell NCs to mouse fibroblast cells. 	[88–90]
	Bifunctional		<ul style="list-style-type: none"> • The cross-linker possesses an ester function at one end, which reacts with a primary amine of a biomolecule to form a stable amide bond and a maleimide group at the other end, which reacts with a sulfhydryl group of the dots to form a stable thioether bond. 	[91–93]
Covalent linkage	Amide		<ul style="list-style-type: none"> • In 1998, Chan and Nie established the second class of adaptor using an amide linker between nanoparticles and biomolecules. 	[56, 94–99]

<p>Hydrophobic ligands exchange</p>		<ul style="list-style-type: none"> • Exchange of the hydrophobic TOP/TOPO ligands with thiolated biomolecules. 	<p>[100–105]</p>
<p>Metal-nitrogen coordination</p>		<ul style="list-style-type: none"> • In 2005, Mattoussi <i>et al.</i> described a linkage of poly-histidine terminated proteins with QDs. 	<p>[106]</p>
<p>Metal-oxygen coordination</p>		<ul style="list-style-type: none"> • Polysaccharides directly bound to the QDs surface by Zn-O bond. 	<p>[107]</p>
<p>Covalent</p>		<ul style="list-style-type: none"> • QDs encapsulated in phospholipid micelles can be selectively coupled to a sulphhydryl group of a biomolecule. 	<p>[108–118]</p>
<p>Hydrophobic attraction</p>		<ul style="list-style-type: none"> • Commercial polymer-coated QDs functionalized with streptavidin available from Quantum Dot Corp. 	<p>[23, 119–127]</p>

Electrostatic attraction	MBP-zb		<ul style="list-style-type: none"> • Electrostatic attraction between negatively charged QDs and positively charged leucine zipper interaction domain of the maltose-binding protein. • Maltose-binding protein is used as a purification tool and protein G (PG-zb) as a molecular adaptor to attach the QDs to an IgG. 	[128–132]
	PG-zb		<ul style="list-style-type: none"> • Electrostatic interactions between negatively charged semiconductor NCs and positively charged avidin which can be attached to biomolecules. 	[133, 134]
	(-) QDs/ (+) biomolecules			[104, 130, 132, 135]

Table 1.3: Conjugation systems between quantum dots and biomolecules.

It should be noted that the surface of a single QD is large enough for linking to multiple biomolecules. Approximately 15-20 maltose binding proteins can be attached to the surface of a 6-nm diameter CdSe/ZnS QD whereas a 3-nm CdSe/ZnS QD could be covered with ~ 12 -15 MBP.[19, 27]

Many other applications of quantum dots as labels in biological applications have been reported in the literature.[136–168] Biomolecule-nanoparticle hybrid systems combine the unique optical and electronic properties of QDs (size-dependent excitation and emission wavelength, resistance to photobleaching², high quantum yield in aqueous solution) with naturally optimized recognition and reactivity functions of biomolecules. This self-assembly approach applied to a wide range of semiconductor nanomaterials employing other recombinant proteins should result in a considerable array of biosensors with various useful properties.

Protein cages can provide structurally constrained reaction environments.[169–175] In our project, we are interested in using the widely studied iron storage protein, ferritin, as a template for the preparation and protective functionalisable coat of inorganic nanomaterials.

1.2 Ferritin, the iron storage protein

The iron storage protein, ferritin plays a key role in iron metabolism.[176–178] Two and a half billion years ago, the solubility of iron became a problem when water began to be used as a source for photosynthesis:

$6\text{CO}_{2(gas)} + 6\text{H}_2\text{O}_{(liquid)} \xrightarrow{\text{light}} \text{C}_6\text{H}_{12}\text{O}_{6(aqueous)} + 6\text{O}_{2(gas)}$. The by-product of such synthesis - dioxygen - created a dilemma for iron-dependent organisms; either to move to media devoid of dioxygen or change to accommodate the low solubility of Fe^{III} produced from Fe^{II} by dioxygen oxidation (the solubility of Fe^{III} is 10^{-9} that of Fe^{II}).

The role of ferritin is to maintain and store iron in a soluble and available form for use

²irreversible destruction of a fluorophore that is under illumination.

as ferrihydrite $[\text{Fe}^{\text{III}}\text{O}\cdot\text{OH}]$. [179–181]

1.2.1 Ferritin structure

Ferritins are found in both eukaryotes (humans, other vertebrates, invertebrates, higher plants, fungi) and prokaryotes (bacteria). [182] Although the primary sequences of ferritin show significant differences among species, the three dimensional conformations are found to be strikingly similar in all cases except for the bacterioferritin (for details, see reference [183]).

In 1962, Harrison and Hofmann suggested that this protein consists of 20 identical subunits. [184–186] Now it is known that all ferritin molecules consist of a protein shell called apoferritin (AFt), composed of 24 polypeptide subunits (total molecular weight of ca. 480 kDa), [187–192] and a central core of hydrated iron(III) oxide $[\text{Fe}^{\text{III}}\text{O}\cdot\text{OH}]$ [193, 194]. The apoferritin subunits assemble into a hollow sphere with an outer diameter of 12 nm, and an inner core of 8 nm in diameter (Figure 1.15).

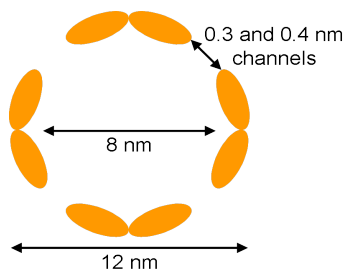


Figure 1.15: Schematic representation of the ferritin structure.

Up to 4,500 iron atoms can be encapsulated within the protein shell to give ferritin, although normally only 2,000-2,500 iron atoms are present in the form of microcrystals as shown by electron and X-ray diffraction [195] and high-resolution dark-field electron microscopy [196]. Thus, ferritin is characterised as an inhomogeneous protein due to the iron content that varies from one ferritin molecule to another (molecular weight around 750,000 for high loading). [197, 198] The iron core is generally thought to be formed from oxidation of Fe^{2+} upon admission of oxygen, resulting in Fe^{3+} which hydrolyzes

within the cavity.[181, 199–201] In addition to iron, the mineral core of various ferritins also contains phosphate in variable amounts influencing the size of the core.[202]

The apoferritin shell is a heteropolymer composed of a variable proportion of two subunits designated by H (for heavy or heart, molecular weight 21,000) and L (for light or liver, molecular weight 19,000). Differences in the subunits of apoferritin are due to variations in the sequence of amino acids throughout the chain, in chain length, and in mass.[203, 204] Ferritins isolated from vertebrates are composed of two types of subunit (H and L), whereas those from plants and bacteria contain only H-type chains, where H-chains are important for Fe^{II} oxidation and L-chains assist in core formation. Furthermore, the relative proportions of H and L subunits appears to be organ specific, heart generally giving a higher proportion of H subunit, while liver and spleen ferritins contain mainly the L subunit.[179–181, 205–208]

In our study, the protein cages used are the horse spleen apoferritin and the human liver apoferritin whose DNA sequences are reported in Table 1.4.

	↗	↘
Horse H	MTTA F P SQVRQNYHQDSEAAINRQINLEL H ASYVYLSMS F YFDRDDVALKNFAKYFLHQ S	
Human H	MTTA S T SQVRQNYHQDSEAAINRQINLEL Y ASYVYLSMS Y YFDRDDVALKNFAKYFLHQ S	
Horse L	MSSQIRQNYST E VEAAVN R LVNLYL R ASYTYLSLGFYFDRDDVALEGV C HFFRELAEEKR	
Human L	MSSQIRQNYST D VEAAVN S LVNLYL Q ASYTYLSLGFYFDRDDVALEGV S HFFRELAEEKR	
	↗	↘
Horse H	HEEREHAEKLMKLNQNRGGRIFLQDIKKPDQDDW E NG L KAMECALHLEKNVN E SLLLELHK	
Human H	HEEREHAEKLMKLNQNRGGRIFLQDIKKPD C DDW E SG L NAMECALHLEKNVN Q SLLLELHK	
Horse L	EG A ERLLKMQNQGGRALFQD L QKP S QDEWGTTLDAMKAA I VLEK S LNQALLDLHALGSA	
Human L	EG Y ERLLKMQNQGGRALFQD I KKP A EDEWGKTPDAMKAA A MALEK K LNQALLDLHALGSA	
	↗	↘
Horse H	LATDKNDPHLCDF L ETHYLNEQVKAIKELGDHVTNLR R MGAPESGMAEYLFDKHTL G ECDES	
Human H	LATDKNDPHLCDF I ETHYLNEQVKAIKELGDHVTNLR K MGAPESG L AEYLFDKHTL G DS D NES	
Horse L	Q ADPHLCDFLE S HFLDEEVKL IKKMGDHL TN I QRL V GS Q AGLGEYLFERLTLKHD	
Human L	R TDPHLCDFLE T HFLDEEVKL IKKMGDHL TNLHR L GG P EAGLGEYLFERLTLKHD	

Table 1.4: DNA sequences of both H and L apoferritin from horse and human. The discrepancies between species are highlighted in red.

Both of the H horse and human subunits contain approximately 182 amino acids whereas both of the L subunits contain 175 amino acids (Table 1.5). After biosynthesis, the first methionine residue (shown in green in Table 1.4) is removed.

Amino acid	No. residues subunit			
	Horse H	Horse L	Human H	Human L
Asp	14	12	15	13
Glu	18	15	16	16
Lys	13	9	13	12
Arg	8	11	7	10
Asn	11	6	12	6
Gln	10	11	10	7
Ser	9	10	12	8
Thr	6	6	7	7
Phe	8	8	6	8
Trp	1	1	1	1
Cys	3	2	3	1
His	11	6	10	7
Tyr	7	6	9	7
Gly	7	11	7	12
Ala	13	15	13	15
Val	6	8	6	6
Leu	22	28	22	27
Ile	5	4	6	3
Met	6	4	5	5
Pro	4	2	3	4

Table 1.5: Amino acid composition of H and L subunits of horse spleen apoferritin and human liver apoferritin.[209, 210]

Furthermore, each subunit of apoferritin is folded in a bundle of two pairs of α -helices

joined by a long loop (Figure 1.16):

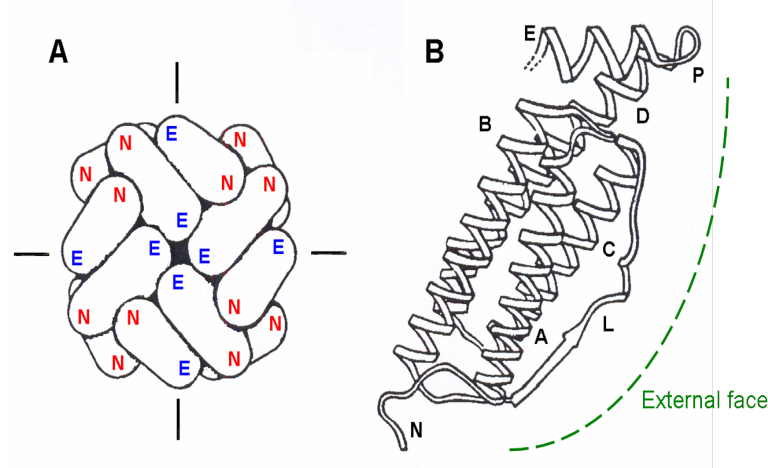


Figure 1.16: Schematic representation of the horse spleen ferritin molecule. (A) Subunit arrangement. (B) Conformation of the horse spleen apoferritin subunit showing alternative connectivities between helical sections (adapted from reference [181]).

Each subunit is roughly cylindrical ($l = 5.5$ nm, $d = 2.7$ nm)[211] and contains four long nearly parallel right-handed helices (A, B, C, D), a shorter helix (E), a helical turn (P), a long length of extended chain (L), some regions of irregular conformation and a *N*-terminus (N). Helices A-E are joined in alphabetical order and L connects opposite ends of B and C. The *N*-terminus is on a short non-helical region preceding A. Helix A on the outside of the molecule turns into B on the inner surface; following the long loop L, the polypeptide chain runs along C on the outside of the subunit, and after a tight corner turns along D on the inside surface, then *via* a twisted segment and a single helical turn P, the chain ends with E.

Ferritin is a thermally stable protein up to 82°C . Granick observed some changes in ferritin when a dialyzed protein solution was slowly heated.[212, 213] Coagulation occurred at $T = 82^\circ\text{C}$ which redissolved on cooling, whereas at higher temperatures, the protein was irreversibly denatured.

1.2.2 Electrostatic features

One of the most interesting feature of the apoferritin shell is the presence of channels formed by the different types of interactions of the 24 subunits (Figure 1.17).[193, 214]

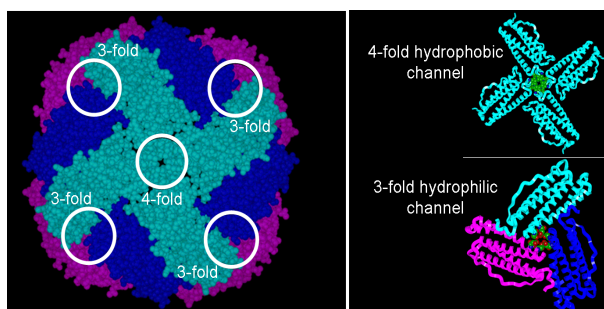


Figure 1.17: Schematic representation of the hydrophobic and hydrophilic channels of apoferritin.[215]

These channels are responsible for the entrance and exit of cations. Eight hydrophilic channels - referred to as 3-fold channels - are formed by interactions of three *N*-terminus of glutamate and aspartate residues and six hydrophobic channels - referred to as 4-fold channels - are formed by interactions of twelve leucine residues (three from each subunit) (Figure 1.18).

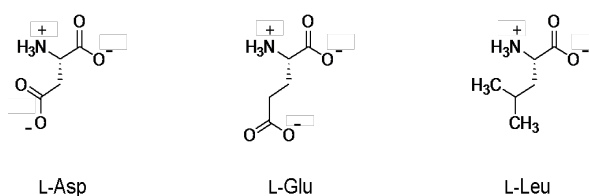


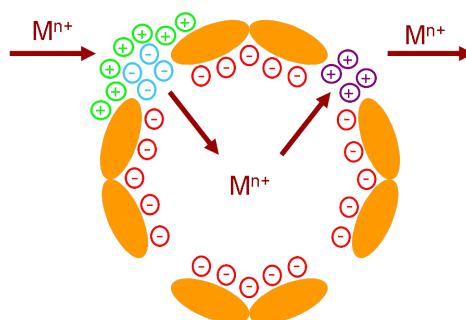
Figure 1.18: Structures of the amino acids L-aspartate (Asp), L-glutamate (Glu) and L-leucine (Leu).

The presence of charged amino acids gives specific electrostatic potential to the protein. The potential on the interior surface is, like the outer surface, mostly negative with only a few regions with an excess of positively charged amino acids.[216]

The external entrance of the 3-fold channel has a negative potential value due to the presence of glutamic acid and aspartic acid residues. These acids are also responsible

for the negative potential along the channel across the protein shell from the outside to the inside. Furthermore, the outer entrance is surrounded by regions of positive potential values giving rise to an electrostatic field directing cations toward the channel entrance. This channel might function as a funnel to direct cations into the apoferritin cavity.

The potential on the exterior of the 4-fold channel tends to be positive due to the presence of the free *N*-terminal amino acid amine, thus resulting in a repulsive surface to positively charged ions. It has been proposed that this channel may function as a pathway for the removal of cations (Scheme 1.3).



Scheme 1.3: Schematic representation of the channels across the protein shell.

Many studies have been performed investigating the permeation of small molecules into apoferritin but with conflicting results.[217–219] Diffusion studies have shown that glucose (7 Å across) is capable of slowly entering the interior of the ferritin capsule, but sucrose (approximately twice the size of glucose) is not.[220, 221] On the contrary, X-ray studies have shown that maltose (13 Å) can enter into the cavity of ferritin through the channels (3-4 Å) which implied that the latter are sufficiently flexible to allow entrance of molecules larger than their own size.[222]

1.2.3 Dissociation of the protein shell subunits

The first demonstration that apoferritin could be converted into subunits was made by Hofmann and Harrison in 1962, using the anionic detergent SDS (sodium dodecyl sulphate) and other denaturants. Furthermore, ferritin and apoferritin were not affected

by the addition of 10 M urea. However, the optical rotatory properties changed in presence of 6 M guanidine hydrochloride at pH 6.0 consistent with helix disruption in the protein.[185, 188, 223, 224]

By far the most useful procedure for the reversible dissociation of apoferritin is that described by P. M. Harrison and D. W. Gregory in 1965 in which they observed the disassembly of the protein shell into its subunits as a function of pH.[225] In 1968, they also showed that apoferritin subunits are able to assemble in the absence of iron as determined by electrophoretic mobility and sedimentation coefficient analyses, which led to the conclusion that the reassembled apoferritin is identical to the native ferritin.[226, 227]

Crichton and Bryce studied the dissociation of apoferritin by sedimentation velocity techniques and established that between pH 2.8-10.6 the apoferritin is only present as a 24 subunit capsule whereas between pH 1.6-2.8 and 10.6-13.0 both the capsule and a low molecular weight component were detected.[228] The dissociation into subunits is more easily observable by ^1H NMR analysis at low pH and it has been shown that at pH ~ 3.5 , ferritin starts to dissociate and at pH ~ 1.8 , the protein is completely dissociated.[229] This phenomenon can be explained by the subunit-subunit interactions. At low pH values, one tryptophan residue per subunit as well as four to five tyrosine residues per subunit are exposed to the solvent. These transfers are accompanied by the protonation of the different carboxyl groups present on the subunit. During the reassociation process at high pH values, the carboxyl groups are deprotonated and the sequence described above is reversed. The extreme stability of the apoferritin is due to intersubunit hydrophobic interactions and surface charges.[230]

As ferritins are robust proteins that can withstand high temperature (82°C) and high pHs (8.5-9.0) for an appreciable period of time, this dissociation-reassociation process of the protein shell is an attractive asset in order to entrap small molecules inside the cavity. Effectively, the apoferritin shell can be dissociated into subunits at pH 2.0 in the presence of the nanomaterials and then by increasing the pH to 7.0 the subunits reassemble into the 24-subunit shell, thereby trapping molecules within its

interior.

1.3 Apoferritin as a protein cage for quantum dots

Preparation of semiconductor nanocrystals in a controlled manner is a very interesting challenge as their optical and electronic properties depend on the size, shape and chemical composition of the particles. One possible issue for the preparation of an ideal isolated nanomaterial involves the use of a preorganized matrix as a chemically and spatially confined environment for its construction.

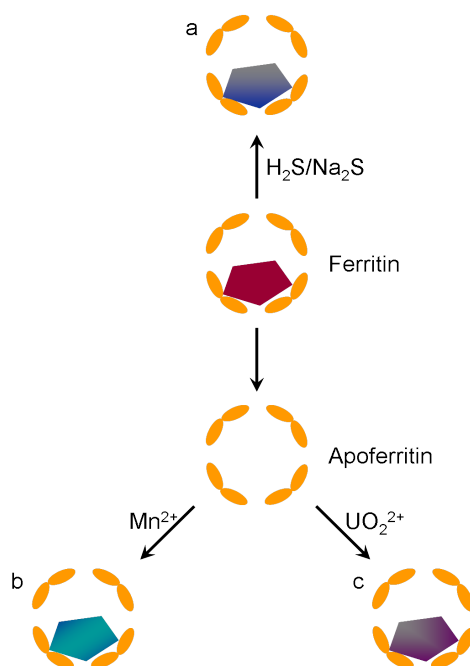
For several years, Stephen Mann, Director of the Centre for Organised Matter Chemistry at the University of Bristol, has been interested in using biological systems as templates for materials synthesis.[81, 231–236] He has been working on the encapsulation of different types of nanoparticles in the cavity of apoferritin and his results illustrate that the protein cavity can be a preferred environment for non-hydrolytic reactions.

The procedures currently used to entrap small molecules within the cavity of ferritin are the channels providing pathways for the entry and expulsion of ions and the dissociation-association process of the protein shell according to the pH.

1.3.1 Entrapment of materials in apoferritin: The nanoreactor route

Although only phosphate-containing iron cores of ferritin are able to bind incoming metal ions with high affinity, a wide number of dicationic metals (M^{2+}) such as Cd^{2+} , Zn^{2+} , Cu^{2+} , Ni^{2+} , Co^{2+} , Mn^{2+} and Mg^{2+} have been reported to bind to phosphate-free apoferritin.[237]

In 1991, Mann and co-workers established for the first time the use of protein structures as reaction cages to generate nanoscaled materials. His group synthesized iron(III) sulphide loaded-apoferritin by transformation of the hydrated iron(III) oxide core to an iron sulphide in alkaline reactions conditions (*in situ* chemical reaction of native oxide cores with H_2S or Na_2S) (Scheme 1.4).[238, 239]

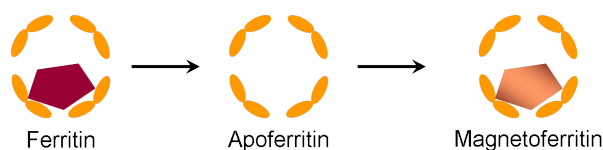


Scheme 1.4: Representation of the use of ferritin in the synthesis of nanophase materials. (a) iron sulphide; (b) manganese oxide reconstitution; (c) uranyl oxyhydroxide deposition (adapted from reference [240]).

Four years later, the demetallation-reconstitution process was also used to accumulate FeS nanoparticles within the protein cavity.[241]

By modifying the iron core, iron phosphate, arsenate, vanadate and molybdate could be synthesised within the apoferritin.[242]

Mann and Meldrum demonstrated an *in vitro* synthesis of magnetoferritin - apoferritin loaded with iron oxide magnetite (Fe_3O_4) cores (Scheme 1.5). Two preparation techniques were established: reconstitution of apoferritin with Fe^{II} solution was achieved in 1992 under slow oxidation conditions (high temperature 60°C and pH 8.5)[243, 244] and in 1998, a new synthesis was reported involving incremental addition of Fe^{II} followed by stoichiometric amounts of the oxidant triethylamine-*N*-oxide Et_3NO . [245]



Scheme 1.5: Synthesis of the magnetoferritin (adapted from reference [243]).

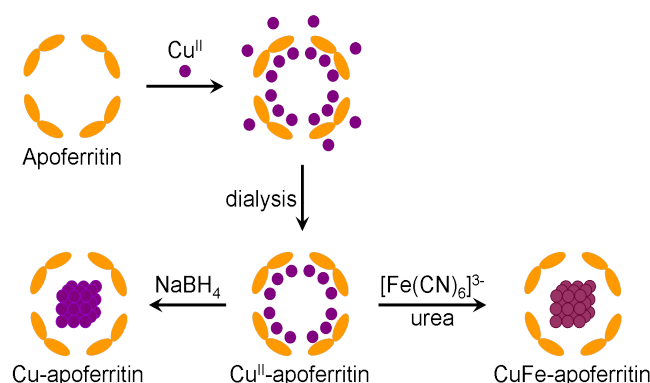
Using ion uptake methodology, manganese ions have been deposited as Mn oxyhydroxide cores MnOOH (Scheme 1.4).[238, 239] Mann pointed out the roles of the inner and outer surfaces of ferritin proposing that the outer surface acts as a polyelectrolyte inhibiting the formation of MnOOH in the external phase whereas the inner surface is inactive enabling nucleation and growth within the cavity.[246]

Uranyl oxyhydroxide cores (6 nm) have also been accumulated in apoferritin cavity by ion-binding and hydrolytic polymerization. Uranyl acetate $\text{UO}_2(\text{CH}_3\text{COO})_2 \cdot 2\text{H}_2\text{O}$ reduced by sulphonic acid at pH 8.0 led to 4,000 U atoms accumulating in the apoferritin cavity (Scheme 1.4).[238, 239] In 1992, J. Hainfeld reported the accumulation of 800 uranium atoms by incubation of uranyl acetate in pH 4.0 buffer. The encapsulated uranium atoms had reduced toxicity and antibodies could be attached to the outer shell for tumour imaging.[247]

Since the beginning of the 21st century, more and more researchers have been interested in the use of apoferritin as a confined environment for the encapsulation of nanoparticles.

Cobalt has been synthesized as cobalt(III) oxyhydroxide CoOOH within the protein cage by oxidative hydrolysis of Co^{II} with hydrogen peroxide H_2O_2 . [248–250] Nickel and chromium have been accumulated as their metal hydroxides through an hydroxylation process using carbonate ions.[251] Ni and Cr cores were formed by adding Na_2CO_3 to ammonium nickel(II) sulphate hexahydrate $(\text{NH}_4)_2\text{Ni}(\text{SO}_4)_2 \cdot 6\text{H}_2\text{O}$ and ammonium chromium(III) sulphate dodecahydrate $\text{NH}_4\text{Cr}(\text{SO}_4)_2 \cdot 12\text{H}_2\text{O}$, respectively. HCO_3^{3-} ions substitute the coordinate water molecules and form a complex which penetrate into apoferritin through the channels. In the cavity, HCO_3^{3-} is decomposed into CO_2 and OH^- accelerating the hydroxylation process. Gold sulphide particles were also incorporated by mixing Au_2S and apoferritin at RT at pH 6.0-9.0.[252]

In 2005, Domínguez-Vera reported loading apoferritin with Cu^{II} which entered by the channels and, then can react with $[\text{Fe}(\text{CN})_6]^{3-}$ resulting in $\text{Cu}^{\text{II}}\text{-CN-Fe}^{\text{III}}$ Prussian blue (PB) nanoparticles (Scheme 1.6).[253]



Scheme 1.6: Preparation of the PB $\text{Cu}^{\text{II}}\text{-CN-Fe}^{\text{III}}$ -loaded apoferritin (adapted from reference [253]).

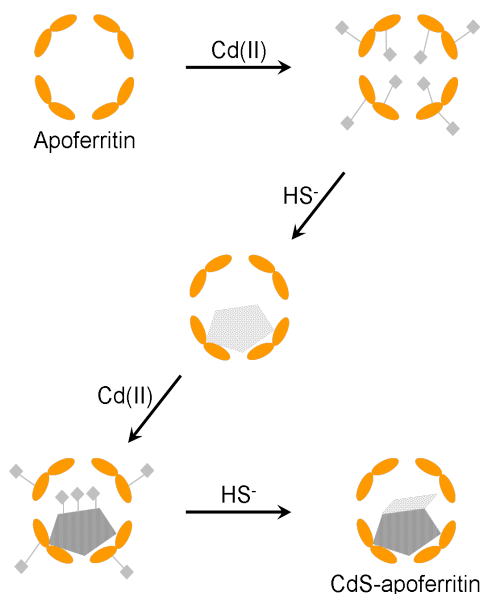
Using the same procedure, superparamagnetic nanoparticles of nickel and cobalt have been encapsulated within the apoferritin cavity by treatment of apoferritin with Ni^{II} and Co^{II} at pH 8.0. Addition of sodium borohydride NaBH_4 , a reducing agent small enough to pass through the channels led to the formation of Ni^0 and Co^0 particles.[254]

Mineralization of cobalt-platinum by ferritin has been achieved by adding ammonium tetrachloroplatinate $(\text{NH}_4)_2\text{PtCl}_4$ solution and cobalt acetate tetrahydrate $\text{Co}(\text{CH}_3\text{COO})_2 \cdot 4\text{H}_2\text{O}$ to an apoferritin solution at pH 8.0. Then, NaBH_4 was introduced to the buffered solution to reduce the metal ions precursors Co^{II} and Pt^{II} to form CoPt .[255, 256]

A size-selective hydrogenation catalyst has been synthesized as a Pd-loaded apoferritin complex. K_2PdCl_4 was mixed with a solution of apoferritin at pH 8.5 and NaBH_4 was added to the resulting solution for reduction of palladium.[257, 258]

More interestingly, semiconductor nanocrystallites such as CdS , CdSe and ZnSe were formed in the cage-shaped protein. Because the cavity surface of the apoferritin has acidic amino acid residues, the inner space has a negative electrostatic potential which condenses the positively charged metal ion in the cavity.[216] In 1996, S. Mann

and K. Wong prepared CdS-loaded ferritin.[259] They proceeded by the addition and reaction of stoichiometric amounts of Cd^{II} and HS^- to deaerated buffered solutions (pH 7.5) of apoferritin (Scheme 1.7).

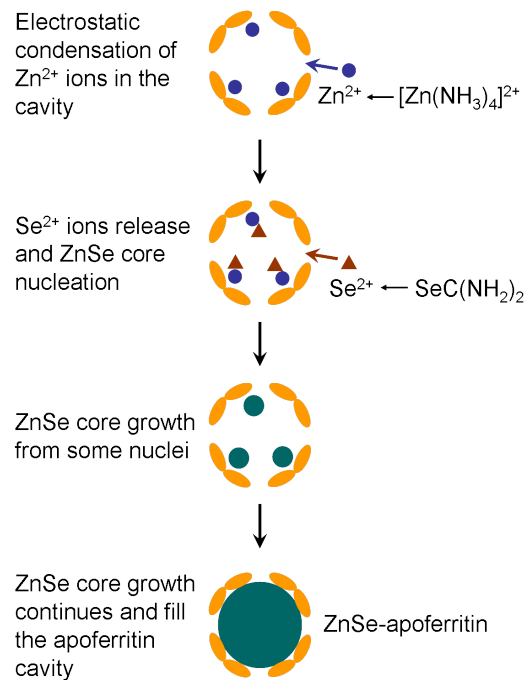


Scheme 1.7: Reaction scheme for the synthesis of CdS-apoferritin nanocomposites (adapted from reference [259]).

The first step of the synthesis was the nucleation of CdS clusters inside the cavity generated by the addition of Cd^{II} atoms followed by the addition of excess sulphide and dialysis. These clusters were then considered as growth centres for the binding of a second addition of cadmium and sulphide atoms. These CdS nanocrystals did not fully develop in the cavity and the obtained CdS nanoparticles had irregular morphologies. The UV-visible spectrum for CdS-apoferritin composites showed two absorption peaks: an excitation peak at around 350 nm for the CdS nanoparticles and an absorption peak at 280 nm corresponding to the peptide bonds of the protein.[260] Transmission electron microscopy (TEM) micrographs of CdS-loaded apoferritin showed discrete electron-dense nanometre-size particles (size estimated to be 4.5 nm and 2.5 nm at 55 and 110 Cd^{II} per molecule). Furthermore, energy dispersive X-ray analysis (EDX) confirmed the presence of cadmium and sulphide.

In 2004, Yamashita and co-workers reported the synthesis of uniform CdSe nanoparticles within the cavity of apoferritin (509 CdSe/cavity).[261, 262] They designed a slow chemical reaction between Cd^{2+} stabilized by ammonia solution (formation of tetraaminecadmium ions $\text{Cd}(\text{NH}_3)_4^{2+}$) and Se^{2-} from selenourea. The pH of this reaction mixture was adjusted to 8.0, and then apoferritin molecules were added. This resulted in CdSe QDs with a narrow size distribution and an average diameter of 6 nm.

In 2005, Yamashita and his group established the fabrication of 1,000 ZnSe nanoparticles in one apoferritin cavity using the same procedure with tetraaminezinc ions $\text{Zn}(\text{NH}_3)_4^{2+}$ (Scheme 1.8).[263] The average crystal size was determined to be 7 nm, which is the same as the internal diameter of apoferritin cavity. The same group also recently produced CdS encapsulated-apoferritin composites following this procedure starting from $\text{Cd}(\text{NH}_3)_4^{2+}$ and thioacetic acid CH_3COSH . [264]



Scheme 1.8: Schematic representation of the ZnSe-encapsulated quantum dots within the apoferritin cavity (adapted from reference [263]).

As can be seen, a number of semiconductor nanocrystallites have been encapsulated through the channels in the protein shell of apoferritin. In the next paragraph, the

encapsulation of different molecules through the dissociation-reassociation process is discussed. To date, no quantum dots have been entrapped using this methodology and the luminescence properties of the composites reported above have not been described.

1.3.2 Entrapment of materials in apoferritin: The reassembly route

In 2002, a gadolinium complex GdHPDO3A, an extra cellular MRI contrast agent currently used in clinical practice was introduced into the internal cavity of apoferritin by the dissociation (pH 2.0)-association (pH 7.0) process (Figure 1.19).[265]

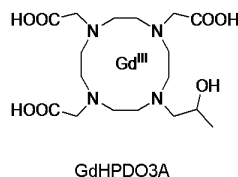
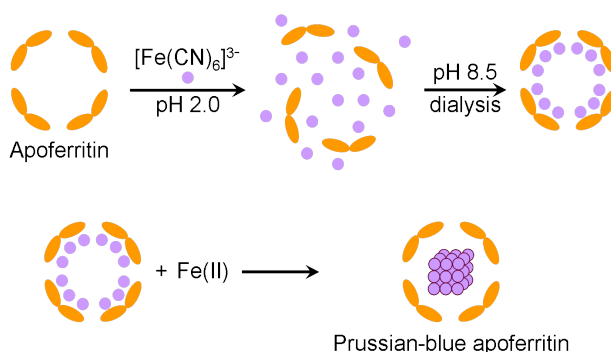


Figure 1.19: Representation of the gadolinium-DO3A complex.

In 2003, a new Prussian blue ferritin was reported by Domínguez-Vera: apoferritin was loaded with a metal complex (hexacyanoferrate(III) $[\text{Fe}(\text{CN})_6]^{3-}$) by the disassembling-reforming process, isolated and then the trapped metal complex reacted with a second metal ion (Fe^{II}) to build a new material giving confined $\text{Fe}^{\text{II}}\text{-CN-Fe}^{\text{III}}$ ferritin (Scheme 1.9).[266]



Scheme 1.9: Preparation of the PB $\text{Fe}^{\text{II}}\text{-CN-Fe}^{\text{III}}$ -loaded apoferritin (adapted from reference [266]).

Larger cores could be formed by the dissociation process of the apoferritin shell. Indeed,

using the reassembly route, the PB cores were observed to be 5 nm exhibiting an UV-vis broad band at 710 nm, whereas the nanoreactor route described in section 1.3.1 led to PB complexes of 3.5 nm cores with an UV-vis broad signal at 470 nm.

Desferrioxamine B (DFO) - a drug for iron chelation therapy - has been introduced within the protein shell by dissociation of the ferritin at pH 2.0 followed by reassociation at pH 7.4. It has been shown that this DFO-loaded apoferritin could react with Fe^{III} to form about three [DFOFe] complexes within the cavity, this confirms that apoferritin could be used as a confined environment for the construction of nanoparticles. When apoferritin/[DFOFe] composites were synthesized by adding previously prepared [DFOFe] complexes to apoferritin, only one [DFOFe] complex was encapsulated. These results can be explained by the size of the hydrophilic channels (4 Å) and by the size of the cavity: 1) [DFOFe] complexes are much bigger than DFO molecules, thus more DFO can be encapsulated within apoferritin cavity than [DFOFe], 2) In the case of encapsulated DFO, Fe^{III} atoms access to the cavity by the hydrophilic channels which are too small to allow the release of DFO.[267]

The same procedure has also been used for the encapsulation of the marker fluorescein,[269] and the drugs doxorubicin,[268] cisplatin[270] and carboplatin[270] which were incorporated by adding the drugs to apoferritin at pH 2.0 followed by reassociation of the subunits at pH 7.5 (Figure 1.20).

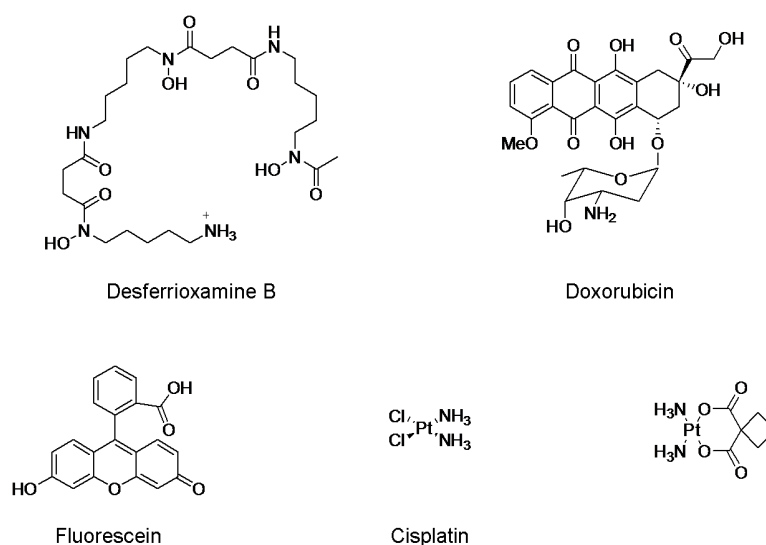


Figure 1.20: Molecular structures of desferrioxamine B, doxorubicin, fluorescein, cisplatin and carboplatin.

Although the efficiency of the reassembly procedure has been shown for diverse molecules, it is important to re-iterate that this encapsulation method has not been previously achieved for the entrapment of quantum dots within the apoferritin cavity.

1.4 Applications of apoferritin-encapsulated materials

Zborowski, Mann and co-workers reported for the first time in 1996 a new application for a derived-ferritin composite.[271] They used magnetoferritin for immunogenetic isolation of lymphocytes from mononuclear cell samples. Magnetoferritin was synthesized as described previously.[243] Monocytes were first depleted from the cells which were then labelled with an antibody anti-IgG (mAb). A second biotinylated antibody (Ab-biotin) was added to the first and finally biotinylated-ferritin was attached through an avidin bridge leading to the system cell-mAb-Ab-biotin-avidin-biotin-magnetoferritin shown in Figure 1.21. Lymphocytes were isolated by depositing the cells on glass slides through a magnetic field.

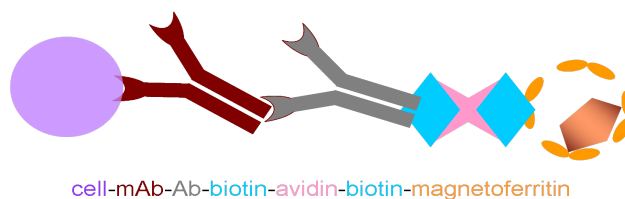


Figure 1.21: Magnetoferritin used as a label for lymphocytes isolation.

Apo ferritin with iron oxyhydroxide has been used for the synthesis of Cr^{III} from Cr^{VI} and Cu^0 from Cu^{II} . [272, 273]

Ferritin can also be used as a template for the design of arrays of particles as shown by Yamashita. [274, 275] Ferritin was deposited on a silicon substrate and then submitted to heat treatment (450°C) in order to remove the protein shell. Ordering of iron cores was observed by X-ray powder diffraction and high resolution scanning electron microscopy (HRSEM) before and after heat-treatment (Figure 1.22). Dried ferritin samples contained 6 nm diameter ferrihydrite iron cores. After heating, the core was transformed in FeO and $\text{Fe}_2\text{N}\cdot\text{FeO}$. This technique could be used to fabricate quantum electronic devices based on FeO and InO particles. [276, 277]

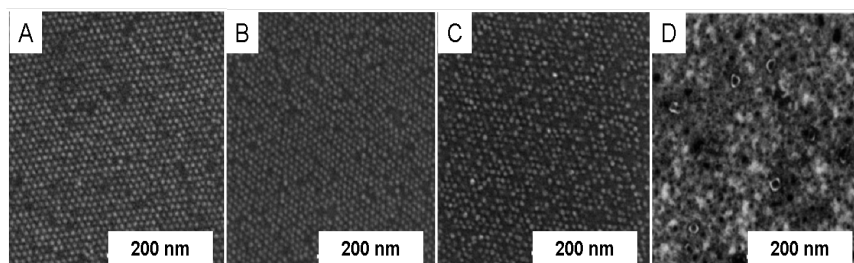
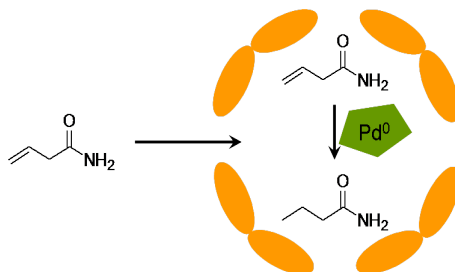


Figure 1.22: HRSEM images of arrays of the ferritin molecules A) before and B), C), D) after heat-treatment under nitrogen at 300°C , 500°C and 700°C for 1 h, respectively (adapted from reference [274]).

Size selective olefin hydrogenation was realised using a Pd cluster incorporated in apoferritin. Ueno *et al.* reported that olefin substrates could enter the cavity through the channels and could undergo hydrogenation catalyzed by palladium (Scheme 1.10). [257] Hydrogenation of neutral olefins was faster using the Pd/apoferritin composite than hy-

drogenation with Pd alone. Also, the greater size or negative charge of the olefin leads to slower hydrogenation.



Scheme 1.10: Hydrogenation of olefins by Pd-loaded apoferritin.

Cobalt-filled carbon nanotubes were prepared from cobalt-encapsulated apoferritin. The apoferritin shell of Co-AFt composites was removed by heat-treatment leaving free cobalt on a substrate.[278]

Recently, Iwahori and Yamashita reported the preparation of a nanodot gate memory based on apoferritin with a Co_3O_4 core.[279] Co/apoferritin composites were synthesized following Douglas and Stark procedure.[248] The gate was prepared by a silicon oxide surface positively charged by poly(ethyleneimine) (PEI) on which negatively charged Co/apoferritin composites could be deposited by electrostatic attraction. By heat-treatment, apoferritin and PEI could be removed leaving Co nanoparticles on the substrate. Electric measurement showed that the NP array was responsible for storage of electrons or holes depending on the voltage.

Metallic phosphate nanoparticles encapsulated within the apoferritin cavity through nanoreactor and reassembly routes showed good voltammetric signals for bioanalytical applications.[280]

The conjugation of ferritin to other biomolecules have been studied by different techniques.

Modification of the lysines residues on the outside of apoferritin have been exploited as a method of connection. Mann *et al.* reported the creation of networks of ferritin molecules by cross-linking ferritin through biotin-avidin bridges.[281] Biotinylation of

horse spleen ferritin led to 72 modified lysines residues/ferritin molecule. Figure 1.23 shows TEM and SDS-PAGE analyses confirming the formation of networks once streptavidin was added to biotinylated ferritin molecules.

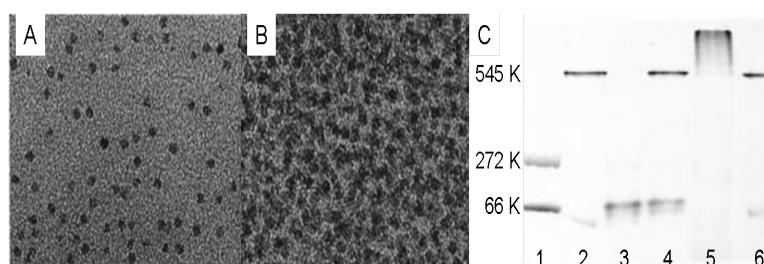


Figure 1.23: TEM micrographs of A) streptavidin added to native ferritin and B) networks of ferritin molecules formed by the addition of streptavidin to biotinylated ferritin. C) SDS-PAGE of (1) protein marker, (2) native ferritin, (3) streptavidin, (4) native ferritin + streptavidin, (5) biotinylated ferritin + streptavidin, (6) biotinylated ferritin (adapted from reference [281]).

Hexacyanoferrate(III)- and fluorescein-encapsulated apoferritin composites were used as bioassay labels for the detection of DNA.[282] Eight amino-modified DNA strands were covalently linked to the carboxylic amino acids of apoferritin through EDC (1-ethyl-3-(3-dimethylaminopropyl) carbodiimide hydrochloride) coupling.

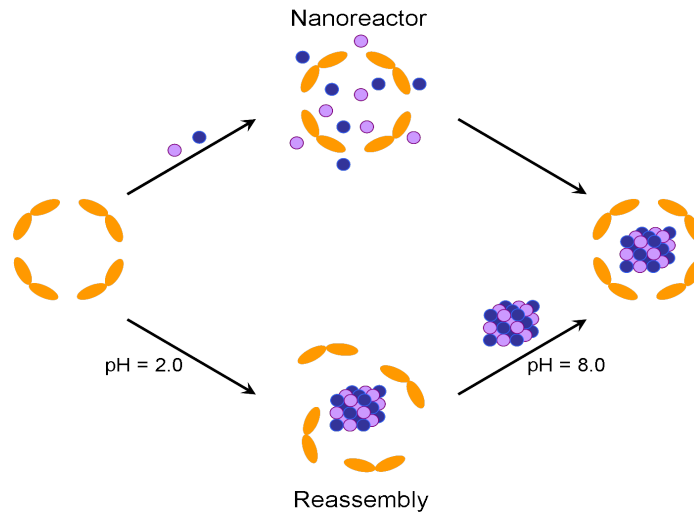
Lysines residues were recently modified with different sized *N*-hydroxysuccinimidyl ester derivatives. Four acetyl/alkyne derivatives were attached to each subunit.[283]

1.5 Project aims

This project focuses on 1) the synthesis of QDs and tuning of their properties; and 2) the encapsulation of quantum dots within the cavity of apoferritin using the two methods described previously:

- The nanoreactor route: inorganic ions enter apoferritin cavity through the 3-4 Å diameter channels between the subunits of the protein shell. QDs formation is then stimulated by the presence of a high density of aspartate and glutamate amino acid residues on the inner surface of the protein shell (Scheme 1.11).

• The reassembly route: apoferritin shell disassembles into its subunits at $\text{pH} = 2.0$ and re-assembles at $\text{pH} > 8.0$ in the presence of preformed quantum dots in aqueous solution (Scheme 1.11).



Scheme 1.11: Encapsulation of QDs within the cavity of apoferritin either by the channels (upper scheme) or by the disassembly/reassembly process (lower scheme).

In the following section, the solubility of the protein ferritin in organic media, the preparation of the protein cage apoferritin and the synthesis of PbS quantum dots are discussed.

We show that the formed apoferritin/PbS QD composites emit in the near infrared (NIR) wavelength range. This makes the composite an attractive tool for biological applications as hemoglobin and water have their lowest absorption coefficient in the NIR region where the light scattering is minimum.[75, 284]

The QDs/protein bionconjugate system could:

- 1) simplify the conjugation of QDs to other biomolecules (proteins, peptides, carbohydrates),
- 2) improve the QDs stability/solubility in aqueous solution,
- 3) reduce the immune response induced *in vivo*,
- 4) reduce the QDs toxicity *in vivo*,
- 5) control the size of the QD to ~ 7 nm.

Chapter 2

PbS quantum dots

2.1 Introduction

Of the various nanocrystals, PbS-based QDs have emerged as promising candidates for optical applications in the near-infrared (nir) region of the electromagnetic spectrum.[285–288] In particular, since the wavelength emission of PbS dots can be controlled and tailored within the spectroscopic window 900-1,200 nm of low absorption of biological systems, water soluble PbS nanocrystals have the potential to be used as biocompatible fluorescent labels to replace traditional organic fluorescent dyes in *in vivo* biological applications.

2.1.1 Previous syntheses

In the literature, the synthesis of lead-sulphide nanocrystals (IV-VI materials) in aqueous solution has been reported where PbS cores were coated by various organic molecules such as PVA (poly(vinyl-alcohol)), PVP (poly(vinyl-pyrrolidone)), DNA, etc.

PVA, PVP and DNA-coated PbS quantum dots were synthesized from an aqueous solution of $\text{Pb}(\text{NO}_3)_2$ stabilized by PVA, PVP, or DNA solution at 0 °C under argon. H_2S was added in excess to induce the formation of PbS dots.[289–291] The particle size was generally between 4 to 12 nm and showed different particles shapes: spherical for PVA capping, needle/cubic for PVP capping and cubic for DNA capping.

Using the same procedure of DNA coating, Levina *et al.* showed that PbS/DNA conjugates have a luminescence efficiency half-life of one week in blood plasma.[286]

Wu *et al.* established the synthesis of subnanometre-size PbS nanoparticles *via* the electroporation of vesicles.[292] Previously dried vesicles were hydrated with a $\text{Pb}(\text{NO}_3)_2$ aqueous solution. Na_2S was added to the vesicle suspension and the precipitates of PbS were removed by centrifugation. The supernatant containing less than 0.4 mg mL^{-1} of vesicles was subjected to electroporation to form PbS quantum dots in the bulk solution with 3-10 Å in diameter. Nevertheless, it was reported that PbS QDs have a tendency to adsorb at the surface of the vesicles.

Adenosine, uridine, cytidine, guanosine triphosphates (ATP, UTP, CTP and GTP respectively) (Figure 2.1) were also used to coat PbS QDs.[293]

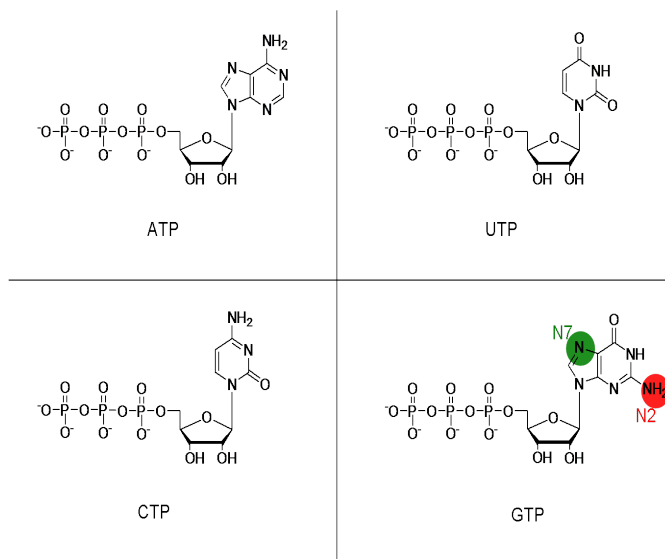


Figure 2.1: Representation of ATP, GTP, UTP and CTP nucleotides.

The geometries and structures of the nucleotide GTP have been shown to play an important role in the PbS synthesis. Only GTP was able to stabilize dots with luminescence at $\sim 1,300 \text{ nm}$, whereas ATP, UTP and CTP led to aggregation of particles. Positions N2 and N7 of G have been reported to act as binding sites for Pb^{2+} or PbS. Indeed, syntheses with inosine triphosphate (ITP) (G with N2 deleted) did not produce

any PbS QDs and syntheses using a derived-compound from G (CH₃ group at position N7) showed a blue-shifted luminescence of the PbS dots.

PbS have also been synthesised microbiologically where the yeast *Torulopsis* has been used as a sulphur source. Lead nitrate was added to a *Torulopsis* yeast culture. After cell breakage, PbS particles were characterized as 2-5 nm nanocrystallites exhibiting an absorption maximum at 330 nm. The emission maximum of the PbS dots was not recorded, the authors reported a broad-range luminescence (350-500 nm) which could be due to the presence of the aromatic amino acids of the microorganisms.[294]

Aptamer coated-PbS QDs were prepared by mixing thrombin-binding aptamer (TBA) and Pb(CH₃COO)₂·3H₂O in TAE (Tris-Acetate-EDTA) buffer at pH 8.0, followed by injection of Na₂S.[295] The resulting conjugates are 3 to 6 nm diameter. Choi *et al.* reported that the aptamer-functionalized QD binds specifically to its target, the blood-coating human α -thrombin inducing a decrease in the PL emission of PbS QDs due to a charge transfer where thrombin acted as a quencher.

Recently, PbS quantum dots were prepared in HEPES buffer by ligand exchange. PbS dots were first synthesised with oleic acids ligands at 130 °C and transferred in water by exchange of the organic ligands with ethylene glycol or thiol groups. These water-soluble PbS QDs were shown to emit in the NIR region and to have a quantum yield of 26%.[296, 297]

2.1.2 Synthesis of colloidal thiol-capped PbS quantum dots

Bakueva *et al.* prepared PbS quantum dots in aqueous solution using a mixture of thiols, thioglycerol (TGL) and dithioglycerol (DTG), as capping/stabilizing agents (Figure 2.2).[300] The ratios between Pb, TGL and DTG have been shown to influence the stability and the optical properties of the PbS dots. Indeed, PbS dots (Pb:TGL 6:1) with molar ratio DTG:Pb < 1:1 led to rapid growth of the dots with aggregation and low optical features; ratio DTG:Pb > 3.4:1 involved a slow formation of the dots (several hours); ratio DTG:Pb 1.28:1 to 3.4:1 produced stable dots with an increase in

the emission maximum as the size increases.[298, 299]

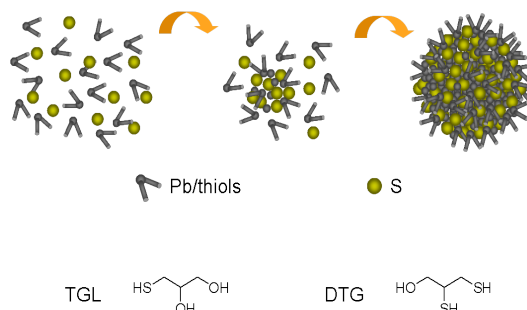


Figure 2.2: Schematic representation of PbS synthesis using thiols: thioglycerol (TGL) and dithioglycerol (DTG).

During the synthesis, the pH of the $\text{Pb}(\text{CH}_3\text{COO})_2 \cdot 3\text{H}_2\text{O}$ solution was adjusted to a value of 11.0 by adding triethylamine and the synthesis of the dots was completed by adding a 0.1 M solution of sodium sulfide Na_2S .

2.2 Objectives

To investigate the possibility of using near-infrared PbS QDs as biological labels, it was necessary to study their optical stability as a function of time and temperature (4 to 300 K). Therefore, we studied the morphology and photoluminescence of a series of thiol-capped PbS QDs in aqueous solution with Pb/S molar ratio varying from 1:0.2 to 1:0.7. This work was realised in collaboration with L. Turyanska from the Physics Department of Nottingham University.

2.3 Results & discussion

We synthesised PbS quantum dots in deionized water with a molar ratio Pb:TGL:DTG of 1:6:2 following the one-step method described by Bakueva *et al.*[301] By varying the Pb/S molar ratio (MR) from 1:0.2 to 1:0.7, we were able to obtain colloidal PbS dots with different sizes. The resulting colloidal solution was either kept

in the laboratory atmosphere or stored at a temperature of 5 °C under N₂ atmosphere. These were examined several times over a period of six months by photoluminescence (PL) spectroscopy at low (4 K) and room (300 K) temperature.[301, 302]

2.3.1 Morphological properties of PbS quantum dots

During the first three weeks after the synthesis, the photoluminescence maximum of a given MR of Pb/S solution was shifted to longer wavelengths (by up to 30 nm). This behaviour is likely to arise from Ostwald ripening effects that lead to formation of nanocrystals with larger size and hence longer wavelength emission. This process can be reduced by storing the solution at low temperature ($T < 280$ K).[302]

Figure 2.3 shows the typical RT photoluminescence spectra of the different Pb/S molar ratios investigated:

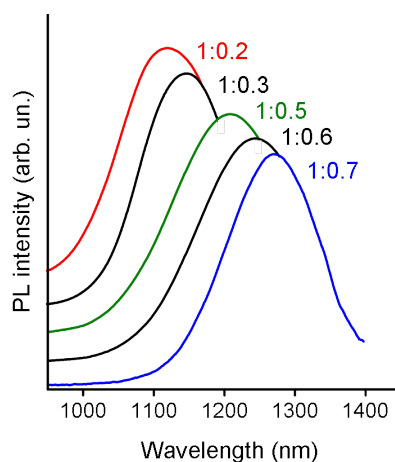


Figure 2.3: RT PL spectra of thiol-capped PbS dots with various Pb/S MR. The optical excitation was provided by the 514.5 nm line of an Ar⁺ laser.

PbS samples were analysed both as dried samples on a glass substrate and as liquid solution in a glass vial. Under both conditions, the emission wavelength/energy values are similar for a given molar ratio.

As expected for quantum dots, the increase in size and thus in PL emission is straight-

forward and has a tendency to stabilize over time (Figure 2.4):

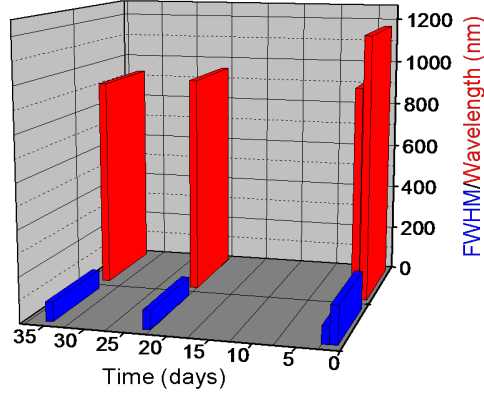


Figure 2.4: Variation of the full width at half maximum (blue) and emission wavelength (red) of PbS dots over the time (days).

By increasing the Pb/S MR from 1:0.2 to 1:0.7, the luminescence from the PbS dots can be tuned in the wavelength range 1,100 nm to 1,300 nm. The shift of the dot emission towards longer wavelengths with increasing MR is due to the increase of the QD size. Our atomic force microscopy (AFM) study, shown in Figure 2.5, indicates that the PbS quantum dots have an approximately spherical shape with a diameter d increasing from about 3 to 12 nm as determined from Z (heights) analysis of AFM images for Pb/S MR increasing from 1:0.2 to 1:0.7.[302]

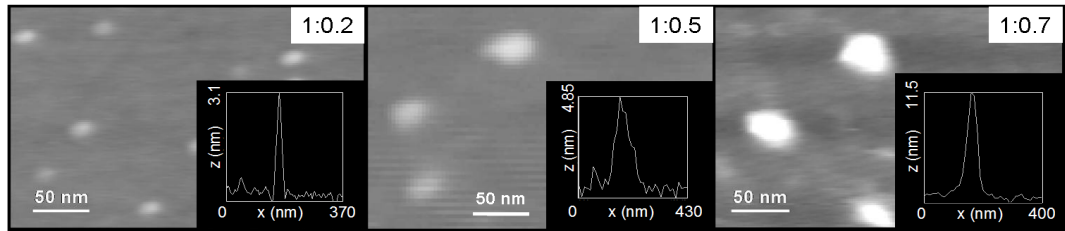


Figure 2.5: AFM images of PbS dots with Pb/S MR equal to 1:0.3, 1:0.5 and 1:0.7.

Figure 2.6 shows the energy of the PL peak as a function of the dot diameter:

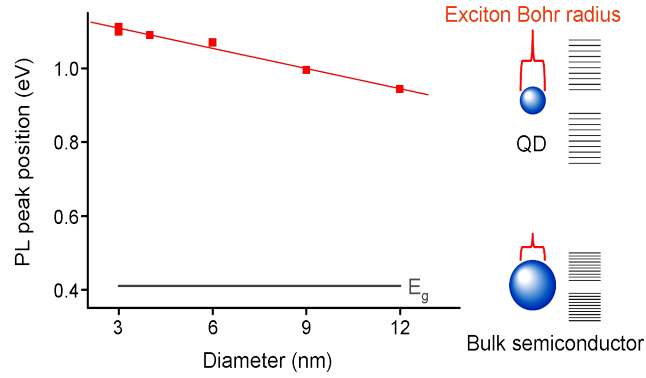


Figure 2.6: Strong confinement of the thiol-capped PbS QDs.

Due to the strong confinement of the exciton in the dot, the PL emission peaks at energies that are significantly larger than the band gap of bulk PbS (E_g). Also, the emission energy tends to shift to lower energies with increasing diameter d due to a decreasing quantum confinement potential of the exciton.

2.3.2 Optical properties of PbS quantum dots

The effect of temperature, T , on the optical properties of PbS quantum dots is of great importance for their use in room temperature (RT) applications. Recently, an unusually large linewidth (~ 100 meV) for the RT photoluminescence emission from an individual PbS QD was reported.[303] However, the effect of temperature on the spectral linewidth of the emission from either an individual or an ensemble of PbS dots is still largely unknown.

Figure 2.7 shows the PL spectra at various temperatures and excitation power $P = 100$ W cm $^{-2}$ for a representative QD sample with Pb/S MR equal to 1:0.5.[302]

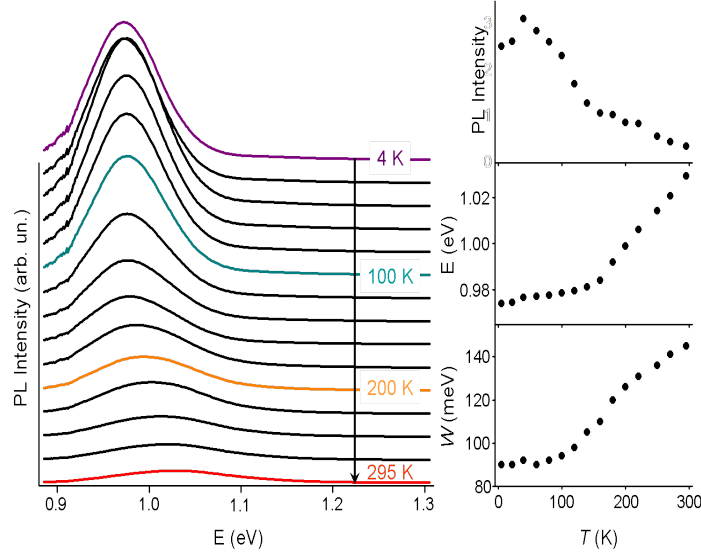


Figure 2.7: Temperature dependence of the PL spectra of thiol-capped PbS QDs with Pb/S MR equal to 1:0.5. The insets show the T -dependence of the peak intensity (top-inset), the energy peak, E (middle-inset), and the full-width at half-maximum, W (bottom-inset), of the QD PL emission.

Increasing the temperature has three main effects on the PL spectrum: 1) The peak intensity of the QD PL emission reveals a maximum at a temperature $T = 50$ K and thereafter it decreases monotonically (top-inset of Figure 2.7); 2) The peak energy, E , of the QD emission blue-shifts and its T dependence for $T > 150$ K can be described by the coefficient $\alpha = \partial E / \partial T = 0.3 \text{ meV K}^{-1}$ (middle-inset of Figure 2.7). The value of α is smaller than that of bulk PbS ($\alpha = 0.5 \text{ meV K}^{-1}$).^[304] This difference is attributed to the atomic-like character of the dot energy levels and the strong quantum confinement of the exciton, whose Bohr radius (20 nm)^[285, 289] is considerably larger than the dot diameter (< 10 nm).^[285] 3) The blue-shift and quenching of the dot emission are accompanied by a significant increase of the full width at half maximum, W , of the dot emission (bottom inset of Figure 2.7).

The enhancement of the QD PL intensity observed for increasing T below 50 K indicates a thermally activated redistribution of carriers in the dot in the presence of defects: with increasing T , carriers (electrons or holes) trapped in a defect in or around the

dot overcome shallow energy barriers and fall down into the ground state of the dot, thus increasing the PL intensity. A further increase of T from 50 to 295 K decreases the PL intensity by only a factor of 10; this T -dependence and high thermal stability of the PL emission were observed for all our samples. These are important features for applications and indicate a low level of thermal escape of carriers from the ground state of the dot towards the excited states and a relatively low density of non-radiative recombination centres.

The T -dependence of W for Pb/S solutions with different MRs is shown in Figure 2.8.[302] For $T < 150$ K, different T dependencies and/or values of W are observed ($W = 80$ -100 meV). In particular, for some structures, W exhibits a small decrease with increasing T (see circles in Figure 2.8(a)). In contrast, for $T > 150$ K, all samples show a characteristic thermally activated increase of W . This behaviour is revealed more clearly in Figure 2.8(b) which plots W versus $1/T$. It can be seen that at high T , the T -dependence of W is well described by an exponential dependence.

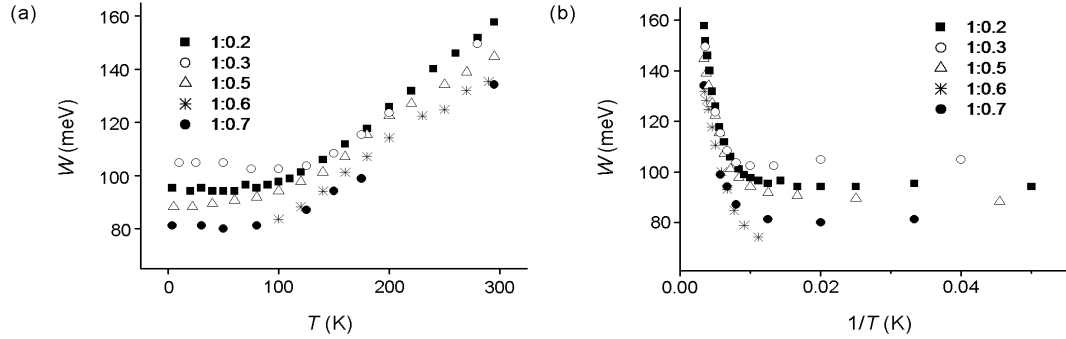


Figure 2.8: (a) T -dependence of W for all samples. (b) Plot of W vs. $1/T$. [302]

In order to understand the effect of the temperature on W , the mechanisms that can give rise to the broadening of the emission from an ensemble of dots have to be considered quantitatively.

When an atom in the crystal is submitted to excitation by photons, electrons absorb energy and reach an excited energy level. Then, the energy is released by the electrons, the latter either go back to the ground state or to a lower excited state and here the

remaining energy is transmitted to the crystal lattice. In turn, the lattice reaches an excited quantized energy level depending on the amount of energy absorbed inducing lattice/atom vibration (Figure 2.9). In a crystal, these lattice vibrations are called phonons.

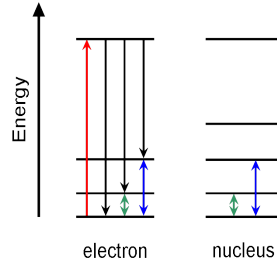


Figure 2.9: Representation of the energy levels of the electron and the nucleus. The red arrow corresponds to the absorption of the electron, the black arrows show the emission and the blue and green arrows are the lost energy transferred to the nucleus that in turn reaches an excited state.

A zero phonon line (ZPL) in a PL spectrum corresponds to an electron-hole recombining without any loss of energy. A phonon sideband corresponds to an emission side peak that appears next to the ZPL in response to the energy transferred to the crystal lattice (Figure 2.10).

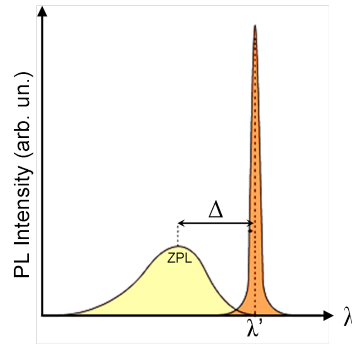


Figure 2.10: Representation of a zero-phonon line and a phonon sideband in a PL spectrum.

The gap Δ between the ZPL and a phonon sideband is proportional to the amount of energy transferred from the electron to the atoms in the crystal. We also note that the

interaction of electrons with the crystal can lead to an homogeneous broadening of the PL spectrum due to the dephasing of the electronic states. In the light of these general consideration, we now consider our measured PL spectra.

At low T , carriers are frozen randomly into the dot states and the PL spectrum simply reflects the distribution of the dot energies. Although the optical linewidth depends largely on the variation of the dot size and spectral diffusion due to charge trapping on dot defects, the thermally activated increase of W indicates that at high T the optical linewidth is also controlled by an intrinsic scattering process due to carrier interactions with phonons. The coupling of carriers to phonons in a QD leads to PL emission, which consists of a ZPL and a broad band with (longitudinal optical) LO phonon sidebands and a continuum of acoustic-phonon assisted transitions.[305–308] The contribution of phonon sidebands to the QD PL spectrum was found to be important for CdSe QDs[305], and much weaker for nanocrystals based on (InGa)As[306] and GaAs QDs[308]. Previous PL studies have also shown single broad PL emissions for both individual PbS and ensembles of dots[303] with PL line shapes typically reproduced by a single Gaussian function. Therefore, the measured thermally activated broadening of the dot emission observed in all the PbS QDs does not arise from the contribution of phonon sidebands, but instead from homogenous broadening of the ZPL for each dot in the ensemble caused by interaction with the increasing thermal population of optical phonons.[302]

The T -dependence of W can be described by the relation $W = \gamma n + W_0$, where $n = 1/[\exp(\hbar w_{\text{LO}}/k_{\text{B}} T) - 1]$ is the Bose distribution function for LO phonons of energy $\hbar w_{\text{LO}}$, γ is a constant and W_0 represents the inhomogeneous contribution to W . As shown in Figure 2.8(b), at high T (> 150 K) all data are well described by this expression by setting $\hbar w_{\text{LO}}$ equal to the energy of LO phonons in PbS ($\hbar w_{\text{LO}} = 26$ meV), $\gamma = 110 \pm 20$ meV and $W_0 = 90 \pm 10$ meV.[304] The strength of carrier-phonon coupling, as measured empirically by the parameter γ , tends to be larger for the dots with the higher PL emission energies, see inset of Figure 2.11.

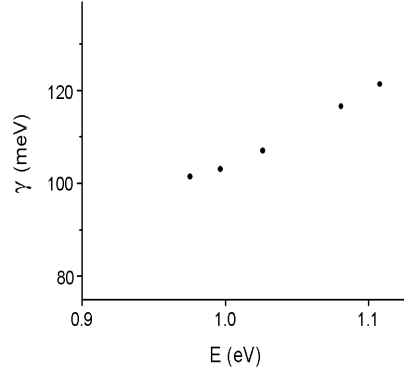


Figure 2.11: Representation of a zero-phonon line and a phonon sideband in a PL spectrum.

In a QD, the interaction of electrons with phonons is expected to be qualitatively different from that occurring in bulk systems. Inelastic interactions such as phonon-assisted excitation of carriers to excited states or energy relaxation processes are unlikely to occur in PbS dots as it is estimated that the confinement energy for electrons and holes is much larger than $\hbar w_{\text{LO}}$.¹ In contrast, elastic collisions involving the virtual absorption and emission of a LO phonon by carriers do not require a specific energy separation between the discrete levels of the dot. Elastic collisions by phonons do not change the energy of the carrier, but they do change the phase of the carrier wavefunction, thus causing a broadening of the spectral lines.[309–311] For a spherical PbS QD, the exciton-phonon coupling strength is expected to be small due to the almost identical form and size of the electron and hole wavefunctions.[312] The calculated exciton wavefunction and its coupling to lattice vibrations depend on the strength of carrier confinement[313, 314] and can be influenced by local electric fields arising from trapping of charges in QD defects[313]. An increase of the strength of carrier-phonon coupling with increasing carrier confinement was observed in Cd(S)Se nanocrystals[315], while an opposite trend was shown for CdTe-based quantum wells[316] and CdS QDs[317].

Our data indicate that the strength of carrier-phonon coupling, γ , is larger for dots with the higher emission energies (> 1 eV at RT) and smaller size ($d < 7$ nm)

¹the estimation of the ground and excitonic transitions is based on the effective mass approximation and a PbS nanocrystal with spherical shape of diameter $d = 10$ nm and infinite potential barriers.

(see Figure 2.8(b)) in qualitative agreement with theory[314]. These dots exhibit the largest values of W . Therefore, the local environment of the dot (*i.e.*, trapped charges on defects) seems to act not only to broaden the optical linewidth at low T but also to enhance the interaction of carriers with the lattice, thus leading to an additional broadening of the dot PL emission.

2.4 Conclusion

We have synthesised PbS quantum dots in aqueous solution emitting in the range 1,100 to 1,300 nm. It was found that by increasing the Pb/S molar ratio from 1:0.2 to 1:0.7, the size of the dot increased from 3 to 12 nm in diameter and the emission maximum shifted to longer wavelengths. Also, we have reported that their photoluminescence intensity and PL peak emission were only weakly affected by temperature. This PL stability allowed us to study the thermal broadening of the QD emission over an extended temperature range (4-300 K). We have showed that the broadening of the emission spectra occurring when T increased was due to phonon interaction. We also reported that for high temperatures, the strength of the carrier-phonon coupling was higher for smaller dots thus leading to the conclusion that at low T ($T < 50$ K), the broadening of PL emission is due to the presence of defects on the surface of the dot, while at high T , the broadening is due to trapped charges on defects as well as phonon interactions.

Chapter 3

Preparation and characterization of the protein cage, apoferritin

3.1 Introduction

Before exploiting the bioconjugation of ferritin with quantum dots, it was necessary to determine the purity of the protein used through all the experiments. To this purpose, ferritin, the cationized ferritin (surface-modified ferritin bearing additional positive groups) and apoferritin were analysed using different techniques.

In the following paragraphs, different types of experiments (size exclusion chromatography, SDS-PAGE, BCA, ICP-MS) have been realised in order to determine the stability of the apoferritin during its preparation as well as the amount of residual iron in the protein after dissolution of the mineral core.

Ferritin, a brown coloured protein, containing over 23% of ferric iron Fe^{III} , can be freed from its core by reductive dissolution to the ferrous state and removal of the Fe^{2+} by dialysis.[193] The colourless protein thus obtained is designated as apoferritin.

Two mechanisms are chemically feasible for the removal of iron from ferritin: reduction followed by chelation of $\text{Fe}(\text{II})$ or direct chelation of $\text{Fe}(\text{III})$. Furthermore, both of these mobilisation pathways involve the penetration of the reducing agent/chelating agent

within the cavity of ferritin to react with the iron core.

The first attempt to remove the iron core of ferritin was reported by Crichton and Michaelis in 1943. In their experiment, they added sodium dithionite as a reducing agent to a ferritin solution at pH 4.6 combined with *o*-phenanthroline or α,α' -bipyridine to form water soluble ferrous complexes.[193]

Chelation of ferric iron is slow when biological[318–320] or synthetic[319, 321, 329, 330] chelators as well as microbial siderophores[322–324] are used, but much more rapid when realised with dithionite and dihydroflavins.[325–328]

Hoy *et al.* have studied the reductive mobilisation of ferritin iron by 1,10-phenanthroline and provided the evidence for the penetration of the reductant within the protein cavity and its interaction with the iron core.[331]

In 1999, Mann *et al.* also reported the reductive mobilisation of the ferrihydrite iron core of ferritin by mercaptoacetic acid in NaOAc buffer at pH 5.5. They synthesised derivatized ferritin/apoferritin proteins in organic solvents by coupling nonylamine molecules to the carboxyl groups present on the external surface of the protein cage.[334, 335]

More recently, aceto-, benzohydroxamic acids and catechol have been used as iron(III)-chelating molecules to free the ferritin from its oxyhydroxide core. Domínguez-Vera and co-workers showed that 60% and 18.35% of the ferric iron was removed using the acids and catechol respectively.[332, 333]

3.2 Objectives

Our strategy to improve the stability and bioconjugation of PbS quantum dots to other biomolecules was to incorporate them into the cavity of apoferritin. To optimise the entrapment of QDs, we studied the efficiency of the iron removal from ferritin. Thus, we prepared the protein cage apoferritin using the reductive mobilisation of Fe(III). The apoferritin cage was then studied using diverse techniques such as column chromatography, gel electrophoresis, and mass spectrometry in order to determine the structure of apoferritin after removal of its iron core. Also, we studied the solubilisation

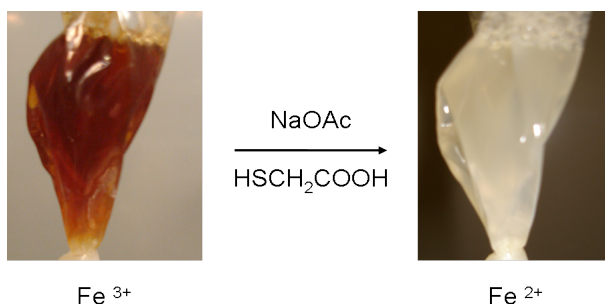
of ferritin and one of its derivatives (cationized ferritin) in organic solvents which could potentially lead to the synthesis of quantum dots in non-aqueous media in a controlled manner.

3.3 Results & discussion

3.3.1 Preparation of the protein cage apoferritin from horse spleen ferritin

In our synthesis of apoferritin, we used a reductive dissolution process established by Mann and co-workers.[334, 335] This preparation consists of 5 repetitions of a demineralization procedure: 1) ferritin protein was dialysed against NaOAc buffer at pH 5.5 for 20 min, 2) mercaptoacetic acid was added to the buffer and dialysed for 3 h, 3) buffer was removed and ferritin was dialysed against fresh NaOAc buffer at pH 5.5 for 20 min.

The progressive release of iron was clearly seen by a decolouration of the protein solution from red-brown solution for ferritin to pale yellow solution for apoferritin to give the demetallated protein consisting of the intact polypeptide shell surrounding a water-filled nanodimensional cage (Scheme 3.1).



Scheme 3.1: Change of colour of the protein during apoferritin synthesis.

The yellow colour of apoferritin is reported as an inherent property of the protein associated with the aromatic amino acids.[336, 337]

Figure 3.1 shows the UV-visible absorption of ferritin and apoferritin samples confirm-

ing the release of iron:

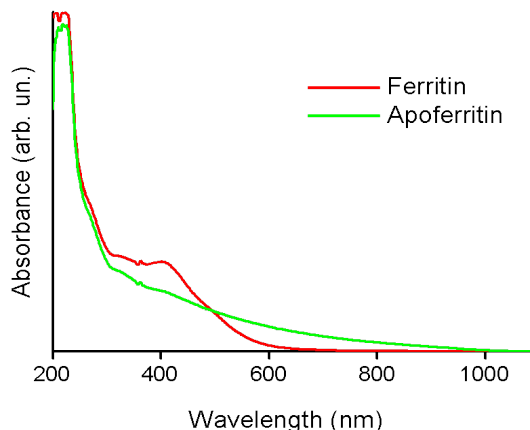


Figure 3.1: UV-visible spectra of ferritin and apoferritin.

The absorbance spectra of ferritin and cationized ferritin shows two peaks around 280 nm and 400 nm. The first peak previously discussed corresponds to the protein moiety (aromatic side chains and peptide bonds) and the second peak is due to the presence of iron within the protein. As expected, the curve of the apoferritin - protein without iron - does not show any peak around 400 nm thus confirming the release of the hydrated iron(III) oxide core.

Sometimes, the apoferritin solution was obtained as a cloudy solution suggesting the formation of aggregates of protein during the procedure. This could be avoided by refreshing the dialysis buffer frequently.

3.3.2 Purification of apoferritin by gel filtration

3.3.2.1 Size exclusion chromatography (SEC) principle

SEC is a chromatographic method in which particles are separated depending on their size or hydrodynamic volume. Particles with different sizes elute through a stationary phase (superdex = dextran over reticulated agarose) at different rates.

The apparatus or column consists of a hollow tube packed with small polymer beads defined to have pores of various sizes (Figure 3.2). Small particles can enter pores or

channels present in the matrix, whereas larger ones cannot. Larger particles can not enter the pores, and thus the larger the particles, the less overall volume to traverse through the column, and the faster the elution.

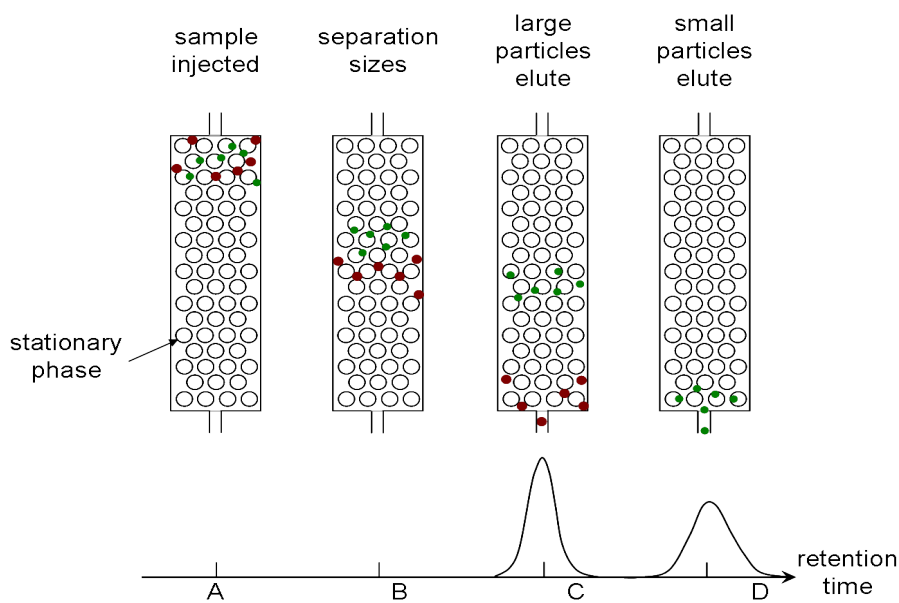


Figure 3.2: SEC principle.

3.3.2.2 Elution profiles of ferritin and apoferritin

After filtration through a $0.20\ \mu\text{m}$ filter, ferritin sample remained a red-brown solution and apoferritin sample became a clear pale yellow solution allowing removal of large aggregates of protein formed during iron reduction (data not shown).

Ferritin and apoferritin samples ($0.25\ \text{mL}$ of each) were loaded onto a column Superdex 75 ($< 100\ \text{kDa}$) and the elution flow was fixed at $0.5\ \text{mL min}^{-1}$. The size exclusion of the column is such that molecules smaller than $100\ \text{kDa}$ were retained on the matrix and eluted last. In order to detect the protein, the absorption of the samples was measured at $280\ \text{nm}$.

Figure 3.3 shows the elution profiles of ferritin and apoferritin:

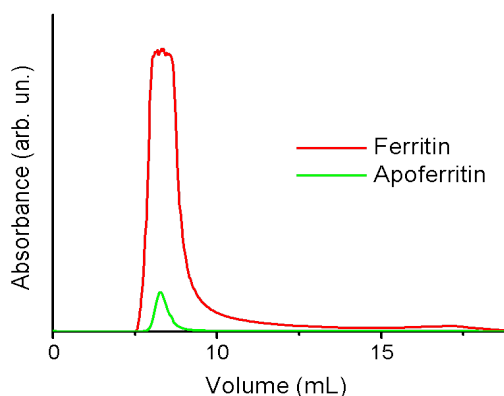


Figure 3.3: Size exclusion chromatography of ferritin and apoferritin.

The peak at $V = 7$ mL represents the biggest component of the two solutions which is the 24 polypeptides structure of ferritin and apoferritin. This results suggests that ferritin and apoferritin have a similar diameter size of 12 nm and is evidence that apoferritin shell is not decomposed/disassembled during the removal of iron. No peak corresponding to subunits or other proteins was found suggesting a good purity of our samples.

For more accuracy, the residues obtained after filtration were analysed by denaturing gel electrophoresis.

3.3.3 Assessment of apoferritin purity by denaturing gel electrophoresis

3.3.3.1 SDS-PAGE principle

SDS-PAGE (sodium dodecyl sulphate polyacrylamide gel electrophoresis) is a technique used to separate proteins according to their electrophoretic mobility and their relative molecular mass (Figure 3.4).

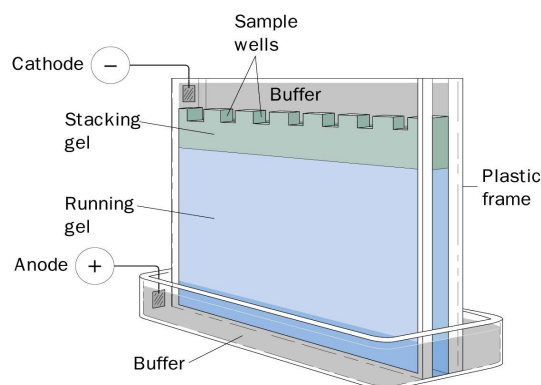


Figure 3.4: SDS principle.

The matrix is made by polymerisation of a mixture of acrylamide and polyacrylamide where the size of the pores are generated by the amount of acrylamide. The proteins are first concentrated on the stacking gel and then separated on the resolving gel. Separated proteins are finally visualized by staining with Coomassie followed by destaining with methanol/acetic acid/water.

3.3.3.2 Ferritin and apoferritin under denaturing conditions

Four samples (F1 ferritin 8.5 mg mL^{-1} , F2 ferritin 4.25 mg mL^{-1} , A1 apoferritin 8.5 mg mL^{-1} , A2 apoferritin 4.25 mg mL^{-1}) were first mixed with SDS, an anionic detergent that denatures secondary and non-sulphide-linked tertiary structures. The SDS binds to the protein and applies a negative charge to the protein in an uniform proportion, so that the distance of migration through the gel is directly related to the size of the protein. Boiling all samples at 95°C for 1 minute further denatured the proteins.

Protein samples were then deposited and submitted to an electric current causing the negatively charged proteins to migrate from the negatively charged stacking gel to the positively charged resolving gel. Contrary to the previous experiment of size exclusion column, larger molecules encounter more resistance and do not migrate easily in the gel while smaller molecules fit through the pores and travel farther down the gel.

Below is the SDS-PAGE obtained for our four samples (Figure 3.5).

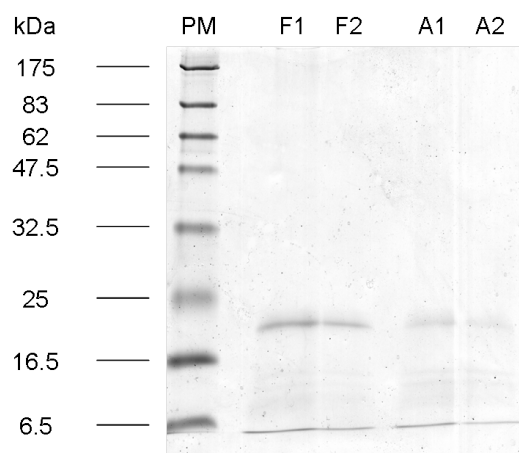


Figure 3.5: SDS-PAGE of ferritin (F1 and F2) and apoferritin (A1 and A2). The protein marker (PM) is on the left lane.

The SDS anionic detergent causes the apoferritin to disassemble into its subunits. The subunits could thus move through the gel matrix depending on their global charges and respective molecular masses. As can be seen, only one band is visible for ferritin and apoferritin in different concentrations corresponding to approximately 20,000 Da, which is in agreement with the subunits molecular weight of ferritin (21,000 for H- and 19,000 for L-subunit).[335, 338]

This observation underlines the result of the size exclusion experiment i.e. our protein is pure and does not contain significant amounts of any other protein.

Now that the purity of both the commercial protein ferritin and the protein apoferritin have been studied, it is useful to know the actual amount of protein present in solution as well as the amount of iron before and after reductive dissolution of the iron core. This is described in the following paragraphs by conducting a bicinchoninic assay (BCA) to detect the protein content and by mass spectrometry for the amount of iron.

3.3.4 Determination of apoferritin purity by BCA assay

The BCA assay is a colorimetric biochemical assay for detecting the concentration of proteins in a solution; it is based on the Biuret reaction where the peptide bonds of proteins/polypeptides react with copper(II) under alkaline conditions producing Cu^+ that complexes with bicinchoninic acid forming a purple product. The amount of protein present in a solution can be quantified by measuring the absorption spectra at 562 nm and comparing it with protein solutions of known concentrations (bovin serum albumin (BSA) in our case).

It is important to note that the commercial proteins that we use (ferritin and cationized ferritin) are dissolved in 0.15 M NaCl solutions. BCA assays were undertaken by testing the samples without and with NaCl salt.

Table 3.1 shows the results of the BCA assay realised in water:

	Concentration expected (mg mL^{-1})	Concentration given by BCA assay (mg mL^{-1})	%
Ferritin	0.5	0.25	50
	0.25	0.12	48
Cationized ferritin	0.5	0.043	8.6
	0.25	0.015	6

Table 3.1: Results of the BCA assay for ferritin and cationized ferritin prepared in water solutions only.

These results show that 49% of protein is present in the ferritin commercial solution and only 7.3% in the commercial solution of cationized ferritin.

Table 3.2 allows the comparison of proteins in water only to proteins prepared in 0.15 M NaCl solutions in order to produce the same environment for the proteins than the commercial solutions:

	Concentration expected (mg mL ⁻¹)	Concentration given by BCA assay (mg mL ⁻¹)	%
Ferritin	0.11	0.08	73
	0.21	0.12	57
	0.43	0.21	49
	0.64	0.30	47
	0.85	0.39	45
Cationized ferritin	0.07	0.035	50
	0.14	0.072	51
	0.28	0.133	48
	0.55	0.257	47

Table 3.2: Results of the BCA assay for ferritin and cationized ferritin in NaCl solutions.

When the samples are prepared in 0.15 M NaCl solutions, a clear increase in the protein content present in the commercial solutions is observed for both of the ferritins. Nevertheless, there is a clear diminution of the protein fraction when the concentration of the protein is increased, this can be explained by the presence of detergents in the samples or by a variation in the pH during the solution preparation.

Making an average of the results, we can assume that 49% of protein is present in the commercial solution of cationized ferritin and approximately 54% in the ferritin solution. These observations are of importance in order to compare the amount of protein to the amount of dots used during our experiments on the formation of biocompatible composites based on QDs and apoferritin.

3.3.5 Determination of iron content by ICP-MS analysis

Inductively Coupled Plasma-Mass Spectrometer (ICP-MS) is a highly sensitive instrument capable of the determination of a range of both metals and non-metals between nanograms per litre to 100 milligrams per litre. This is based on the coupling of a

plasma torch producing ions and a mass spectrometer for separating and detecting ions. The sample is injected by an auto sampler, nebulized and then converted to a plasma under high temperature (6,000 °C to 8,000 °C). The ions pass through different cones and are separated depending on their atomic mass and charge.

Ferritin (85 mg mL⁻¹) and apoferritin (8.5 mg mL⁻¹) samples were analysed and the presence of iron was determined (Table 3.3):

Metals ($\mu\text{g L}^{-1}$)	Mn	Fe	Cu	Zn	Se	Mo	Cd	Pb
Diluent blank	0.00	0.00	0.00	0.00	0.00	0.00	0.00	0.00
Control \times 20,000	0.06	491.07	0.73	5.37	0.00	0.00	0.02	0.04
Test \times 20,000	0.00	0.39	-0.03	-0.48	-0.02	0.01	0.00	0.00
Test \times 5,000	0.00	0.33	0.03	-0.43	-0.01	-0.01	0.00	0.00
2 nd Test \times 5,000	0.01	0.15	0.09	-0.05	-0.02	-0.01	0.00	0.00

Table 3.3: Metals analysis present in ferritin (control sample) and apoferritin (test sample) by ICP-MS.

In the 20,000 times diluted ferritin sample, 491.07 $\mu\text{g L}^{-1}$ of iron were detected, which means that $9821.4 \times 10^3 \mu\text{g L}^{-1}$ were present before dilution in the original sample of 85 mg mL⁻¹. Thus, in 1 mL of the commercial solution of ferritin, there is 9.82 mg of iron that represents 11.5% of the sample. However, as shown previously, this sample only contains 50% of ferritin, so in 1 mL of sample, there is 42.5 mg of ferritin, which means that 23% of iron is present in the protein itself which is in agreement with the literature.[195, 338] Following this, the calculations made for apoferritin gave 0.18% of iron remaining after reductive dissolution of the iron core. This is lower than the residual iron percentage (2%) previously reported by Price and Joshi as determined using thioglycolate.[339]

3.3.6 Solubility studies of ferritin in organic solvents

As the syntheses of quantum dots in aqueous solution are more complex and less developed than in organic media, the solubilisation of horse spleen ferritin in organic

solvents was studied by hydrophobic ion pairing (HIP) methodology and UV-visible absorption.[340–342] The solubilisation of a commercially available solution of cationized ferritin was additionally studied.

The cationization of ferritin is based on the covalent blocking of the free carboxyl groups on the protein shell by small molecules containing a positive charge at the unattached end (*N, N*-dimethyl-1, 3-propanediamine (DMPA), hexamethyldiamine (HMD)).

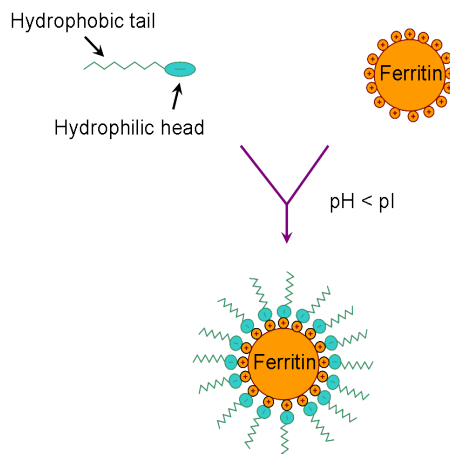
In Table 3.4, the distribution of the charged amino acids inside the cavity (internal phase) and outside (external phase) of ferritin and cationized ferritin are reported:

Protein	Subunit	Amino acid				
		K	R	H	D	E
Ferritin	H	13	8	11	14	18
	interior	1	0	5	2	5
	exterior	6	4	0	8	4
Cationized ferritin	H	13	8	11	6	14
	interior	1	0	5	2	5
	exterior	6	4	0	modified	modified
Ferritin	L	9	11	6	12	15
	interior	5	4	4	4	7
	exterior	3	5	0	6	3
Cationized ferritin	L	9	11	6	6	12
	interior	5	4	4	4	7
	exterior	3	5	0	modified	modified

Table 3.4: Distribution of the amino acids lysine (K), arginine (R), histidine (H), aspartic acid (D), glutamic acid (E) in ferritin and cationized ferritin. Values were estimated using pdb files 2fha and 2fga for H and L ferritin subunits respectively from protein data bank.

Solubilisation of ferritin and cationized ferritin were realised by complexation of the proteins to the surfactant AOT (bis(2-ethylhexyl) sulfosuccinate sodium salt) with and without considering the purity of the proteins. Studies were made in dichloromethane,

hexane and toluene at different concentrations of protein and at different pHs (Scheme 3.2).



Scheme 3.2: Schematic illustration of complexation process between ferritin and AOT surfactant.

No transfer was observed when considering the purity calculated previously in the commercial solutions. Results of complexation considering completely pure samples (100% protein content) are reported in Table 3.5.

	Hexane	DCM
Ferritin (ratio 1:1 to 1:5)	×	×
Cationized ferritin (ratio 1:1)	✓	✓

Table 3.5: Transfer of ferritin and cationized ferritin from aqueous solution to organic solution through complexation with the surfactant AOT.

Ferritin/AOT complexation was exploited over a range of ferritin/AOT ratios from 1:1 to 1:5 in NaOAc 1 mM buffer pH 3.8 and in NaOAc 100 mM buffer pH 4.4, unfortunately the increased amount of AOT surfactant did not induce any solubilization of ferritin in organic solvents. Interestingly, different results were obtained for the cationized ferritin with transfer in the organic phase for a protein concentration of 10 mg mL⁻¹ in 100 mM NaOAc buffer (no transfer was observed in the case of a concentra-

tion protein of 2 mg mL^{-1}). This phase transfer was indicated by the colour of the sample (Table 3.6):

	Hexane	DCM
<u>Before mixing</u>		
lower phase	orange	colourless
upper phase	colourless	orange
<u>After mixing</u>		
lower phase	colourless	orange
upper phase	orange	colourless

Table 3.6: Changes of colour observed during the transfer of cationized ferritin from aqueous solution to organic media.

The transfer of cationized ferritin could be easily seen with the naked eye as shown in Figure 3.6:

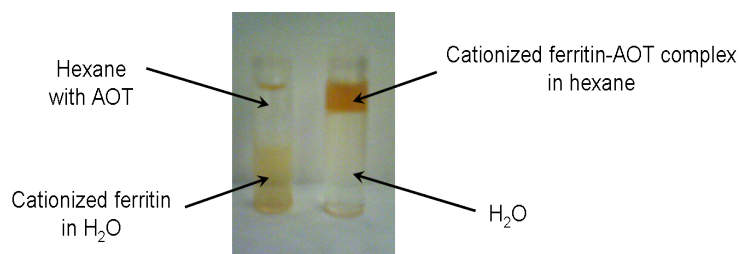


Figure 3.6: Transfer of the cationized ferritin from the aqueous media to the organic solvent, hexane.

Figure 3.7 shows the UV-visible absorption spectra of cationized ferritin in hexane and DCM.

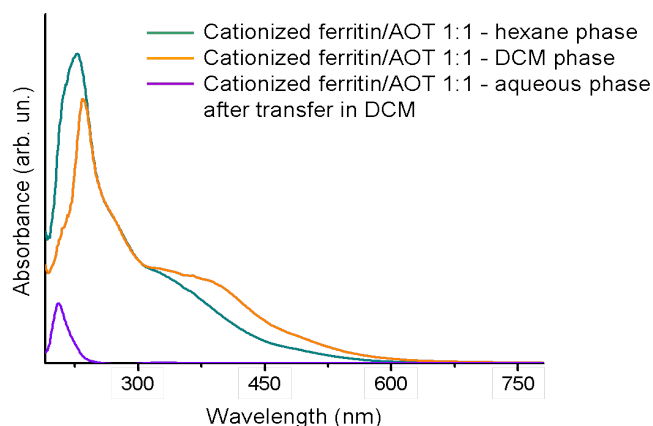


Figure 3.7: UV-visible spectra of cationized ferritin in different organic solvents.

Because of its iron core, ferritin has a broad absorption band in the ultraviolet region that tails into the visible region of the spectrum. The UV-visible spectra of cationized ferritin/AOT in hexane and DCM phases show the shoulder around 280 nm of the protein moiety[260] and clearly demonstrates the successful transfer of the cationized ferritin protein from the aqueous phase to the DCM phase. In the case of the DCM experiment, the UV-visible absorption spectra of the aqueous phase showed no absorption peak around 280 nm as expected, thus confirming the solubilization of cationized ferritin in organic media.

At this stage, it is important to point out that:

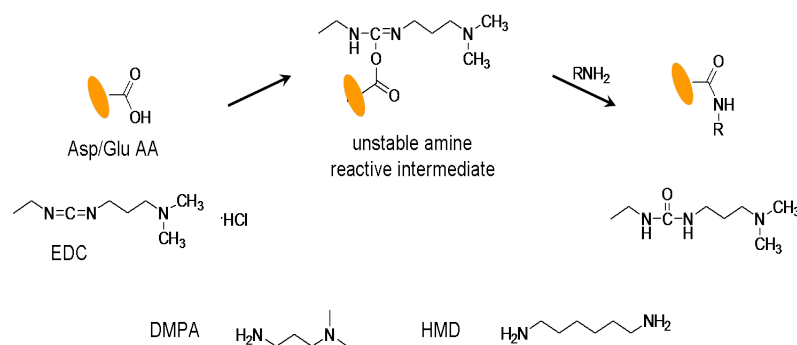
- The cationized ferritin is soluble in different organic solvents, but not the ferritin.
- The commercially available cationized ferritin is relatively expensive.

For these reasons, we then undertook the synthesis of the cationized ferritin.

3.3.7 Preparation of the cationized ferritin

Cationized ferritin was obtained by the activation of carboxyl groups of ferritin with a water-soluble carbodiimide, 1-ethyl-3(3-dimethylaminopropyl)carbodiimide hydrochloride (EDC) followed by the subsequent reaction of the activated carboxyls with an

amine of the general type RNH_2 such as *N,N*-dimethyl-1, 3-propanediamine (DMPA) giving tertiary amine derivatives or, hexamethyldiamine (HMD) giving primary amine derivatives (Scheme 3.3).[343]

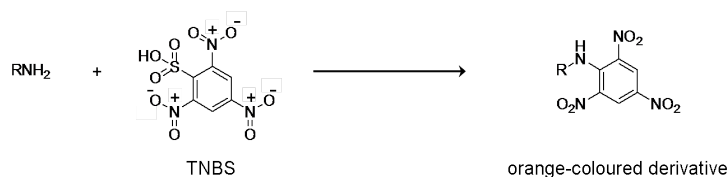


Scheme 3.3: Mechanism of activation of carboxyl groups by EDC and further reaction with amines resulting in the amide bond formation.

Both of these amines were used in the reaction at pH 6.5 (*i. e.* with apoferritin assembled) giving cationization of the external Asp and Glu amino acid only as transparent orange solutions.

The modification of protein carboxyls by such a procedure causes a change in charge of two units per modified carboxyl group from -1 to +1: the overall pI of the molecule changes from 4.5 for the ferritin[344] to higher values depending on the degree of cationization of the carboxyl groups.

The degree of cationization can then be resolved by determining the number of -NH_2 amine groups formed. There are several methods for the measurement of amine groups in proteins and other molecules using commercially available reagents such as TNBS (trinitrobenzene sulfonic acid) or OPA (*o*-phthaldialdehyde).[345, 347] In our case, we detected amine groups with TNBS reagent that is simpler to use. Ferritin containing primary amines can react with the TNBS (extinction coefficient $14,400 \text{ cm}^{-1}$) to form a highly chromogenic derivative (Scheme 3.4).



Scheme 3.4: Mechanism of the free NH_2 of the cationized ferritin with an amine detection reagent.

The amine content of the compound was then determined by measuring the absorbance of the orange-coloured product at 335 nm by comparison to a standard curve generated by use of an amine-containing compound, the alanine (Figure 3.8).

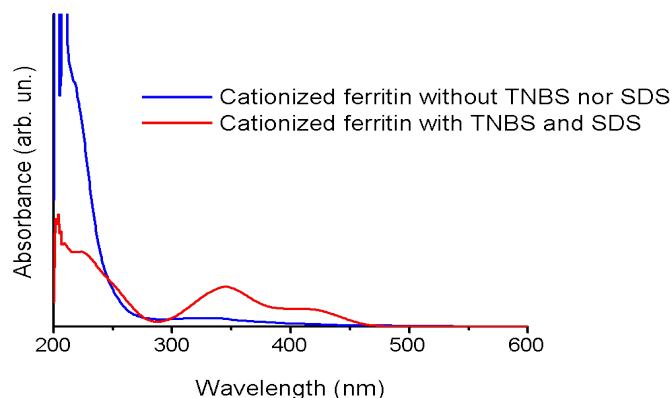


Figure 3.8: UV-visible of the cationized ferritin before and after blocking of the $-\text{NH}_2$ groups by TNBS.

After calculations, we found that 25% of the amino groups remain free and this result is in good agreement with the data reported in the literature.[209]

It is interesting to note that the successful cationization of the commercially available ferritin could be applied to the apoferritin as the structure of the protein shell is conserved during the preparation of the protein cage as described in section 3.3.1.

3.4 Conclusion

The protein cage apoferritin has been prepared from ferritin by reductive mobilisation of its iron(III) core. We have showed that apoferritin has been efficiently freed from its ferrihydrite core with only 0.18% of iron remaining. Furthermore, apoferritin and ferritin showed the same elution profile by size exclusion chromatography and the same characteristic bands of the subunits around 20 kDa after denaturation with SDS, leading to the conclusion that the structure of the apoferritin has been conserved along the removal of the iron core. The transfer of cationized ferritin in organic solvents leads to the potential of cationizing ferritin and apoferritin in order to synthesize quantum dots in a controlled manner in non-aqueous media.

Chapter 4

PbS-apoferritin composites

4.1 Introduction

This chapter describes the synthesis of a biocompatible aqueous NIR fluorescent label based on a PbS QD entrapped in the hollow core of a horse spleen apoferritin (AFt) protein cage.[346] As mentioned in the chapter 1, section 1.3.1, only CdSe, ZnSe and CdS nanoparticles have been entrapped within the apoferritin cavity by the entrance of Cd, Zn, Se and S precursors through the protein channels, but no luminescence studies have been reported on the composites formed.

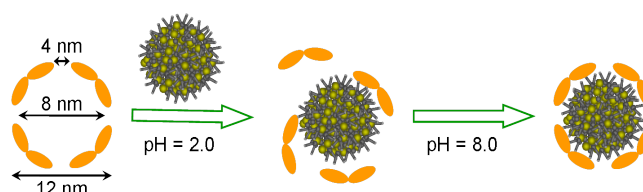
4.2 Objectives

The hollow core of the apoferritin protein limits the size of the encapsulated QD to ~ 8 nm and provides an exterior protein coat to the QD that allows covalent attachment of other biomolecules, such as oligosaccharides, peptides and fatty acids, using well established chemical techniques.[347]. In addition, this composite provides an efficient fluorescent label in the NIR. Therefore, it could provide an attractive system for biological and medical studies.

In this chapter we investigated two routes of synthesising the AFt-PbS composite:

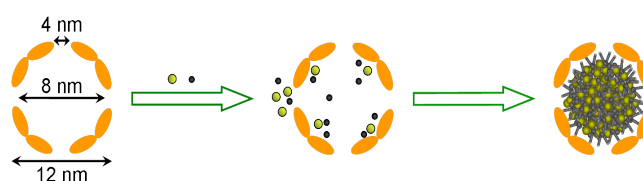
- The first route involves disassembly of the apoferritin shell into its component

protein subunits, and then reassembly of the protein shell in the presence of pre-formed PbS QDs, see Scheme 4.1. As mentioned previously, to our knowledge, this method has never been used to ‘trap’ quantum dots.



Scheme 4.1: Encapsulation of PbS QDs within the cavity of apoferritin by the disassembly/reassembly process.

- In the second route the apoferritin is used as a ‘nanoreactor’ to promote the formation of the dots from their precursors, see Scheme 4.2.



Scheme 4.2: Encapsulation of PbS QDs within the cavity of apoferritin either by entrance of ions through the channels.

4.3 Results & discussion

For the reassembly route, disassembled apoferritin in 0.1 M NaCl adjusted to $\text{pH} = 2.0$ with 2 M $\text{HCl}_{(aq.)}$ was added slowly to the preformed PbS quantum dots in deionized water. PbS dots were synthesized as described in chapter 2 and were used as a solution of $\text{pH} 9.0$. The pH of the PbS solution was high enough (~ 9.0) to induce the reassembly of the apoferritin subunits around the dots without further addition of base.

For the nanoreactor route, $\text{Pb}(\text{CH}_3\text{COO})_2$ and Na_2S were injected in deionized water to apoferritin in 0.1 M NaOAc buffer at $\text{pH} = 5.5$.

In both routes, the colour of the Aft-PbS composites solutions varied from pale brown for the lowest Pb/S molar ratio 1:0.3 to black solutions for the highest Pb/S MR 1:0.7.

Furthermore, apoferritin-PbS composites seemed to be sensitive to storage conditions in that the composites were stable when kept under nitrogen in the dark at 4 °C, but decomposed quickly when exposed to light and air at RT . [346]

4.3.1 Structural study of the PbS-apoferritin composites

The solutions were examined several times over a period of 3 months by photoluminescence (PL) spectroscopy. For PL experiments, the AFt-PbS composites were studied as liquid solutions in a glass vial or deposited on a glass substrate.

Figure 4.1 shows AFM images of AFt, PbS QDs and AFt-PbS composites prepared by the reassembly route. [346]

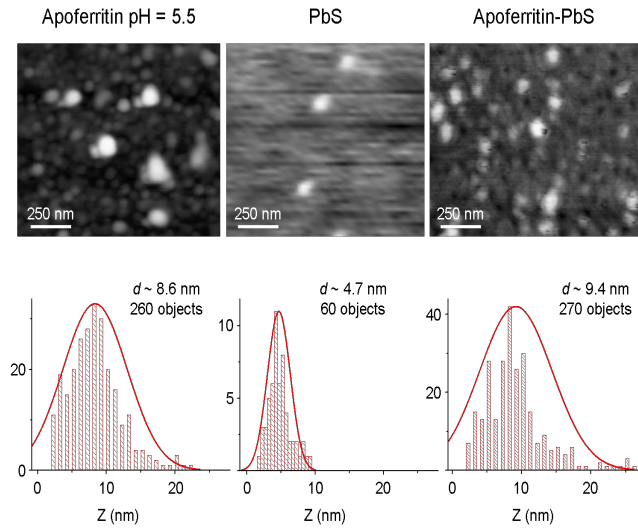


Figure 4.1: AFM images of PbS QDs (Pb/S MR = 1:0.3), AFt and AFt-PbS composites and their corresponding size distributions. This work was realised in collaboration with L. Turyanska from the Physics Department of Nottingham University.

Preliminary AFM studies of the PbS QDs indicate that the dots had spherical shape with average height, d , increasing from 3 to 12 nm for Pb/S molar ratio increasing from 1:0.3 to 1:0.7. [302] Here we focus on PbS MR 1:0.3 and average height $d = 5 \pm 2$ nm. The size of the AFt-PbS composite indicated by our AFM studies is *i.e.* $d = 9 \pm 5$ nm, a value close to that measured for our apoferritin ($d = 9 \pm 4$ nm), but smaller

than that expected for the external shell of ferritin and apoferritin ($d = 12$ nm). This discrepancy is thought to be caused by the compression of the apoferritin shell induced by the AFM-tip, an effect also observed by other groups for ferritin.[348]

To reveal the morphology and structure of our AFt-PbS composite, we have performed TEM experiments (Figure 4.2).[346]

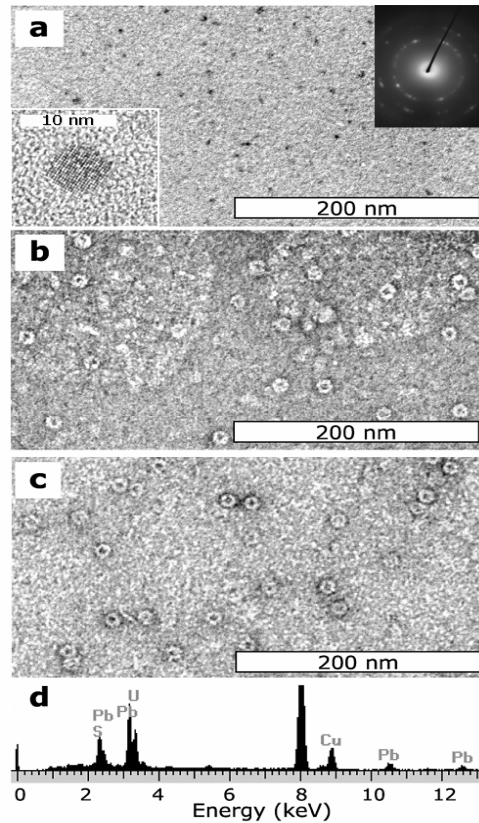


Figure 4.2: (a) TEM image of unstained AFt-PbS (PbS MR = 1:0.3) composites synthesized using the ‘nanoreactor’ route. (b-c) TEM images of AFt-PbS (PbS MR = 1:0.3) composites stained with uranyl acetate and synthesized using the ‘nanoreactor’ (b) and reassembly (c) routes. (d) EDX spectra of stained AFt-PbS (PbS MR = 1:0.3) composites. The U- and Cu- lines arise from the uranyl acetate stain and TEM grid, respectively. The inset in part (a) shows the HRTEM image and X-ray diffraction (XRD) pattern for unstained AFt-PbS composites synthesised using the reassembly route. These analyses of our AFt-PbS composites were produced by Dr. M. Li and Prof. S. Mann from the University of Bristol and Dr. T. Ben, A. Beltrán and Prof. S. Molina from Cádiz Universidad in Spain.[346]

Initially, the contrast in the TEM image of Figure 4.2a is completely dominated by the PbS core of the composite. However, the rather weaker contrast of the protein shell can be clearly revealed when the composites are negatively stained with uranyl acetate (Figure 4.2b-c). The TEM images of Figure 4.2b-c show AFt-PbS composites made of an intense central core and a lighter shell. From the analysis of the TEM images of Figure 4.2b-c, we find that the diameter of the composite is $d = 13 \pm 1$ nm, which is consistent with the value expected for apoferritin ($d = 12$ nm).

Energy Dispersive X-ray (EDX) spectra for stained and unstained samples (Figure 4.2d) also reveal characteristic Pb- and S-lines, thus supporting the presence of PbS core inside of the apoferritin as well as the presence of cysteine and methionine residues in the protein shell.

To reveal the crystal structure of the core inside the AFt-PbS composite, we have examined Selected Area Electron Diffraction (SAED) pattern and High Resolution TEM (HRTEM) images with the help of Dr. T. Ben, A. Beltrán and Prof. S. Molina from Cádiz Universidad in Spain. The SAED pattern in the inset of Figure 4.2a displays peaks corresponding to interplanar distances of 1.31 ± 0.02 Å and 2.09 ± 0.01 Å, characteristic of the (420) (1.327 Å) and (220) (2.098 Å) planes of bulk PbS.[27] Analysis of HRTEM images for 35 particles also indicate that the PbS core has an average diameter $d = 6 \pm 2$ nm. This estimate is close to the size of the PbS QDs (without apoferritin) derived from our AFM ($d = 5 \pm 2$ nm) and HRTEM ($d = 6 \pm 2$ nm) experiments.[346]

As further proof of the incorporation of PbS in apoferritin, we have examined High Angle Annular Dark Field (HAADF) (Figure 4.3b) and Electron Energy Loss (EEL) spectra (Figure 4.3c) taken with a Scanning TEM (STEM) microscope. This is a well-suited technique to investigate the chemical composition of nanostructures[349, 350] and does not require the use of staining agents as the contrast in the image is determined by the atomic number of the constituting elements.

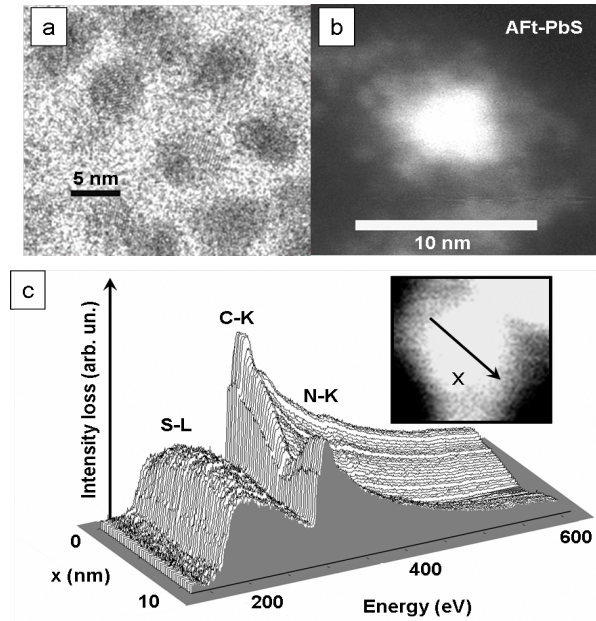


Figure 4.3: (a) HRTEM images and (c) spatial sequence of EELS spectra for Aft-PbS composites synthesized using the nanoreactor route. The spectra were recorded with an acquisition time of 1 s and show the characteristic signals of S-L (~ 165 eV), C-K (~ 285 eV) and N-K (~ 401 eV) edges. The inset shows the HAADF image for one composite. Each EEL spectrum was taken at a particular x-position along the arrow crossing the composite in the HAADF image. (b) STEM-HAADF image of unstained Aft-PbS composites synthesized using the reassembly route.[346]

The HAADF-STEM image in Figure 4.3b reveals composites made of a lighter shell surrounding a brighter core, which supports the shell-core structure of the Aft-PbS composite.

Figure 4.3c presents a sequence of EEL spectra, each taken at a particular position along the line crossing the circular particle marked in the inset of Figure 4.3c by an arrow. The EEL spectra indicate that the outer layer of the composite contains N-, C- and S-atoms as expected for the shell of Aft, while a larger number of S-atoms is revealed in the particle core as expected for PbS.

4.3.2 Optical properties of the PbS-apoferritin composites

Figure 4.4 shows the room temperature PL spectra of representative PbS QDs (Pb/S MR = 1:0.3) and AFt-PbS composites prepared by the ‘nanoreactor’ and reassembly routes. The PbS and AFt-PbS composites provide efficient and stable photoluminescence in the NIR spectral region of the electromagnetic spectrum. However the encapsulation of the PbS dots in apoferritin tends to shift slightly the PL emission to higher energy values.[346]

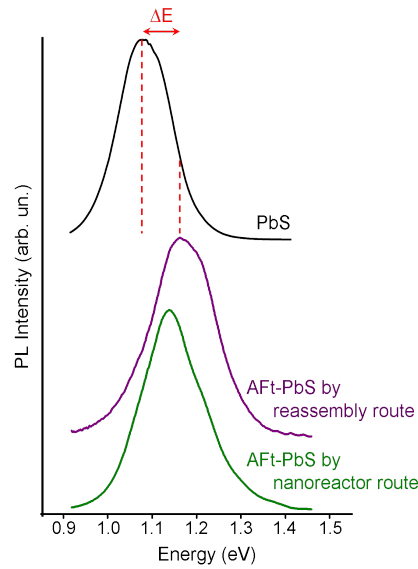


Figure 4.4: Room temperature PL spectra of PbS QDs (Pb/S MR = 1:0.3) and AFt-PbS composites. ΔE is the energy shift of the PL emission of the AFt-PbS solution relative to that of PbS QDs.[346] This work was realised in collaboration with L. Turyanska from the Physics Department of Nottingham University.

The small energy shift, ΔE , is similar for the two encapsulation methods and suggests that apoferritin acts to limit the size of the encapsulated dot. In turn this would prevent Ostwald ripening and coalescence of the dots thus leading to smaller dots and corresponding higher emission energies.

The value of ΔE is different for AFt-PbS solutions based on dots with different average diameter d . It tends to be larger in dots with higher energy and smaller values of d

and changes its sign when d becomes larger ($d \sim 10$ nm) than the diameter of the apoferritin core ($d = 8$ nm) as shown in Figure 4.5.

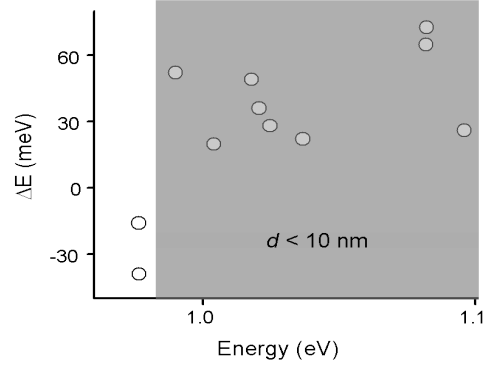


Figure 4.5: Dependence of ΔE on the peak energy of the QD PL emission. The value of ΔE is derived by comparing the PL spectra of PbS QDs and of AFt-PbS composites synthesized using the reassembly route. The grey area indicates dots with average size $d < 10$ nm.[346]

This shift is also observed when comparing the PL spectra of the different particles resulting from the centrifugation of the AFt-PbS solution. Centrifugation on the AFt-PbS composite solution causes a partial phase separation into a light brown upper solution and a dark brown lower solution (not a solid precipitate) with an ill-defined interface. The AFt-PbS composite, which tends to concentrate in the lower phase, was carefully removed using a syringe and deposited on a glass substrate for PL studies. As shown in Figure 4.6, the emission energy of the lower phase is very similar to that of the original AFt-PbS solution, while that of the remaining solution is shifted to lower energy and coincides with that of PbS dots formed in the absence of apoferritin.[346]

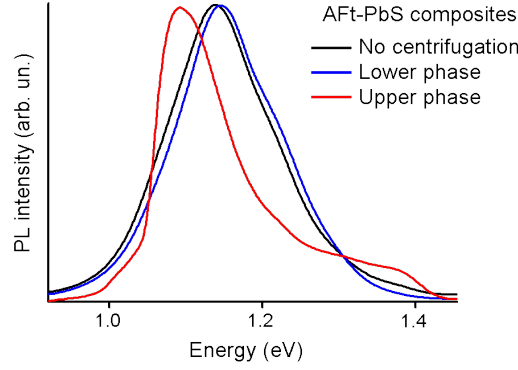


Figure 4.6: RT PL spectra for the AFt-PbS solutions with and without centrifugation.[346]

The intensities of the PL emissions from the PbS QDs and AFt-PbS composites are comparable and found to be stable over a period of at least 3 months. The stable and efficient PL signal of the AFt-PbS composites allowed us to study their optical properties over a wide range of temperatures from 4 K to room temperature, and of excitation powers, P (10^{-3} - 10 W cm $^{-2}$). For the temperature study, the as-prepared sample was dried on a glass substrate. As shown in Figure 4.7, with increasing T from 4 to 292 K, the peak energy, E , of the PL spectrum for the AFt-PbS composites blue-shifts and its T -dependence for $T > 150$ K can be described by the coefficient $\alpha = 0.3$ meV K $^{-1}$ as expected for PbS QDs.[302, 346]

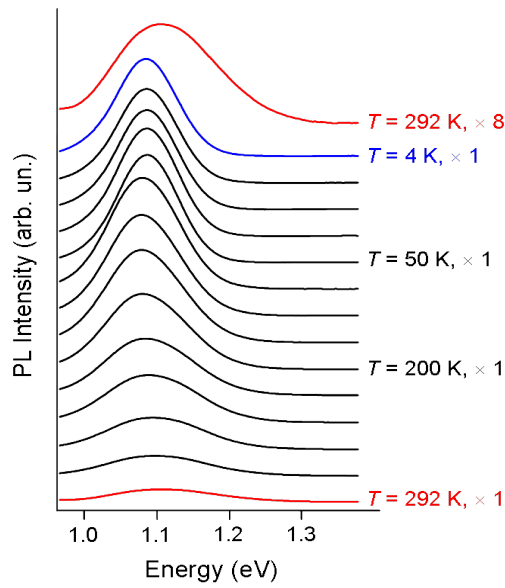


Figure 4.7: PL spectra of AFt-PbS composites at various T and excitation power $P = 0.2 \text{ W cm}^{-2}$. This work was realised in collaboration with L. Turyanska from the Physics Department of Nottingham University.

Also, the peak intensity of the PL emission decreases monotonically by less than a factor 10; this high thermal stability of the PL intensity indicates strong carrier confinement in the QD and a relatively low density of non-radiative recombination centres in the AFt-PbS composite.

4.3.3 Native gel electrophoresis of PbS-apoferritin composites

The effectiveness of the reassembly route employed for the synthesis of our AFt-PbS composites was tested by native polyacrylamide gel electrophoresis (PAGE). Proteins are not denatured and therefore they are separated based on their charge-to-mass ratio.

Figure 4.8 shows the native PAGE of AFt-PbS composites in comparison to ferritin and apoferritin.

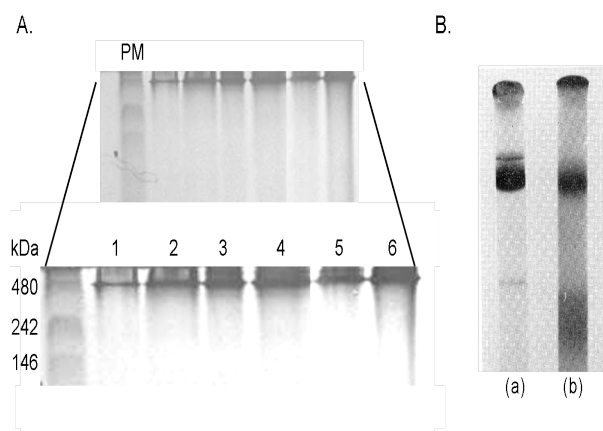


Figure 4.8: A. Native PAGE of 1) apoferritin 8.5 mg mL⁻¹, 2) apoferritin 0.85 mg mL⁻¹, 3) ferritin 8.5 mg mL⁻¹, 4) ferritin 0.85 mg mL⁻¹, 5) and 6) AFt-PbS synthesised by the reassembly route. The protein marker is on the left lane. B. Native PAGE of reconstituted ferritin stained for the protein (a) and iron (b) (adapted from reference [351], no protein marker).

Bryce and Crichton analysed reconstituted ferritin (addition of ferrous ammonium sulphate to a solution of apoferritin in imidazole buffer pH 7.45 plus oxidants) by polyacrylamide gel electrophoresis (6.5% gels in buffer at pH 8.6).[351] By using the amido black and potassium ferrocyanide dyes to stain the protein and the iron, respectively, they showed that apoferritin and iron migrated together over the gel as seen in Figure 4.8B. After running our different samples on a 10% native gel (Figure 4.8A), we observed that staining revealed two bands for each sample which were also seen for the reconstituted ferritin and correspond to apoferritin monomer (at 480 kDa) and dimer (the latter is visible on an enlarged image).[225] As Bryce *et al.* also showed that horse spleen apoferritin and horse spleen ferritin migrate at the same level[203], we affirm that the encapsulation of PbS QDs using the disassembly/reassembly route does not influence the external electrostatic potential of the protein shell. Furthermore, PbS QDs did not migrate, remaining in the stacking gel (data not shown) and no accumulation of dots was observed for AFt-PbS composites, which implies that PbS QDs are encapsulated within the apoferritin cage.

4.4 Conclusion

We have exploited both the self-assembly and nanoreactor properties of apoferritin to incorporate PbS quantum dots in the apoferritin cavity. Apoferritin-PbS composites have been prepared in aqueous solution with photoluminescence emission in the wavelength region ($\sim 1,000$ nm) of interest for studies of biological media. We have proved by several spectroscopic techniques that AFt-PbS composites are made of PbS cores surrounded by the apoferritin shell. Furthermore, it is the first time that the disassembly/reassembly route has been employed for the encapsulation of quantum dots within the apoferritin cage. The efficiency of this technique has been confirmed by native gel electrophoresis showing that the external surface of the protein is conserved and quantum dots do not bind on the outer surface of apoferritin.

Chapter 5

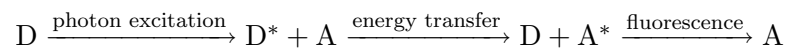
Bioluminescence resonance energy transfer (BRET) with PbS quantum dots

5.1 Introduction

5.1.1 Introduction to FRET phenomena

Fluorescence (or Förster) resonance energy transfer (FRET) is a powerful spectroscopic technique that occurs whenever the emission spectrum of an excited fluorophore (called donor **D**) overlaps with the absorption spectrum of a neighbouring molecule (called acceptor **A**). [352] FRET measures small variations in the separation distance between **D** and **A** coupled by a dipole-dipole interaction. This sensitive technique allows the detection of molecular interactions and conformational changes. [82, 353–356]

The principle of this method can be explained as following:



In the first step, a fluorescent donor molecule **D** is excited by the normal absorption of a photon and transfers this excitation energy to an acceptor molecule **A** in the second

step. At this stage, the energy transfer is a non-radiative transition (interaction of the transition dipoles of **D** and **A**, it does not occur *via* emission of a photon from **D**^{*} and reabsorption by **A**). Finally, **A** may lose its excess energy by fluorescence. As a result of FRET, a quenching of the fluorescence of **D** and an enhancement of fluorescence of **A** can be observed. The efficiency of FRET increases as the overlap between the emission of **D** and the absorption of **A** increases. FRET is only significant if the donor and acceptor groups are part of the same molecule or hold on close molecule complex. The efficiency E is described by the equation (5.1):

$$E = \frac{R_0^6}{R_0^6 + r^6} \quad (5.1)$$

where r is the distance between **D** and **A** and R_0 is the Förster distance at which half the **D** molecules participate in the FRET and half decay by the usual radiative and non-radiative processes (transfer rate equal to the decay rate of the donors in the absence of the acceptors). The Förster distance R_0 is dependent on individual **D** and **A** pairs typically 10-100 Å.

Oligomers (peptides, nucleic acids) of different lengths and steroids have been employed as spacers between **D** and **A** to demonstrate that greater separation leads to less efficient energy transfer.[357]

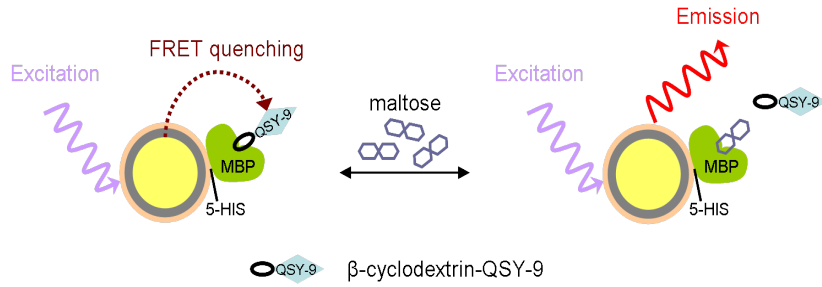
Semiconductor nanoparticles have been employed in a wide range of FRET applications as both donor and acceptor roles. QDs have proved their ability to be used as efficient donors whereas their use as energy acceptors is still uncertain.[358–361]

During FRET experiments, some rules apply:

- Increasing the number of energy acceptors per QD, increases FRET quenching efficiency,
- Increasing Förster radius, R_0 , increases constraints of FRET quenching. The size of QDs can be a limitation of using dots as donors for FRET compared to organic dyes (QDs are larger than traditional fluorophores).

In experiments where the dots are used as donors due to their broad absorbance, the energy acceptors are organic fluorophores (such as BIPS (1'-3-dihydro-1'-(2-carboxyethyl)-3,3-dimethyl-6-nitrospiro-[2H-1-benzopyran-2,2'-(2H)-indoline]), [362] β -cyclodextrin [363], cysteine [363–366], rhodamine [367]) and non fluorescent dyes or quenchers (QSY9, BHQ-10, DABCYL (4-(dimethylaminoazo)benzene-4-carboxylic acid), squaraine) [368–370].

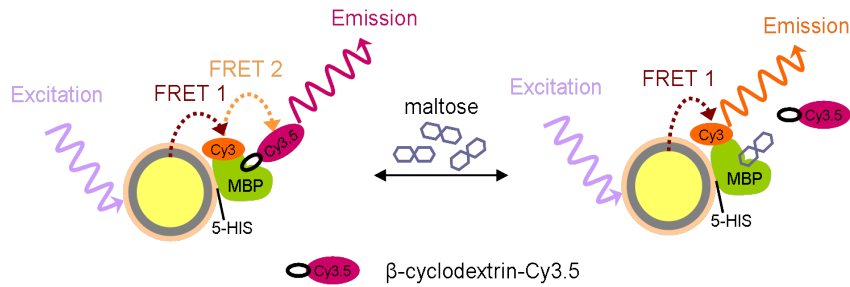
The general idea of these experiments is described in Scheme 5.1:



Scheme 5.1: One-step FRET mechanism with a QD as a donor and α -cyclodextrin-QSY-9 as an acceptor (adapted from reference [363]).

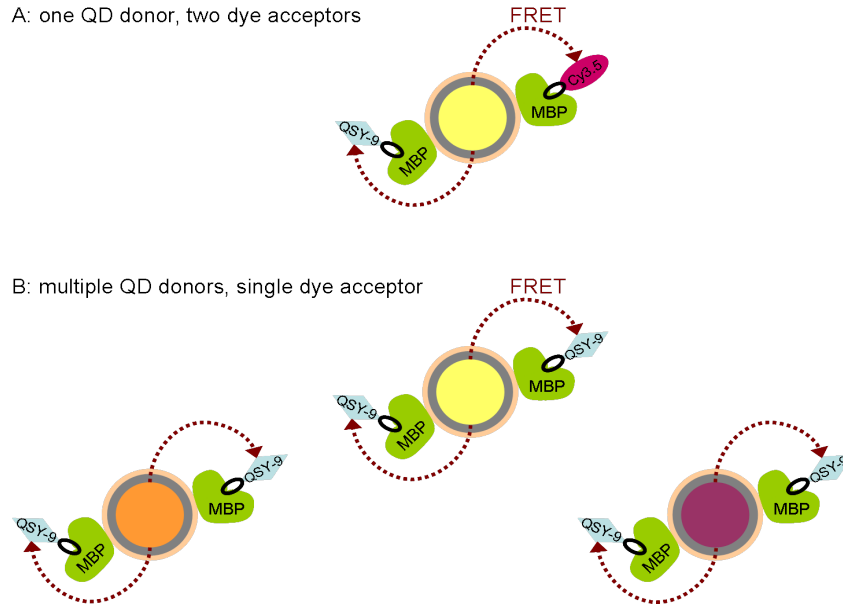
β -cyclodextrin-QSY-9 used as a dye conjugate binds to the MBP domain and this assembly results in FRET quenching: the energy of the excited dot is adsorbed by the organic dye. When maltose is added to this system, the quencher is displaced and the QD photoluminescence is restored.

To accomplish FRET over long distances, multistep energy transfer processes have been described (Scheme 5.2). [363, 371]



Scheme 5.2: Two-step FRET mechanism (adapted from reference [363]).

Multiplexed FRET can be realised with two configurations: A) a single colour QD can interact with multiple distinct acceptors and B) multiple donor populations can interact with one type of acceptor (Scheme 5.3).[372]



Scheme 5.3: Schematic representation of the FRET multiplexing configurations (adapted from reference [372]).

Moreover, some groups reported the application of FRET between II-VI QDs and fluorescent dyes linked together by different biomolecules such as antibody,[369, 373, 378] BSA,[374, 377] peptide,[367, 375, 376, 382, 383] and DNA[379–381].

CdTe nanoparticles (NPs) of different sizes were used as energy donors and acceptors in antigen/antibody immunocomplexes. The luminescence of green-emitting QDs ($\lambda_{max} = 555$ nm) was quenched whereas the emission of red-emitting QDs ($\lambda_{max} = 610$ nm) was enhanced.[373]

CdTe NPs conjugated to bovin serum albumin (BSA) through a glutaric dialdehyde cross-linker showed an increase in their emission attributed to an energy transfer from the tryptophan moieties of albumin to the NPs.[374]

More recently, QDs have been employed as energy donors and gold nanoparticles as acceptors. The QD luminescence was reduced by 71% due to their conjugation to

the gold NPs. After collagenase exposure, the peptidic linkage is cleaved and emission of luminescence from QDs is restored.[375, 376] Also, in such a system, rhodamine acts as an efficient energy acceptor.[367]

Van Orden *et al.* established a FRET transfer using CdSe/ZnS quantum dots as energy donors and tetramethylrhodamine (TMR) as dye acceptor.[377] Biotinylated BSA conjugated to QDs were bound to streptavidin-labelled TMR. An enhancement of the dye fluorescence was observed while the emission from the CdSe/ZnS NCs was quenched.

The antibody/antigen interaction has proved to be an efficient system for FRET between CdSe/ZnS core-shell NCs as donors and the ‘black hole’ quencher BHQ-10.[378] The hybrid sensor consisted of anti-trinitrotoluene (TNT) antibody attached to the QDs by metal affinity coordination through the histidine tail of the antibody and a dye-labelled TNT analogue. The addition of TNT replaced the quencher-labelled analogue, restoring the luminescence of the NCs.

Thrombin activity has been detected by a similar method where CdSe/ZnS QDs were conjugated with an anti-thrombin aptamer itself conjugated to a DABCYL quencher.[369]

Willner *et al.* reported a FRET in CdSe/ZnS-DNA conjugates.[379, 380] Thiolated DNA-functionalised QDs were hybridized with the complementary DNA-functionalized Texas-Red. An energy transfer was observed from the QD to the dye. The addition of a cleaving reagent, DNase I, resulted in a photoluminescence recovery of the nanocrystals.

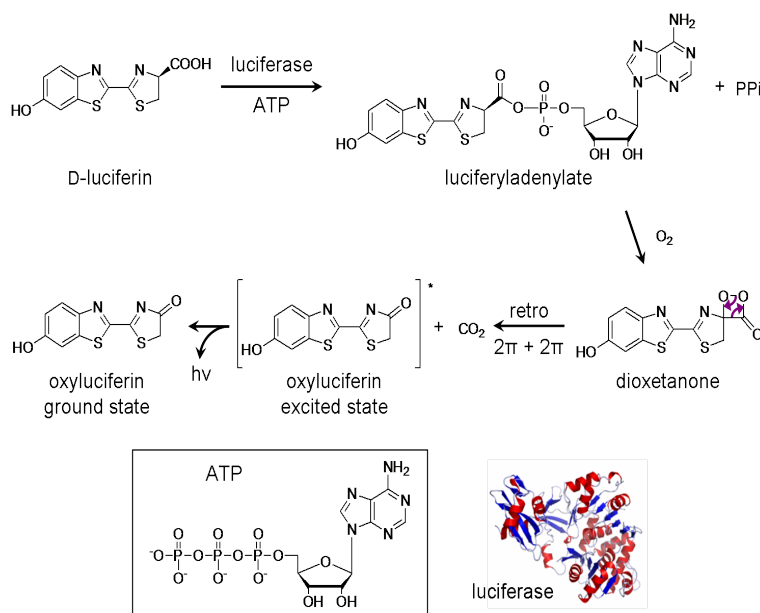
A sandwich assay of DNA target has been established by Wang and co-workers.[381] The nanosensor consisted of two oligonucleotide probes, one reporter probe labelled with the fluorophore Cy5 as acceptor and one capture probe labelled with biotin and conjugated to streptavidin-derivatized CdSe/ZnS QDs. Thus, the desired DNA target is sandwiched between the two probes.

Recently, an amino-terminated histidine modular peptide was used as a linker between CdSe/ZnS NCs and a dye to show the effective proteolytic activity of proteases such as collagenase, caspase-1, thrombin and chymotrypsin which were able to cleave

the peptide linker.[382, 383]

5.1.2 PbS as energy acceptors in a BRET process

The BRET (Bioluminescence Resonance Energy Transfer) process is similar to the FRET process discussed in the introduction. Nevertheless, an important limitation of FRET is the requirement for external illumination to initiate the fluorescence transfer, which can lead to background noise due to direct excitation of the acceptor. To overcome this difficulty, the technique of BRET using a self-illuminating system has been developed.[384, 385] Bioluminescence is an enzyme-catalysed reaction involving the enzyme luciferase, the most well known being firefly luciferase from the firefly *Photinus pyralis*. [386] The luciferase catalyzes the conversion of D-luciferin (substrate) to a luciferyladenylate intermediate using ATP (adenosine 5'-triphosphate). Then, the latter is oxidized by molecular oxygen. This gives rise to an excited oxyluciferin *via* a dioxetanone intermediate. The light is emitted when oxyluciferin falls from the excited state to the ground state (Scheme 5.4).



Scheme 5.4: Bioluminescence reaction involving the enzyme luciferase and the substrate luciferin.

A derivative of *Renilla* luciferase, Luc8, was used as an energy donor in a BRET system with commercial CdSe/ZnS quantum dots.[387, 388] Luc8 was attached to acid-capped QDs through a peptide bond. The bioluminescence of Luc8 was decreased and the luminescence of the QDs increased. Once the peptide bond was cleaved, bioluminescence from Luc8 was recovered and the QDs emission was negated.

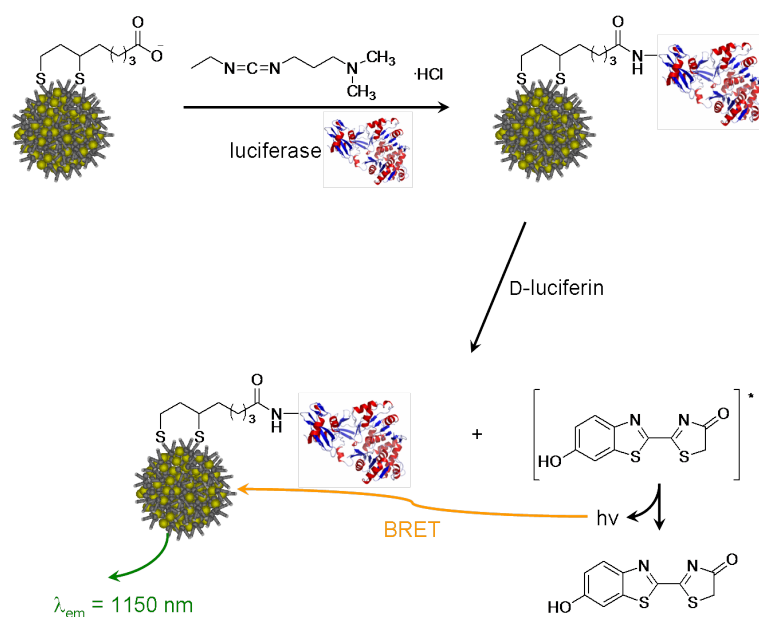
5.2 Objectives

The objective was to create an energy transfer from the luciferin to the PbS quantum dots *via* the luciferin/luciferase system. The experiment was realised following the bioluminescence conditions reported by Nakatsu *et al.* with the luciferase and luciferin from *Luciola mingrelica* and ATP ratios of approximately 1:0.0022:5.3.[389]

5.3 Results & discussion

PbS dots MR 1:0.3 were capped with lipoic acid, substituting dithioglycerol which was used as a capping agent in the previous syntheses. Lipoic acid and dithioglycerol have a similar structure with two thiol groups that increase ligand binding to the dot surface. Photoluminescence analyses under an Ar⁺ laser with an excitation wavelength at 514.5 nm indicated a higher emission wavelength ($\sim 1,220$ nm) of the acid-capped dots compared with thiol capped-PbS QDs, which can be due to the effect of capping as AFM images from the acid-capped QDs reveal a similar diameter ($d = 3\text{-}5$ nm) to the thiol-capped QD.

The BRET system was realised by activating the lipoic acid capped-PbS MR 1:0.3 by the coupling agent EDC (1-ethyl-3-(3-dimethylaminopropyl) carbodiimide hydrochloride) in order to create a linkage with the enzyme luciferase through an amide bond (Scheme 5.5).



Scheme 5.5: Coupling of dihydrolipoic acid-capped PbS QDs with luciferase using EDC coupling agent and bioluminescence energy transfer from the luciferin excited state to the PbS dots.

Thus the luciferase would be covalently attached to the PbS QD surface, additionally the close proximity of the enzyme and the substrate should allow energy transfer. Luciferin and ATP were then successively added to initiate the reaction. Bioluminescence from luciferin and photoluminescence from PbS QDs were measured separately using a 250-800 nm/900-1,400 nm range detector, respectively, see (Figure 5.1).

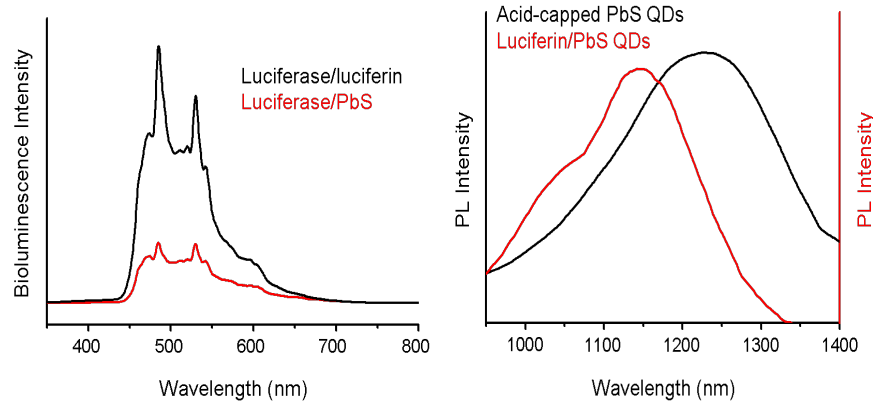


Figure 5.1: Bioluminescence and photoluminescence intensities of D-luciferin/luciferase and PbS dots respectively before (black lines) and after (red lines) coupling reaction.

The PL emission from PbS QDs was detected with an InGaAs detector in a dark room in order to minimize a possible direct excitation of the quantum dots by any source of light. With an integration time of 60 s and despite a low intensity, a PL emission from the PbS dots could be observed at 1,142 nm whereas the emission of the luciferase ($\lambda_{em} = 490$ nm) and D-luciferin ($\lambda_{em} = 550$ nm) decreased when subject to the proximity of PbS dots.

Repetition of such experiment was problematic due to D-luciferin being stable in Tris-Acetate only for a short period of time of 8 to 24 h while the BRET measurement takes ~ 10 h.

Also, So *et al.* reported that the binding of polymer coated-CdSe/ZnS with wild-type firefly luciferase from *Renilla reniformis* (sea firefly) was unsuccessful. The use of luciferase mutant could allow more stable conjugates.[390, 391]

5.4 Conclusion

We obtained emission from PbS quantum dots where the system D-luciferin/luciferase from *L. mingrelica* acts as an energy donor and PbS quantum dots act as energy acceptors through a bioluminescence resonance energy transfer. Luciferase, the enzyme

catalysing the reaction, was covalently attached to acid-capped PbS QDs. The addition of D-luciferin to the medium led to a transfer of energy from the D-luciferin to the PbS dots. As expected, the emission of PbS QDs was observed while the emission from D-luciferin/luciferase decreased. This successful transfer of energy makes these nanoparticles promising tools for *in vivo* biomedical imaging. A similar energy transfer could be achieved using our AFt-PbS bioconjugate system where the apoferritin protein shell surrounding the QDs would offer a greater binding to biomolecules for labelling experiments.

Chapter 6

Incorporation of un-natural amino acids into human apoferritin

6.1 Introduction

Through the past decade, the engineering of the genetic code with new functionalities (halogeno, keto, cyano, azido, nitroso, silyl, alkene and alkyne groups) has developed as an emerging research field with the use of non-canonical or non-coded amino acids.[392–396]

Non-canonical amino acids such as photoactivable amino acids, isotopically labelled amino acids, and amino acids bearing biophysical probes have been incorporated in order to improve the study of protein structure-function relationships and to generate proteins with novel properties.

In this chapter, our studies on the expression of human H and human L apoferritin proteins are described followed by the incorporation of un-natural amino acids into these proteins. The purpose of this research is to render the apoferritin shell easier to specifically attach to other biomolecules in order to use our PbS-encapsulated apo-

ferritin conjugates as labels for imaging. Thus, it is interesting to incorporate amino acid analogues with new functionalities such as azido or alkyne groups which have been reported to react specifically with alkyne and azido reagents respectively ('click' or bio-orthogonal chemistry) through an Huisgen cycloaddition reaction.

6.1.1 Introduction to protein bio-synthesis

Protein biosynthesis is a two-step process involving transcription of double-stranded deoxyribonucleic acid (DNA) into messenger RNA (mRNA) followed by translation of the mRNA into a protein biopolymer (Figure 6.1).

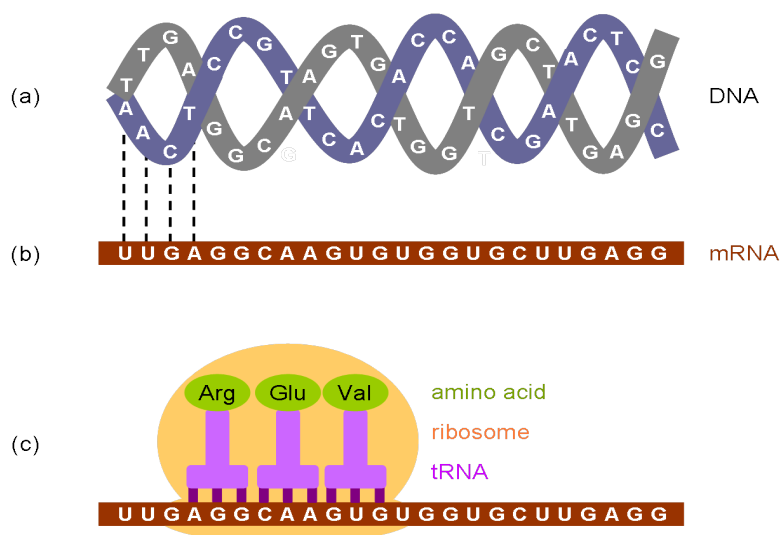


Figure 6.1: Representation of DNA transcription and RNA translation during protein biosynthesis.

During transcription as shown in Figure 6.1b, the four 2'-deoxy nucleotides of the DNA (guanine, cytosine, thymine and adenine) are replaced by their complementary nucleotides, respectively cytosine, guanine, adenine and uracil.

During translation as shown in Figure 6.1c, the mRNA codons (triplets of nucleotides) are 'translated' by tRNA on ribosomes into amino acids through a codon/anticodon recognition. Each codon codes for a specific amino acid. The transfer RNA (tRNA) plays the role of an adaptor between the amino acid and mRNA molecules showing

high substrate (amino acid) specificity.

Thus, the requirement for a non-canonical amino acid or analogue to be incorporated into the protein sequence is that its shape and size have to be similar to those of the natural amino acid to prevent interferences with the folding of the protein.

Two approaches are available to expand the protein synthesis with non-canonical amino acids:

- Site-directed mutagenesis. Mutagenesis is a biological technique based on the substitution of a specific amino acid by one of the other nineteen common amino acids given by the genetic code. For the incorporation of non-canonical amino acid, this technique is a variation of conventional site-directed mutagenesis whose details will be discussed below.
- Use of an amino acid auxotroph: culture medium lacking a defined natural amino acid.

Both of these techniques require: 1) an un-natural amino acid of interest, and 2) a translation system containing ribosomes. The differences between site-directed mutagenesis and auxotroph strains is the codon/anticodon recognition event. In the case of mutagenesis, the suppressor tRNA must be charged with the un-natural amino acid of interest and contain an anticodon recognizing a non-sense or terminal codon in the DNA strand.[397, 398] Here, the non-canonical amino acid would be incorporated as a 21st amino acid in the RNA strand. In the auxotroph method, the tRNA contains an anticodon recognizing a natural amino acid which is depleted in the culture medium, thus the non-canonical amino acid acts as a replacement for the canonical amino acid.[399–407]

6.1.2 Previous incorporation of un-natural amino acids into proteins.

The first incorporation of a methionine analogue was reported in 1957 by Cowie and Cohen who replaced sulphur-containing methionine (Met) by selenium-containing methionine (SeMet) using the Met-auxotroph *E. coli* ML304d strain.[408] They observed slower growth rate of the culture when the growth medium was supplemented with

SeMet instead of Met.

Almost 40 years later, Kothakota, Tirrell *et al.* realised the incorporation of a phenylalanine (Phe) analogue into a protein of sequence $-[(\text{GlyAla})_3\text{X}]_{13}-$ where X is the analogue or the natural Phe. The plasmid encoding the protein was incorporated into phenylalanine auxotroph cells AFpLysS and expressed in M9 medium containing the 20 natural L-amino acids. After 10 min of induction with IPTG (isopropyl β -D-thiogalactopyranoside), cells were sedimented and washed with M9 medium only. Cell pellets were resuspended into M9 containing the Phe analogue and the 19 other natural amino acids. Phe analogue incorporation was observed by UV spectra and NMR analysis to an extent of 90% of natural Phe substituted.[399]

Following this procedure, Tirrell's group expressed the mouse dihydrofolate reductase (DHFR) protein incorporating methionine analogues using the methionine auxotroph CAG18491 (Figure 6.2).[400, 401, 403–405] Also, a leucine auxotroph has been used to incorporate a fluorinated leucine analogue into the leucine zipper protein.[406]

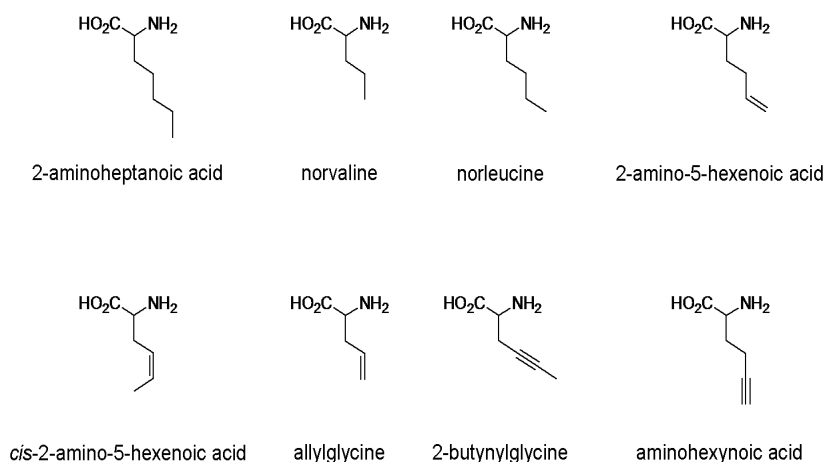


Figure 6.2: Methionine analogues incorporated into proteins.[400, 401, 403–405]

6.2 Objectives

To further improve the potential use of AFt-PbS composites in bio-labelling or bio-imaging applications, we aimed to improve the binding of our composite to biomolecules

by modifying the structure of amino acids of the apoferritin cage. Thus, the goal was to introduce new functionalities (azido and alkyne groups) into human apoferritin through the incorporation of un-natural amino acids. The protein cage thus modified could be easily linked to other molecules through basic organic reactions.

6.3 Results & discussion

6.3.1 H-human and L-human apoferritin expressions

Over-expression conditions were first studied for the synthesis of H and L human apoferritins. The DNA coding for these two proteins were incorporated into the plasmids pET-11a (rHuHFt) and pET-26b(+) (rHuLFt) constructed and kindly provided by Steven Aust (Utah State University, USA), see Figure 6.3.[409]

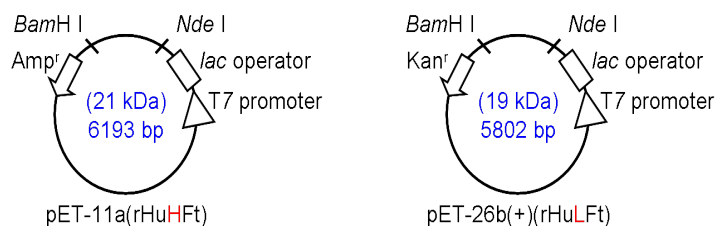


Figure 6.3: Plasmids pET-11a and pET-26b(+) for the expression of H and L human apoferritin respectively.

Both vectors contain *NdeI* and *BamHI* restriction enzymes. The pET-11a plasmid possesses genes resistant to chloramphenicol (Chl) and ampicillin (Amp) antibiotics whereas pET-26b(+) possesses genes resistant chloramphenicol and kanamycin (Kan) antibiotics.

Cell cultures growth of pET-11a and pET-26b(+). H and L human apoferritins were grown following the procedure developed by Grace *et al.* for the co-expression of human apoferritin heteropolymer.[409] Both vectors were transformed into B834(DE3)pLysS competent cells by heat shock. The respective antibiotics were added to LB (Lysogeny broth also known as Luria broth or Luria-Bertani broth) plates over

which cells are grown overnight at 37 °C. LB is a medium nutritionally rich used for the growth of bacteria.

Positive transformants (a single colony) were grown in LB medium containing the antibiotics chloramphenicol and ampicillin for H apoferritin expression or chloramphenicol and kanamycin for L apoferritin expression. The cultures were subsequently used to inoculate a large volume of M9 minimum salts medium at pH 7.0. In order to produce higher growth rate, the M9 medium was supplemented with glucose (20%), salts (CaCl_2 (0.1 mM), $\text{ZnSO}_4 \cdot 7\text{H}_2\text{O}$ (8.0 μM), $\text{MnSO}_4 \cdot 7\text{H}_2\text{O}$ (10.0 μM), $\text{MgSO}_4 \cdot 7\text{H}_2\text{O}$ (1.0 mM), CuSO_4 (2.0 μM), $\text{CoSO}_4 \cdot 7\text{H}_2\text{O}$ (2.0 μM), H_3BO_3 (1.0 μM), $\text{Na}_2\text{MoO}_4 \cdot 2\text{H}_2\text{O}$ (1.0 μM), thiamine-HCl (0.3 nM), and amino acids (L-arginine hydrochloride, L-histidine hydrochloride, L-isoleucine, L-leucine, L-lysine hydrochloride, L-phenylalanine, L-threonine, L-tryptophan, L-valine) at 120 mg mL⁻¹.

The growth of the bacterial cultures were monitored spectrophotometrically at 610 nm by measuring the optical density (OD). An absorbance unit or OD unit is directly proportional to the concentration of the solute.[410] When OD₆₀₀ reaches a value of 0.4, stimulation of protein synthesis was induced by the addition of IPTG at a final concentration of 0.75 mM. The protein synthesis is regulated by the presence of a *lac* repressor which binds tightly (dissociation constant $K_d = 10^{-6}$ M) to a DNA sequence downstream of the T7 promoter thus inhibiting any protein synthesis. When added, IPTG binds to the repressor with more affinity ($K_d = 10^{-13}$ M) causing it to dissociate from the DNA and allows the mRNA for the protein of interest to be synthesised.

Purification of H human apoferritin. Cell pellets were resuspended in Tris-HCl buffer with DNase I, RNase and lysozyme in order to remove any contamination from DNA (e.g. plasmid), RNA and cells.

Deoxyribonuclease I (DNase I) is an enzyme catalysing the hydrolytic cleavage of phosphodiester linkage in the DNA backbone. Cleavage preferentially occurs adjacent to pyrimidine (C or T) residues. Major products are 5'-phosphorylated di-, tri- and tetranucleotides.

Ribonuclease A (RNase) is an enzyme catalysing the hydrolytic cleavage of phosphodiester linkage in the RNA backbone. Cleavage preferentially occurs at the 3' end of pyrimidine residues and degrades the RNA into 3'-phosphorylated mononucleotides and oligonucleotides.

Lysozyme is an enzyme catalysing the hydrolysis of linkages present in the bacteria cell wall.

The bacterial suspension was then subjected to three freeze-thaw cycles to perform lysis of the cell walls and centrifuged to remove the cellular debris. The supernatant was then purified by column chromatography.

Fast protein liquid chromatography. Fast Column Liquid Chromatography is an ion exchange column chromatography used to separate and/or purify proteins from mixtures (Figure 6.4). Analytes are retained on the stationary phase, which displays opposite ionic functional groups, by coulombic interactions.

Cation exchange chromatography retains positively charged molecules on a negatively charged stationary phase. Anion exchange chromatography retains negatively charged molecules on a positively charged stationary phase.

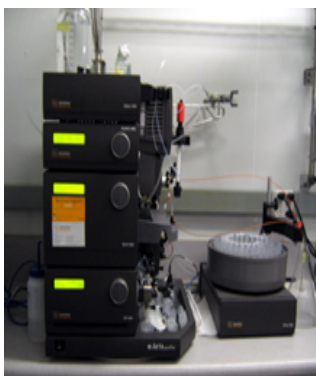


Figure 6.4: Fast column liquid chromatography apparatus. A sample is introduced into a sample loop of 2 mL volume. A buffered aqueous solution known as the mobile phase carries the sample from the loop onto a column (stationary phase). The analytes are then detected by conductivity and UV/visible absorbance.

Proteins have a wide number of both negatively and positively charged functional groups. Ion exchange chromatography separates proteins according to their net charge which is dependent on the mobile phase whose pH can be varied owing to the separation needed.

H human apoferritin was purified using an anion exchange chromatography and the different fractions were then analysed by SDS-PAGE (Figure 6.5).

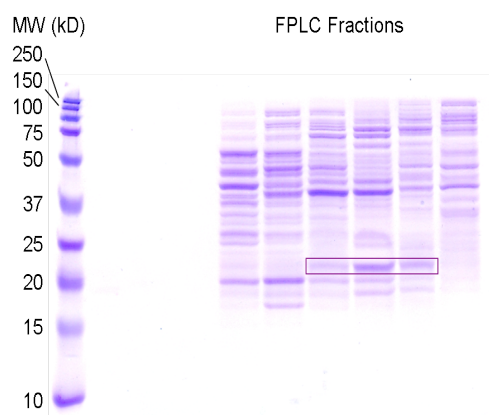


Figure 6.5: SDS-PAGE of the FPLC fractions of H human apoferritin.

On the electrophoresis gel, the characteristic band of the H subunit at 21 kDa was observed in different fractions (surrounded by the purple rectangle in Figure 6.5). Although, H human apoferritin has been synthesized successfully, it is clear that the purification of the protein needs to be further developed. After SDS-PAGE, Grace *et al.* purified the synthesized heteropolymer of apoferritins with a second size exclusion chromatography.

6.3.2 Incorporation of methionine analogues

Organic synthesis of the methionine analogues. Alkyne and azide methionine analogues were prepared by members of Prof. Neil Thomas and Dr. Chen Wang groups (Figure 6.6).

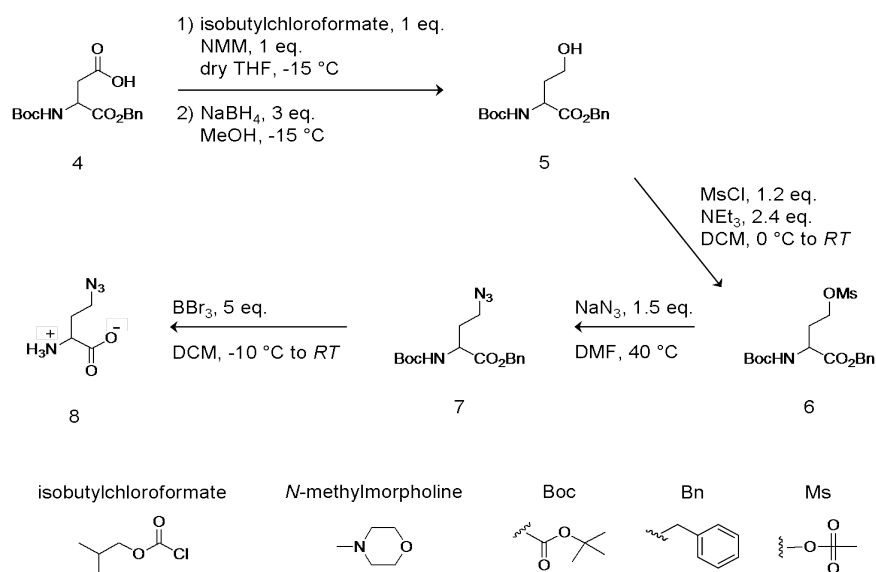


Figure 6.8: Synthesis of azidohomoalanine.

Azidonorleucine was prepared from *N*- α -Boc-lysine (Figure 6.9).[413] Sodium azide was added to triflic anhydride (Tf_2O , 9) leading to TfN_3 (10). The addition of the azido group from (10) to the Boc-protected lysine (11) was catalysed by copper(II) forming the Boc-protected azidonorleucine which underwent deprotection of the Boc group with concentrated hydrochloric acid giving azidonorleucine (13).

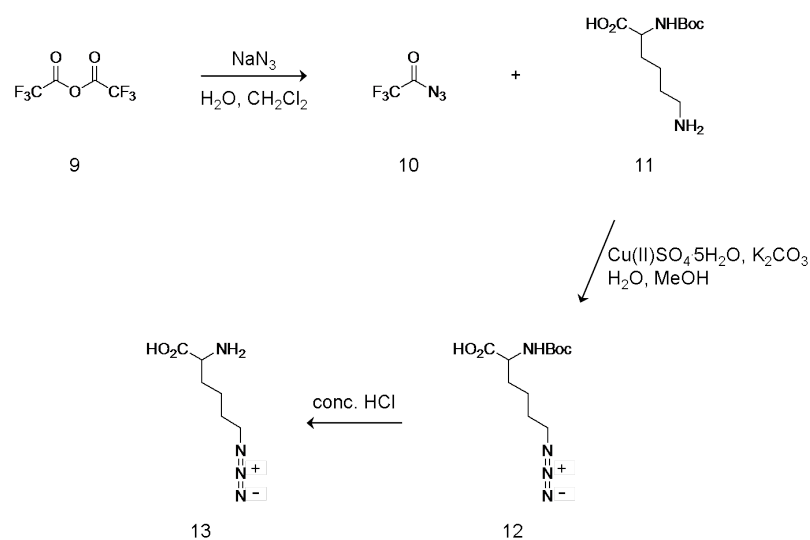


Figure 6.9: Synthesis of azidonorleucine.

H and L human apoferritins expressions with methionine analogues. The incorporation of the different methionine analogues was studied following the protein expression reported by van Hest *et al.*[401]

First H and L apoferritins were grown in M9 medium containing all amino acids including methionine. After a few hours of growth ($\text{OD}_{600} = 0.4$), a medium shift was performed: the cells were sedimented and washed several times with M9 medium containing no amino acids. These washing steps led to depletion of natural methionine substrate in the medium. The cells were resuspended in M9 and divided into 10 aliquots of M9 medium containing the methionine analogue (Table 6.1). All cultures were tested by analysis by Western blotting.

	Protein H or L apoferritin	Incubation temperature (°C)	IPTG (mM)	Incubation time (h)
1	positive control	37	0.75	2
2	negative control	37	0.75	2
3	aminohexynoic acid	37	0.75	2
4	azidohomoalanine	37	0.75	2
5	azidonorleucine	37	0.375	2
6	azidonorleucine	37	1.5	2
7	azidonorleucine	37	0.75	2
8	azidonorleucine	37	0.75	4
9	azidonorleucine	20	0.75	o/n

Table 6.1: Expression conditions of H and L human apoferritins containing natural methionine (positive control), no methionine (negative control) and methionine analogues (aminohexynoic acid, azidohomoalanine, azidonorleucine).

Western blotting. Immunoblotting or Western blotting is a technique used to detect a specific protein by an antigen/antibody recognition. Usually, samples are solubilized and denatured with SDS. The different antigens are then separated by SDS-PAGE and electrophoretically transferred on a nitrocellulose membrane where they are immunodected with a primary antibody (Figure 6.10). The antigen/antibody complexes are finally identified with horseraddish peroxidase (HRPO).[414]

HRPO is an enzyme catalyzing the oxidation of a substrate, the luminol (Figure 6.10).

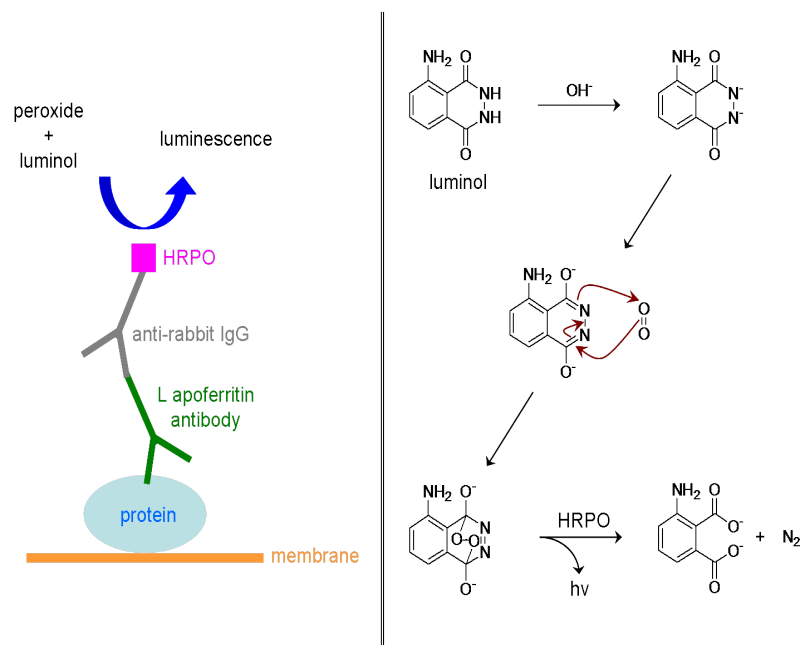


Figure 6.10: Detection of protein target using HRPO/luminol chemiluminescent system.

When luminol reacts with the hydroxide salt, a dianion is formed. The oxygen produced from the hydrogen peroxide then reacts with the luminol dianion. The product of this reaction, an organic peroxide, is very unstable and immediately decomposes with the loss of nitrogen to produce 3-aminophthalic acid with electrons in an excited state. As the excited state relaxes to the ground state, the excess energy is liberated as a photon, visible as blue light ($\lambda_{max} = 425 \text{ nm}$).

Figure 6.11 shows the Western blotting performed for L human apoferritin containing the three different methionine analogues aminohexynoic acid, azidohomoalanine and azidonorleucine.

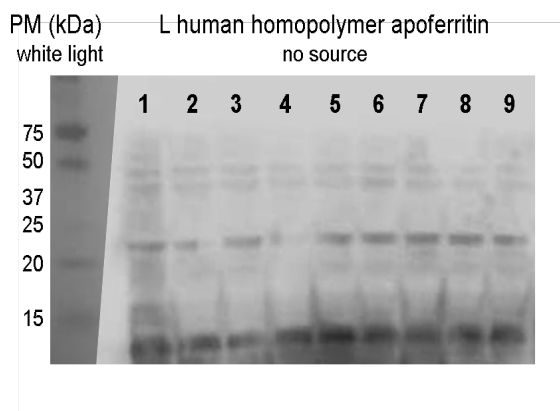


Figure 6.11: Western blot results.

From the images with no source of light (chemiluminescence from the luminol) and the gel under white light, a band around 19 kDa can be seen which is the molecular weight of L apoferritin subunit. Nevertheless, this band is observed in all samples, even the negative sample which does not contain methionine. This implies that protein expression starts before adding IPTG to the medium. To clearly see the formation of L apoferritin with the methionine analogues, specific reagents should be used to label azido and alkyne molecules. These hypothetical experiments are described in the chapter 7.

Other techniques of observing the incorporation of analogues into proteins have been reported. Coumarin was used to successfully label methionine analogues incorporated into mammalian[416] and bacterial[415] cells. Tirrell *et al.* reported the labelling of the azido-modified surface of *E. coli* with a biotinylated alkyne reagent.[417] Also, azido methionine analogues can be labelled through the Staudinger ligation where azido groups react with a phosphine reagent.[418] Bertozzi *et al.* have reported the use of these two techniques to label azides incorporated into proteins.[419–421]

6.4 Conclusion

The introduction of specific and highly functional groups into human apoferritin protein has been studied. Un-natural methionine amino acids with azido and alkyne groups were synthesised and used for the generation of apoferritin. These analogues were incorporated as substitutes for natural methionine residues using methionine auxotroph. Western blot analysis showed characteristic bands proving the synthesis of human apoferritin with natural methionine as well as with methionine analogues which led to the conclusion that the incorporation of new functional groups into apoferritin is possible and could be further developed for the binding of apoferritin to biomolecules.

Chapter 7

Conclusions and future work

To summarize, we have synthesised thiol-capped PbS quantum dots of different sizes in aqueous solution and reported their fluorescence properties. We observed a thermally activated increase of the emission linewidth and have rationalised this behaviour in terms of dephasing of the electronic states by interaction with longitudinal optical phonons.

PbS QDS have been incorporated in the cavity of the protein cage apoferritin by both reassembly and the ‘nanoreactor’ routes in aqueous solution. The AFt-PbS composites have a photoluminescence emission at $\sim 1 \mu\text{m}$, which is in the wavelength window of low absorbance of biological media. The apoferritin cages provide an exterior coat to the quantum dot that is amenable to the attachment of further proteins, saccharides or other biomolecules using standard conjugation chemistry.

AFt-PbS composites have been characterised by atomic force microscopy, transmission electron microscopy, energy dispersive X-ray, high angular dark field and electron energy loss techniques, selected area diffraction pattern, photoluminescence and polyacrylamide gel electrophoresis.

Further work will involve the purification of PbS quantum dots and PbS-encapsulated apoferritin composites by ultracentrifugation using speeds of 20,000/150,000 g for PbS/-AFt-PbS composites respectively.[198] The different density levels could be separated using a fractionator and further analysed using UV-near IR spectrophotometer. This

technique would allow the separation of empty AFt, non-encapsulated PbS dots and AFt-PbS composites.

PbS QDs could be used as energy acceptors in a bioluminescence resonance energy transfer where luciferin acts as the energy donor. BRET allows the emission of PbS QDs whilst negating the use of laser excitation, which could be harmful to the human body. Such a system could be further developed to produce photoluminescence emission for our AFt-PbS composites.

By using human apoferritin rather than horse spleen apoferritin, the immunogenicity of the systems could also be reduced for *in vivo* use once the toxicity of the composite has been determined. The Western blot technique indicated the possibility of the incorporation of methionine analogues into human apoferritin. To improve this result, we can perform other detection methods such as fluorescence using coumarin or a FLAG peptide.

In order to simplify the purification of H and L human homopolymer apoferritins and thus the purification of modified apoferritins with methionine analogues, the coding regions of H and L could be inserted into a vector bearing a polyhistidine-tag such as vector pET-30 (Figure 7.1). An His (histidine) tag is an amino acid motif in proteins that consists of at least six histidine residues, often at the *N*- or *C*-terminus of the protein.

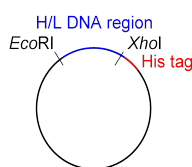


Figure 7.1: Simplified structure of plasmid pET-30a.

This His tag would make the purification steps easier, but may prevent the assembly process or inclusion of the QDs in the apoferritin cavity. Indeed, proteins synthesised with the His tag can be purified using affinity column chromatography as histidine binds to Ni^{2+} with strong selectivity. The tag can then be easily removed from the protein by the enzymes exopeptidase/endopeptidase which act to break peptide bonds. This

project would involve several steps: 1) polymerase chain reaction (PCR) (duplication of H/L inserts), 2) ligation of H/L inserts into pET-30a, 3) transformation into cells followed by expression and purification of the proteins and finally 5) removal of the His tag.

Primers to replicate the coding regions of H and L apoferritins were designed at the Molecular Foundry with the restriction enzymes *EcoRI* and *XhoI*:

Light chain apoferritin:

Sense primer:

CCTAGAATTCAGCTCCCAGATTCGTCAGAATTATTC, 'LCHFS1'

Antisense primer:

AATTCTCGAGTTAGTCGTGCTTGAGAGTGAGCCTTT, 'LCHFA1'

Heavy chain apoferritin:

Sense primer:

ACTGGAATTCATGACGACCGCGTCCACCTCGCAGGT, 'HCHFS1'

Antisense primer:

CCGGCTCGAGTTAGCTTTCATTATCACTGTCTCCCAGG, 'HCHFA1'

ACGGCTCGAGTTAGCTTTCATTATCACTGTCTCCCAGG, 'HCHFA2'

Chapter 8

Experimental techniques

8.1 Sample preparation

8.1.1 Preparation of apoferritin from ferritin

UV-visible spectra were performed on Varian Cary 100 Bio spectrophotometer thermostatted at 22 °C.

Dialyses bags were purchased from Medicell International Ltd (Visking type, MWCO 12-14,000 Da, size 11, 1.5 inches (38.1 mm) diameter, 56-59 mm width, 11.4 cm length). The pH used during the apoferritin synthesis was adjusted using the pH meter PIC-COLO HI 1290 with an amplified electrode from HANNA.

Horse spleen ferritin (85 mg mL⁻¹ and 111 mg mL⁻¹, sterile filtered solution of ferritin in 0.15 M NaCl) and sodium acetate were purchased from Sigma-Aldrich. The reducing agent mercaptoacetic acid (98%) was purchased from Lancaster.

Before use, dialysis bags were washed first with hot water and then with deionized water.

Apoferritin was prepared by using the procedure described in references [334, 335]. The native horse spleen ferritin protein (255 mg, 0.34 mmol) was diluted in 27 mL 0.1 M NaOAc buffer (2.7 mmol, pH 5.5) and placed into a dialysis bag. The protein was first dialysed against 0.1 M NaOAc buffer (820 mL, 0.082 mol) at pH 5.5 for 20 min under

N₂. Mercaptoacetic acid (0.03 M, 2 mL, 60 μ mol) was then added to the buffer and dialysis was continued for 2 hours against 0.1 M NaOAc pH 5.5 (820 mL, 0.082 mol); further mercaptoacetic acid (0.03 M, 1 mL, 30 μ mol) was added and dialysis continued for an additional hour against 0.1 M NaOAc pH 5.5 (820 mL, 0.082 mol); finally, the protein was dialysed against fresh 0.1 M NaOAc buffer (820 mL, 0.082 mol) at pH 5.5 for 20 minutes and purged with N₂. This process was repeated as necessary until reaching a complete decolouration of the ferritin solution.

Apo ferritin was then stored under N₂ at room temperature with 0.1 M NaOAc buffer (pH 5.5) refreshed every day.

8.1.2 Size exclusion chromatography

The purification by size exclusion chromatography was run on a Pharmacia Biotech ÄKTA explorer and FRAC-900 with a Superdex 75 column (< 100 kDa) of 30 cm height, 10 mm diameter and 24 mL bed volume.

First, the Superdex column was rinsed with the eluent consisting of a mixture of 0.1 M NaOAc pH 5.5 and 0.15 M NaCl.

Ferritin (8.5 mg mL⁻¹) and apo ferritin (8.5 mg mL⁻¹) samples were filtered on a filter unit (Sartorius Minisart 0.20 μ m) removing aggregates larger than 0.20 μ m. This filtration clarified the sample, which was a milky suspension before filtration and became a pale-yellow clear solution after elimination of the aggregates. Then, 0.25 mL of the protein samples (8.5 mg mL⁻¹) were injected into the column, and the conditions set at a pressure of 0.74 MPa, a flow rate of 0.5 mL min⁻¹, an absorption at 280 nm to detect the presence of protein units and the fractions collected had a volume of 0.5 mL.

8.1.3 SDS-PAGE of apo ferritin

Gel electrophoresis were run in a tank from ATTO Corporation (AE-6450) and a PowerPac Basic 300 V/400 mA/75 W from BioRad.

The staining solution was prepared as a solution of Coomassie Blue R250/Brilliant Blue (0.625 g) in 250 mL of methanol, 50 mL of acetic acid and 20 mL of water. Fast destain

solution and low destain solution were prepared as 40% methanol + 10% acetic acid and 10% methanol + 7.5-10% acetic acid respectively. Staining and destaining were performed by shaking on an orbital shaker KS250 (IKA Labortechnik, Germany).

TEMED (99%) was purchased from Sigma-Aldrich. Acrylamide-bisacrylamide (w/v 37.5:1) and the prestained protein marker used as the ladder during SDS-PAGE gel electrophoresis, broad range 6-175 kDa (aprotinin 7 kDa, lysozyme 17 kDa, CBD-BmFKBP13 25 kDa, triosephosphate isomerase 30 kDa, aldolase 46 kDa, MBP-CBD 58 kDa, MBP-paramyosin 80 kDa, MBP- β -galactosidase 175 kDa) were purchased from Severn Biotech Ltd and New England Biolabs respectively.

The SDS-PAGE gel was prepared by adding components in the following order:

1. Preparation of the 16% resolving gel (positively charged): to 3.64 mL of water were added successively 4 mL of Tris 1 M at pH 8.8, 160 μ L of SDS 10%, 8.2 mL of acrylamide 30%, 200 μ L of APS 10% and 20 μ L of TEMED. The ingredients were mixed gently and poured into the glass plate assembly. The gel was left to polymerise for 30 min and then some isopropanol was added to ensure a flat surface and exclude the air. After 15 min, the isopropanol was washed off with plenty of water.

2. Preparation of the 6% stacking gel: to 2.7 mL of water were added successively 1.25 mL of Tris 1 M at pH 6.8, 50 μ L of SDS 10%, 1 mL of acrylamide 30%, 80 μ L of APS 10% and 8 μ L of TEMED. The ingredients were mixed gently and poured onto the top of the resolving gel and insert the comb. The gel was left to polymerise for 30 min and then the comb was removed.

While preparing the gel, 4 samples of protein were prepared as following: 20 μ L of each solution (ferritin (8.5 mg mL⁻¹ and 4.25 mg mL⁻¹) and apoferritin (8.5 mg mL⁻¹ and 4.25 mg mL⁻¹)) were mixed with 20 μ L of the loading buffer (100 mM Tris-HCl pH 6.8, 4% SDS, 0.2% bromophenol blue, 20% glycerol, 4% 2-mercaptoethanol). The control sample was the prestained protein marker of broad range (6-175 kDa) which is a mixture of purified proteins covalently coupled to a blue dye that resolves to 8 bands of even intensity when electrophoresed. All samples were heated 1 min at 99 °C. The gel was installed in the tank and filled with electrophoresis buffer (28.8 g of glycine, 6

g of Tris, 20 mL of 10% SDS, pH 8.8). Each solution (20 μ L) were deposited on the gel, the top tank was installed and the voltage was set on 130 V (current 28 A) for 15 min and then set on the maximum voltage (300 V).

After the migration was completed (1 h 15), the gel was removed and stained with Coomassie Blue R250/Brilliant Blue (0.625 g in 250 mL of methanol, 50 mL of acetic acid and 20 mL of water) for 20 min. The gel was then destained 10 min in a fast destain and 48 h in a low destain.

8.1.4 BCA assay on ferritin and cationized ferritin

UV-Visible spectra were performed on an Agilent 845 spectrophotometer.

BCA assays were performed on a Tecan Sunrise instrument after incubation of the samples in a water bath Grant LTD 6G.

Bicinchoninic acid and copper(II) sulphate (4% (w/v) $\text{CuSO}_4 \cdot 5\text{H}_2\text{O}$ in water, pH \sim 4) were purchased from Sigma-Aldrich.

The protein cationized ferritin and TEMED (99%) were purchased from Sigma-Aldrich. The bicinchoninic assay is an assay employed in biochemistry to determine the level of protein in a given sample. The protein concentration is defined by a colour variation from green to purple depending on the amount of protein present which can then be measured by colorimetric techniques.[422]

Different conditions were tested:

1) Solutions of 0.5 mg mL^{-1} and 0.25 mg mL^{-1} of ferritin and cationized ferritin respectively were prepared in deionized water.

2) Solutions of ferritin (0.11, 0.21, 0.43, 0.64 and 0.85 mg mL^{-1}) and cationized ferritin (0.07, 0.14, 0.28 and 0.55 mg mL^{-1}) were prepared in 0.15 M NaCl solutions.

In both cases, the following solutions were prepared: a solution of 10 mL of bicinchoninic acid and 200 μ L of copper(II) sulphate.

Standards were composed of buffer NaOAc (0.1 M, pH 5.0) and BSA (1 mg mL^{-1} in 0.15 NaCl, $1.5 \cdot 10^{-5}$ mol) as described in the following table:

Standard	buffer (μL)	BSA (μL)	BSA final concentration (mg mL^{-1})
1	200	0	0
2	180	20	0.1
3	160	40	0.2
4	140	60	0.3
5	120	80	0.4
6	100	100	0.5

Then 800 μL of $\text{BCA-Cu}^{\text{II}}$ solution was added to each standard (200 μL) and to ferritin and cationized ferritin solutions (200 μL) as well. Incubation was followed for 30 min at 40 °C.

The protein concentrations of the different samples of ferritin and cationized ferritin were determined by measuring their absorbance at 562 nm and comparing the results with the absorbance of BSA protein standards.

8.1.5 ICP-MS analysis

Samples for ICP-MS analysis were diluted using a Microlab 500 series Hamilton and analysed under an ICP mass spectrometer X series II from Thermo electrocorporation. ICP-MS allows the determination of elements with mass ranges from 7 to 250. The apparatus consists of a plasma producing ions (ionization *via* helium plasma) and a mass spectrometer that separates and detects the ions. Commonly, the sample is introduced as a liquid solution and submitted to a nebulizer which converts the solution into an aerosol. The helium carrier gas is exposed to radio frequency inducing the following reaction $\text{He} \longrightarrow \text{He}^+ + \text{e}^-$ thus converting the gas into a plasma. The sample is then exposed to this plasma whose temperature is high enough to generate the formation of ions which are finally detected by the mass spectrometer.

Ferritin (85 mg mL^{-1}) and apoferritin (8.5 mg mL^{-1}) samples were prepared as solutions in the diluent for blood analysis (0.1% Triton, antifoam-B, 1% nitric acid) to avoid deposition of protein on any of the tubing as follows:

1. Control $\times 20,000$: 0.5 mL of $\times 1,000$ dilution of the control sample and addition of 9.5 mL of diluent to give overall $\times 20,000$ dilution *i.e.* expect 0.11 ppm = 110 ppb,
2. Test $\times 20,000$: 0.5 mL of $\times 1,000$ dilution of the test sample and addition of 9.5 mL of diluent to give overall $\times 20,000$ dilution,
3. Test $\times 5,000$: 2 mL of $\times 1,000$ dilution of the test sample and addition of 8 mL of diluent to give overall $\times 5,000$ dilution,
4. 2nd Test $\times 5,000$: repeat of above,

All samples were then analysed by the ICP mass spectrometer.

8.1.6 Solubility of ferritin and cationized ferritin in organic media

Centrifugations were performed using a C9405-VWR Galaxy 5D microcentrifuge.

In order to render water-soluble molecules dispersible into organic solvents, surfactants are commonly used to form micelles around the desired molecules. Transfer into dichloromethane, hexane and toluene were achieved using the widespread surfactant aerosol OT.

Solutions of protein-AOT were prepared with different molar ratios (moles of basic amino acids¹:moles of surfactant). For examples:

- A 1:1 molar ratio ferritin/AOT solution was prepared by mixing a solution of ferritin (commercially available, 85 mg mL⁻¹) and a solution of AOT (5 mg mL⁻¹, 1.12 10^{-5} mol) as following: a solution of AOT (4.3 10^{-4} mmol, 0.19 mg, 380 μ L) in the organic solvent (620 μ L of dichloromethane, hexane or toluene) was added to a solution of ferritin (4.3 10^{-4} mmol, 10 mg, 118 μ L) in buffer NaOAc (10 mM, 882 μ L, pH 3.8) and stirred at room temperature for 10 min, then centrifuged for 2 min at 4,611 *g* (8,000 rpm).
- A 1:1 ratio cationized ferritin/AOT solution was prepared using a solution of cationized ferritin (commercially available, 11 mg mL⁻¹) and the solution of AOT (5 mg mL⁻¹, 1.12 10^{-5} mol) as follow: a solution of AOT (8.35 10^{-4} mmol, 0.37 mg, 740 μ L) in the organic solvent (260 μ L of dichloromethane, hexane or toluene) was added

¹lysine, arginine + glutamic and aspartic acid residues assuming that they are all cationized.

to a solution of cationized ferritin ($9.38 \cdot 10^{-4}$ mmol, 10 mg, 909 μ L) in phosphate buffer (0.02 M, 91 μ L, pH 7.0) and stirred at room temperature for 10 min, then centrifuged for 2 min at 4,611 g (8,000 rpm).

The effective transfer of the cationized ferritin into the organic phase was observed by the significant orange colouration of the phase due to the presence of the protein. The aqueous and organic phases were analysed by measuring their absorbance over the range 190-900 nm.

8.1.7 Preparation of the cationized ferritin

Hexamethylenediamine (98%) and *N,N*-dimethyl-1,3-propanediamine, hexamethylenediamine (97%) were purchased from Sigma-Aldrich.

The modification of carboxyl groups of ferritin into amino groups was carried out following the conditions reported previously by Danon *et al.*[343]

- Formation of tertiary amines using *N,N*-dimethyl-1,3-propanediamine:

In a 50 mL beaker placed on a magnetic stirrer, 4 mL of a 2 M aqueous solution of DMPA (817.4 mg, 8 mmol) were placed. The pH was adjusted to pH 6.5 with 0.2 M HCl followed by the addition of 1 mL of a 10% ferritin solution (85 mg mL⁻¹, 0.1 mL in 0.9 mL 0.15 NaCl) was added to the previous DMPA solution.

To the orange solution obtained, the coupling agent EDC (400 mg, 2.08 mmol) was added and the pH maintained at 6.5 by addition of 0.2 M HCl with continuous stirring until no measurable changes in pH were recorded (~ 2 h). Finally, the reaction mixture was transferred to a stoppered vial and observed to be stable at *RT* for several months.

- Formation of primary amines using hexamethylenediamine:

In a 250 mL beaker placed on a magnetic stirrer, 4 mL of a 2 M aqueous solution of HMD (930 mg, 8 mmol) were placed. The pH was adjusted to 6.5 with 0.2 M HCl followed by the addition of 1 mL of a 10% ferritin solution (85 mg mL⁻¹, 0.1 mL in 0.9 mL 0.15 NaCl) was added to the previous HMD solution.

To the pale orange solution obtained, EDC (400 mg, 2.08 mmol) was added and the pH maintained at 6.5 by addition of 0.2 M HCl with continuous stirring until no measurable

changes in pH were recorded (~ 2 h). Then the reaction mixture was stored in a stoppered vial and found to be stable at RT for several months.

8.1.8 Determination of amine groups in the cationized ferritin

Incubations were performed in a WTB Binder incubator.

L-alanine (99%) was purchased from Sigma-Aldrich.

The level of cationization of ferritin was determined through a coupling reaction of the primary amine groups of the HMD-cationized ferritin with trinitrobenzene sulfonic acid.

First, a bicarbonate buffer NaHCO_3 (0.1 M, 11.76 g, 1,600 mL, pH 8.2) was prepared as a stock solution.

Alanine (4 mg, $4.5 \cdot 10^{-5}$ mol) standard was also made as stock solutions of $20 \mu\text{g mL}^{-1}$. Aliquots of this standard was dissolved in 0.1 M NaHCO_3 pH 8.2 to a concentration of 15.4, 10 and $5 \mu\text{g mL}^{-1}$.

The aqueous solution of cationized ferritin synthesized using hexamethyldiamine (5 mL) was dissolved into 0.1 M sodium bicarbonate pH 8.2 (5 mL) at a concentration of $50 \mu\text{g mL}^{-1}$.

TNBS (1 mL, $3.47 \cdot 10^{-3}$ mol, 5%) was dissolved in 0.1 M NaHCO_3 pH 8.2 (499 mL) at a concentration of 0.01% (w/v).

The blocking of the amino groups was carried out by adding 0.5 mL of TNBS solution to 1 mL of each sample (alanine, cationized ferritin). After mixture, all samples were incubated at 37°C for 2 h. Then 0.5 mL of 10% SDS and 0.25 mL of 1 N HCl were added to the samples.

The degree of cationization was determined at 335 nm by comparison between the cationized ferritin and alanine.

8.1.9 Synthesis of PbS quantum dots

For the preparation of PbS dots, lead(II) acetate trihydrate (99.99%), 2,3-dimercaptopropanol, monothioglycerol (98%), triethylamine (minimum 99%) and sodium sul-

phide were purchased from Sigma-Aldrich.

PbS nanocrystals were prepared following the procedure reported by Bakueva *et al.*[301] A 60 mL solution containing lead acetate trihydrate ($\text{Pb}(\text{CH}_3\text{COO})_2 \cdot 3\text{H}_2\text{O}$) (0.364 g, 0.96 mmol) and a mixture of thiols, *i.e.* thioglycerol (0.52 mL, 0.006 mol) and dithioglycerol (0.20 mL, 0.002 mol), which act as capping agents yielding a yellow solution of Pb:TGL:DTG 1:6:2 was prepared. The pH of the Pb^{2+} precursor solution was adjusted to 11.0 by adding dropwise triethylamine (~ 4 mL) until complete decolouration of the solution ($\text{pH} \sim 11.0$).

The synthesis of the dots was completed by adding a 0.1 M colourless solution of sodium sulphide Na_2S under vigorous stirring in deionized water in different molar ratios:

Molar ratio	Pb^{2+} precursor solution	Na_2S solution	Colour
1:0.1	15 mL	0.25 mL	pale brown
1:0.2	15 mL	0.5 mL	pale brown
1:0.3	15 mL	0.75 mL	pale brown
1:0.5	15 mL	1.25 mL	dark brown
1:0.6	15 mL	1.50 mL	dark brown
1:0.7	15 mL	1.75 mL	black

Samples 1:0.1 and 1:0.2 have been prepared as well with double the concentration of thiols. To 30 mL of Pb^{2+} solution, 0.26 mL of TGL and 0.10 mL of DTG were added followed by the addition of Et_3N to adjust the pH to 11.0. The synthesis of PbS quantum dots was completed by adding a solution of 0.1 Na_2S in deionized water as given above.

8.1.10 Synthesis of PbS-apoferritin composites

As described in the discussion part, AFt-PbS composites were synthesized using two routes of encapsulation.

For the nanoreactor route, we injected Pb^{2+} precursor solution (5 mL, 0.08 mol) and 0.1 M Na_2S (0.25 mL to 0.58 mL for Pb/S molar ratio (MR) varying from 1:0.3 to 1:0.7) to a solution of apoferritin in deionized water (5 mL, 0.09 mmol) at $\text{pH} = 5.5$

under vigorous stirring. The resulting solution was mixed for 15 minutes after the injection.

For the reassembly route, the pH of a 5 mL solution of preformed PbS QDs was adjusted to 9.5 by adding 0.1 M HCl. Apoferritin (5 mL, 0.09 mmol) was adjusted to pH = 2.0 by dialysis against a 0.1 M NaCl solution (150 mL), whose pH was controlled by 2 M HCl. Then disassembled apoferritin was added slowly to the preformed quantum dots.

Both syntheses were carried out under a N₂ atmosphere. The solutions were stored in a fridge at a temperature of 278 K under a N₂ atmosphere.

For the centrifugation experiment, the AFt-PbS solutions were centrifuged at 402 *g* for 5 min at 16 °C using a Rotor S4180 in a Beckman GS-15R centrifuge.

8.1.11 Synthesis of dihydrolipoic acid-capped PbS QDs

Reduced lipoic acid (98%) used for the surface modification of thiol-capped PbS was purchased from Sigma-Aldrich.

The preparation of DHLA-capped PbS nanocrystals was derived from the synthesis of PbS quantum dots reported in the previous paragraph by simply exchanging the DTG ligands by lipoic acid in order to obtain a molar ratio Pb:TGL:DHLA of 1:6:2.

The capping agent thioglycerol (0.52 mL, $1.5 \cdot 10^{-3}$ mol) was added to a Pb²⁺ precursor solution of lead(II) acetate trihydrate (0.379 g, $2.5 \cdot 10^{-4}$ mol) suspended in deionized water (60 mL) under N₂ yielding a yellow solution with a Pb:TGL MR of 1:6.

To 15 mL of the Pb:TGL solution, 100 mg of dihydrolipoic acid was added ($4.8 \cdot 10^{-4}$ mol, 1.134 g cm⁻³) and the pH adjusted to 11.0 with ~ 0.9 mL of triethylamine giving a colourless solution.

PbS synthesis was achieved by the addition of 0.1 M Na₂S solution in deionized water to the Pb precursor solution.

Pb/S molar ratios 1:0.3, 1:0.5 and 1:0.7 were synthesized:

Molar ratio	Pb ²⁺ precursor solution	Na ₂ S solution	Colour
1:0.3	5.3 mL	0.25 mL	dark brown
1:0.5	5.3 mL	0.41 mL	dark brown
1:0.7	5.3 mL	0.58 mL	dark brown

Dihydrolipoic acid-capped PbS quantum dots were observed to be stable for months when kept in the dark under N₂ at 4 °C.

8.1.12 Bioluminescence of firefly luciferase from *L. mingrelica*

BRET experiments were performed using the recombinant firefly luciferase from *Luciola mingrelica* (minimum 95%), synthetic D-luciferin and adenosine 5'-triphosphate (99%) from Sigma-Aldrich.

The reaction of luciferase, luciferin, ATP and O₂ results in the emission of light.

In our system, the luciferase (5 mg, 2 · 10⁶ light units per mg of protein) was used as supplied: a colourless solution of approximately 10 mg of protein per mL of 23 mM Tris acetate, 5 mM MgSO₄, 1 mM EDTA, and 50% (v/v) glycerol.

D-luciferin (5 mg, 1.65 · 10⁻⁵ mol) was diluted in Tris acetate buffer pH 6.5 to a concentration of 0.5 mg mL⁻¹ (faint yellow solution).

ATP (150 mg, 2.72 · 10⁻⁴ mol) was prepared as a 50 mg mL⁻¹ colourless solution in deionized water.

Luciferase was kept hermetically closed at -20 °C whilst D-luciferin and ATP were stored at 4 °C. During experiments, all solutions were kept on ice and D-luciferin was protected from light.

An ATP solution (0.25 mL) was added to 2.4 mL of D-luciferin solution in a plastic cuvette followed by the introduction of 1.3 µL of luciferase.

Bioluminescence measurements were carried out using a Perkin Elmer LS55B luminescence spectrometer thermostatted at 4 °C. Readings were taken over the range 250-800 nm at a speed of 500 nm min⁻¹ and slit width 5.0 nm in the absence of excitation. Luminescence measurements were carried out over 1 h without any noticeable change in the luminescence emission/intensity.

8.1.13 BRET experiments using firefly luciferase as the energy donor and PbS dots as energy acceptors

In order to create an efficient BRET, the donor and acceptor molecules have to be in close proximity. Thus, EDC was used as a coupling agent between luciferase and dihydrolipoic acid-capped PbS dots.

EDC (30 mg) was dissolved in deionized water (30 mg mL⁻¹).

For optimization of the coupling, EDC was introduced in a 1:1 molar ratio to DHLA. Thus to 0.5 mL of DHLA-capped PbS QDs (1.6 10⁻⁵ mol of DHLA), 0.1 mL of EDC solution and 1.3 μ L of luciferase solution (10 mg mL⁻¹) were introduced in the glass vial used for PL measurement and allowed to mix at room temperature for 2 min. Then, 0.25 mL of ATP solution (50 mg mL⁻¹) was added followed by the rapid addition of 2.4 mL of D-luciferin.

Photoluminescence measurement of the DHLA-capped was carried out in a fully dark room to avoid any excitation of the self-illuminating system luciferin-luciferase and run over the range 900-1,400 nm, integration time 60 s, increment 3 nm, slits 2.0. Bioluminescence measurements were carried out as described in section 8.1.12.

8.2 Measurements techniques

8.2.1 Luminescence spectroscopy

For PL experiments, the PbS quantum dots and AFt-PbS composites were studied as liquid solutions in a glass vial and deposited on a glass substrate. The optical excitation was provided by the 514.5 nm line of an Ar⁺ laser. The luminescence was dispersed by a 1/2 m monochromator and detected by a cooled (InGa)As photodiode.

Photoluminescence is a process in which a substance submitted to an excitation source (here Ar⁺ laser) will absorb photons. Electrons are delocalised to an higher energy level whose returns to the ground state are accompanied by the emission of photons. PL detects an optical transition from an excited electronic state to a lower electronic state, the time period between absorption and emission of photons is extremely short

(~ 10 ns).[423]

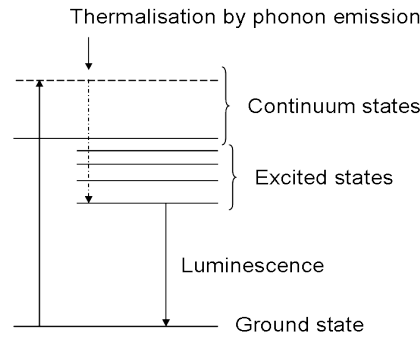


Figure 8.1: PL principle.

8.2.2 Atomic force microscopy

For Atomic Force Microscopy (AFM) measurements, the PbS QDs and AFt-PbS composites were dispersed onto a polished (100)-oriented *p*-type Si-substrate. Following the dilution of the solution with deionised water to 1 part in 100, a small drop was then deposited on the substrate and spin-coated for 30 seconds at a speed of 250 rph (revolutions per hour).

The atomic force microscope was invented in 1986 by Binnig, Quate and Gerber and is one of the foremost tools for imaging, measuring and manipulating matter at the nanoscale.[424]

Like all other scanning probe microscopes, the AFM utilises a sharp probe moving over the surface of a sample in a raster scan. In the case of the AFM, the probe is a tip on the end of a cantilever, which bends in response to the force between the tip and the sample.

The diagram illustrates how this works: as the cantilever flexes, the light from the laser is reflected onto the split photo-diode. By measuring the difference signal, changes in the bending of the cantilever can be measured. When the tip is brought into proximity of a sample surface, forces between the tip and the sample lead to a deflection of the cantilever according to Hooke's law.

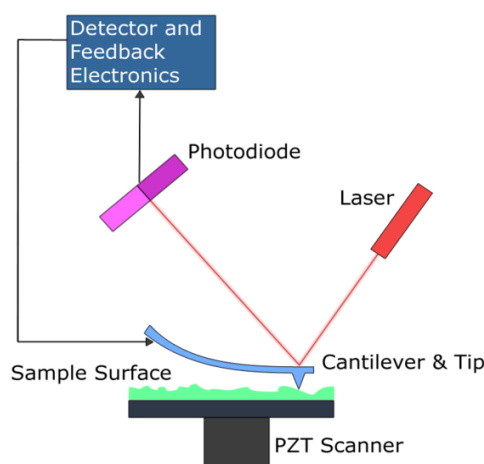


Figure 8.2: AFM principle.

8.2.3 Transmission electron microscopy

Transmission electron microscopy is an imaging technique based on the principle of diffraction of electrons and can reach an enlargement of 1,000,000. The TEM principle was developed by Max Knoll and Ernst Ruska in 1931.

The electron beam passes through the sample. Depending on the thickness, the density or the chemical composition of the sample, the electrons are more or less absorbed. The enlarged picture appears on a fluorescent screen or layer of photographic film or is detected by a CCD camera. This method is used in biology to observe cells or thin sections of organs.

8.2.4 High resolution transmission electron microscopy

High Resolution Transmission Electron Microscopy (HRTEM) images were recorded on a JEOL2011EX microscope operating at 200 kV.

High resolution transmission electron microscopy is an imaging mode of the TEM allowing the determination of the crystallographic structure of a given substance.

8.2.5 High angle annular dark field scanning transmission electron microscopy

High Angle Annular Dark Field Scanning Transmission Electron Microscopy (HAADF-STEM) was performed with a JEOL 2010F microscope operating at 200 keV and equipped with a GIF camera providing an energy resolution of about 1.6 eV.

High angle annular dark field scanning transmission electron microscopy is an imaging technique highly sensitive to the atomic number where scattered electrons are collected with an annular dark-field detector.

8.2.6 Electron energy loss spectroscopy

Electron Energy Loss Spectroscopy (EELS) was performed with a JEOL 2010F microscope operating at 200 keV and equipped with a GIF camera providing an energy resolution of about 1.6 eV.

Electron energy loss spectroscopy was developed by J. Hillier and R. F. Baker in 1944.[425] When a substance is exposed to an electron beam, a part of the electrons is inelastically scattered and which means these electrons lose their energy and have deflected paths. Elemental composition and atomic bonding state can be determined by measuring the amount of energy loss using an electron spectrometer.

8.2.7 Energy dispersive X-ray spectroscopy

Energy Dispersive X-Ray (EDX) spectra were recorded with an Oxford Instruments ultrathin-window EDX detector. The principle of EDX is based on the fact that each element of the periodic table have a unique response (unique electronic structure) to electromagnetic waves. The electrons of a substance exposed to a photon beam are excited which results in the formation of electron-hole. An electron of higher energy fills the hole and the excess of energy of that electron is released as an X-ray which creates a spectral line specific to the element.

8.3 Expression of H and L human apoferritins

The plasmids pET-11a (rHuHFt) and pET-26b(+) (rHuLFt) were kindly provided by Dr. Steven Aust from Utah State University. B834(DE3)pLysS competent cells were supplied by Novagen. LB broth and agarose were purchased from Sigma-Aldrich, Agar from Becton-Dickinson. Antibiotics were used from stocks: ampicillin (Amp) 100 mg mL⁻¹, chloramphenicol (Chl) 30 mg mL⁻¹, kanamycin (Kan) 50 mg mL⁻¹. IPTG (isopropyl β -D-1-thiogalactopyranoside) was used from a stock sample of 0.1 M. DNase I, RNase (31 kDa) I and lysozyme were used from stocks of 1,000 u mL⁻¹, 10 μ g mL⁻¹ and 100 ng mL⁻¹ respectively. Ferritin from human spleen Type V, 10 μ g mL⁻¹ in 0.15 M NaCl, 10 mM Tris, pH 8.0, containing 0.1% NaN₃ was purchased from Sigma-Aldrich.

Samples were shaken using a Thermolyne (AROS160) Adjustable Reciprocating Orbital Shaker at a speed of 250 rpm at 37 °C. Centrifuges apparatus are described when mentioned. Agarose gel and western blot were imaged using Bio-Rad Universal Hood II (50/60 Hz, 200 VA). Fast protein liquid chromatography (FPLC) was performed on a Amersham Åkta FPLC (loop 2mL, P-920 pump, UPC-900 detector, M-925 mixer, INV-907 inj. valve, FRAC-900 fraction collector, flow rate up to 20 ml min⁻¹, pressure 0-5MPa (0-725 psi)) and a HiPrep 16/10 DEAE FF from GE Healthcare.

Freeze-thaw cycles were performed using a Thermolyne liquid nitrogen monitor.

Samples heated at 37 °C before SDS-PAGE were heated on a Standard Heatblock from VWR Scientific Products.

OD₆₀₀ and OD₂₆₀ were measured on a UV/visible spectrophotometer DU530 from Beckman Coulter. Autoclaving was performed using Tuttnauer autoclaves.

8.3.1 Transformation of pET-11a and pET-26b(+) into B834(DE3)pLysS competent cells

LB medium was prepared as 2% LB broth and 1.5% Agar as follows: 500 mL ddH₂O + 10 g LB broth + 7.5 g Agar. The mixture was autoclaved at 121 °C for 20 min. Plates were prepared as indicated:

- for pET-11a: 500 mL LB medium + 100 μL of Amp ($20 \mu\text{g mL}^{-1}$) + 417 μL of Chl ($25 \mu\text{g mL}^{-1}$).
- for pET-26b(+): 500 mL LB medium + 500 μL of Kan ($50 \mu\text{g mL}^{-1}$) + 417 μL of Chl ($25 \mu\text{g mL}^{-1}$).

Both plasmids were dissolved into 50 μL ddH₂O. 2 μL of each plasmid were added to 50 μL of competent B834(DE3)pLysS cells. The mixtures were left on ice for 30 min, heat-shocked at 42 °C for 30 s and back on ice for 2 min. 170 μL of SOC (super optimal catobolite) medium was added to each cell/plasmid sample and place under shaking at 37 °C for 20 min. Cultures were finally spread over plates using glass beads and incubated at 37 °C overnight under shaking.

Positive transformants were grown in 5 mL of LB medium containing 4.17 μL of Chl ($25 \mu\text{g mL}^{-1}$) and their respective antibiotics, 1 μL Amp ($20 \mu\text{g mL}^{-1}$) for pET-11a and 5 μL Kan ($50 \mu\text{g mL}^{-1}$) for pET-26b(+).

Each plasmid DNA (2 mL) were purified using the QIAgen spin miniprep kit and a microcentrifuge. The concentration of the protein was determined by measuring the optical density (OD) at 260 nm: the H apoferritin produced had a concentration of 309 $\mu\text{g mL}^{-1}$ and L apoferritin had a concentration of about 380 $\mu\text{g mL}^{-1}$.

pET-11a and pET-26b(+) (500 μL each) containing genes coding for H and L apofer-ritins respectively were kept in 50% glycerol (500 μL) at -80°C .

Samples were sent for sequencing to the UC Berkeley DNA Sequencing Facility.[426]

8.3.2 Agarose gel of over-expressed H and L apoferritins

The gel electrophoresis apparatus used was a OWI separation system (model B1A 0-150 V/0-100 mA) with a power supply FB300 from Fisher Scientific.

The protein ladder 1 kb was purchased from New England Biolabs.

The protein expression was monitored on a 1% agarose gel.

The gel was prepared as followed: 180 mL of ddH₂O, 2 g of agarose, 20 mL of $10 \times$ TAE (Tris-Acetate-EDTA) to give $1 \times$ TAE. The mixture was heated for 2.5 min at maximum power in a microwave. It was then allowed to cool down and 3 μL of EtBr

(stock of 10 mg mL⁻¹) was added.

The running buffer was made by adding 50 mL of 10 × TAE to 450 mL of ddH₂O and a few mL of 1 × TAE + EtBr.

The following samples were loaded onto the gel and the voltage set to 120 V for 1 h 15:

	H1	L1	H2	L2
pET-11a (μL)	4	/	2	/
pET-26b(+) (μL)	/	4	/	2
TAE (μL)	/	/	6	6
Loading dye (μL)	1	1	2	2
Total (μL)	5	5	10	10

8.3.3 Large-scale expression of H and L apoferritins

pET-11a and pET-26b(+) vectors kept at −80 °C were used to inoculate 100 mL LB medium + 83.3 μL Chl (25 μg mL⁻¹) containing the respective antibiotics: 25 μL Amp (20 μg mL⁻¹) for rHuHFt (pET-11a) and 100 μL Kan (50 μg mL⁻¹) for rHuLFt (pET-26b(+)). The cultures were grown overnight at 37 °C under shaking.

The growth was controlled by the OD at 600 nm. After 4 h of growth, IPTG (133 μL, 0.1 M) was added at a final concentration of 37.5 g mL⁻¹ to induce the expression of the proteins. After 2 h 30, the cells were sedimented for 10 min at 3,080 g (5,000 rpm) at 4 °C using an Avanti centrifuge J26 XP from Beckman Coulter with a J-lite series JLA-10.500 10,000 rpm rotor. The supernatant was removed and the cell pellet was kept at −80 °C.

8.3.4 SDS-PAGE of the large-scale expression culture of H and L apoferritins

The gel electrophoresis apparatus used was Bio-Rad Criterion 80 W/600 V with power supply PowerPac HV 5,000 V/500 mA/400 W from Bio-Rad.

The 2 × loading buffer was supplied by Shelton Scientific Incorporation. β-Mercaptoethanol and Kaleidoscope protein ladder and 10 × Tris/Gly buffer were supplied by Bio-Rad.

Imperial protein stain was supplied by Thermo Scientific.

The 15% Tris-HCl precast gel was purchased from Criterion Bio-Rad (1 mm, 12 + 2 wells comb, 45 μL). The protein buffer was supplemented by adding 1% of β -mercaptoethanol (3 μL) to 300 μL of $2 \times$ loading buffer.

The following samples were prepared and heated at 95 °C for 10 min: 50 μL ddH₂O + 50 μL loading buffer + small amount of H/L cultures frozen at −80 °C. The samples were loaded onto the precast gel and the tank was filled with the running buffer 1 \times Tris/Gly/SDS (1 \times). The gel was run at 200 V for 1 h 10. The gel was washed 3 times by shaking 5 min with 100 mL ddH₂O and stained by shaking with Imperial protein stain for 1 h. The gel was finally destained by shaking with 200 mL ddH₂O for 1 h 30.

8.3.5 Purification of large-scale expression culture of H human apo-ferritin

The purification was followed as described by Grace *et al.* in reference [409]. Cell pellets were resuspended in 50 mM Tris pH 7.0 with DNase I (20 $\mu\text{g mL}^{-1}$), RNase I ($\mu\text{g mL}^{-1}$) and lysozyme (1 mg mL^{-1}). After 30 min on ice, the suspensions were subjected to three freeze-thaw cycles (liquid nitrogen for 5 min - water bath at *RT* for 20 min) and centrifuged at 30,000 g (19,562 rpm, JA-20 rotor) for 30 min to remove cellular debris. The supernatant was concentrated using a Minicon Ultra-4 centrifugal filter device from Millipore and centrifuged at 3,320 g (4,000 rpm) at *RT* using a Sorvall RT7 Plus centrifuge with rotor RTH-750 until the solution was concentrated to 2 mL. The ultrafiltrate was centrifuged for 10 min at 4,000 g (6,131 rpm) at 4 °C using centrifuge 5417R rotor F 45-30-11 from Eppendorf and then filtered using Millex GP syringe-driven filter unit 0.22 μm from Millipore.

The suspension was finally applied to a HiPrep 16/10 DEAE FF-Sepharose Fast Flow anion exchange column. First the FPLC tubing was rinsed with ddH₂O (25 mL) at 5 mL min^{-1} followed by 0.50 mM Tris pH 7.0 containing 300 mM NaCl (5mL) at 5 mL min^{-1} . The column was then equilibrated with 50 mM Tris pH 7.0 (100 mL) at 5 mL

min⁻¹. H human apoferritin (2 mL) was injected and eluted with a stepwise gradient from 50 to 300 mM NaCl in 50 mM Tris pH 7.0. at 3 mL min⁻¹.

The apoferritin-rich fractions were analysed by SDS-PAGE (15% Tris-HCl precast gel) following the procedure described in section 8.3.4. The following samples were prepared and heated at 95 °C for 10 min:

- fractions B12 to C2 + C5 to C9: 17.5 μ L fraction + 17.5 μ L loading buffer,
- fractions C3 and C4: 8.75 μ L fraction + 8.75 μ L ddH₂O + 17.5 μ L loading buffer,
- human spleen ferritin: 2 μ L ferritin + 34 μ L ddH₂O + 36 μ L loading buffer.

The gel was run at 200 V for 1 h, stained and destained as described previously.

8.4 Incorporation of methionine analogues into H and L human apoferritins

M9 minium salts medium (5 \times), glucose (99%) ZnSO₄·7H₂O (99%), MnSO₄·7H₂O (99%), CuSO₄, CoSO₄·7H₂O (98%), H₃BO₃ (99%), Na₂MoO₄·2H₂O (99.5%), thiamine-HCl and the kit of 10 essential amino acids (1 g of each: L-arginine hydrochloride, L-histidine hydrochloride, L-isoleucine, L-leucine, L-lysine hydrochloride, L-methionine, L-phenylalanine, L-threonine, L-tryptophan, L-valine) were purchased from Sigma-Aldrich. CaCl₂, MgSO₄·7H₂O were supplied by Fisher.

Samples were shaken using a Thermolyne (AROS160) Adjustable Reciprocating Orbital Shaker at a speed of 250 rpm at 37 °C and a refrigerated incubator shaker Innova 4230 from New Brunswick Scientific at a speed of 250 rpm at 20 °C.

8.4.1 Preparation of M9 media

The M9 medium was modified by adding a series of salts and glucose as described below:

1. 200 mL M9 medium (5 \times) were mixed with 800 mL of ddH₂O.
2. Salts were added:

Salts	Stocks solutions (M)	Volume added to M9	Final concentration
CaCl ₂	0.1	1 mL	0.1 mM
ZnSO ₄ ·7H ₂ O	0.1	80 μ L	8.0 μ M
MnSO ₄ ·7H ₂ O	0.1	100 μ L	10.0 μ M
MgSO ₄ ·7H ₂ O	1	1 mL	1.0 mM
CuSO ₄	0.1	20 μ L	2.0 μ M
CoSO ₄ ·7H ₂ O	0.1	20 μ L	2.0 μ M
H ₃ BO ₃	0.1	10 μ L	1.0 μ M
Na ₂ MoO ₄ ·2H ₂ O	0.1	10 μ L	1.0 μ M
Thiamine-HCl	0.001	0.3 μ L	0.3 nM

3. Glucose (2%, 20 g) was added.
4. Amino acids (L-arginine hydrochloride, L-histidine hydrochloride, L-isoleucine, L-leucine, L-lysine hydrochloride, L-phenylalanine, L-threonine, L-tryptophan, L-valine) were added at 120 mg mL⁻¹.
5. Mixture was stirred at *RT*.
6. Three M9-based solutions of 100 mL were prepared to each of which was added a different methionine analogue at a concentration of 120 mg mL⁻¹.
7. M9 medium (1,000 mL) with methionine amino acid was prepared using the same procedure.
8. M9 medium (1,000 mL) without amino acids was prepared using the same procedure.

All media were filtered using Express Plus 0.22 μ m filters from Millipore.

8.4.2 Expression of H and L human apoferritins containing methionine analogues.

The protein expression was achieved as described by van Hest *et al.* in reference [401]. pET-11a and pET-26b(+) vectors kept at -80°C were used to inoculate 5 mL M9 medium (with methionine) + 4.2 μL Chl ($25\text{ }\mu\text{g mL}^{-1}$) containing the respective antibiotics: 1 μL Amp ($20\text{ }\mu\text{g mL}^{-1}$) for rHuHFt (pET-11a) and 5 μL Kan ($50\text{ }\mu\text{g mL}^{-1}$) for rHuLFt (pET-26b(+)). The cultures were grown overnight at 37°C under shaking. Small-scale expression was achieved by adding 4 mL of the overnight cultures to M9 medium with all amino acids except methionine (50 mL) + 46 μL Chl ($25\text{ }\mu\text{g mL}^{-1}$) containing the respective antibiotics: 11 μL Amp ($20\text{ }\mu\text{g mL}^{-1}$) for rHuHFt and 55 μL Kan ($50\text{ }\mu\text{g mL}^{-1}$) for rHuLFt. The cultures were grown overnight at 37°C under shaking.

The growth was controlled by the OD at 600 nm until the turbidity reached a value of ~ 0.4 (maximum OD observed in theses conditions). After 5 h, cells were sedimented for 10 min at 3,320 g (4,000 rpm) at *RT* using a Sorvall RT7 Plus centrifuge with rotor RTH-750. The supernatant was removed and the cell pellet was resuspended and washed twice with M9 without amino acids (20 mL). After removal of the supernatant, the cell pellet was dissolved in 50 mL of M9 without amino acids and divided into 10 5 mL-aliquots and sedimented.

The aliquots were prepared by resuspending the cell pellets in 5 mL of M9 medium containing the methionine analogue at 120 mg mL^{-1} and different protein expressions were induced as following:

Protein H or L apoferritin	Incubation	IPTG	Incubation	OD ₆₀₀	
	T (°C)	(mM)	time (h)	H	L
positive control	37	0.75	2	0.410	0.451
negative control	37	0.75	2	0.344	0.323
aminohexynoic acid	37	0.75	2	0.387	0.368
azidohomoalanine	37	0.75	2	0.439	0.353
azidonorleucine	37	0.375	2	0.379	0.332
azidonorleucine	37	1.5	2	0.372	0.437
azidonorleucine	37	0.75	2	0.426	0.371
azidonorleucine	37	0.75	4	0.401	0.354
azidonorleucine	20	0.75	o/n	0.361	0.421

All samples were sedimented at 3,000 g for 10 min and the cell pellets were kept at -80°C .

8.5 Western blot of L human apoferritin containing methionine analogues

The gel electrophoresis apparatus used was Bio-Rad Criterion 80 W/600 V with power supply PowerPac HV 5,000 V/500 mA/ 400 W from Bio-Rad.

Protein ladder Precision Plus Dual Color Standards and Tween 20 were supplied by Bio-Rad. Ponceau S solution (0.1% Ponceau S (w/v) in 5% acetic acid (v/v)) and non-fat dry milk were purchased from Sigma-Aldrich. L apoferritin antibody and goat anti-rabbit IgG-HRP were purchased from Santa Cruz Biotechnology.

Shaking was performed on Speci-Mix from Thermolyne.

The following solutions were prepared:

- Tris-buffered saline ($1 \times$ TBS) (20 mM Tris, 150 mM NaCl, pH 7.5): 30 mL 5 M NaCl, 20 mL 1 M Tris pH 7.4, 950 mL ddH₂O.
- Wash solution (TTBS) (20 mM Tris, 150 mM NaCl, 0.05% Tween 20, pH 7.5): 0.5 mL Tween 20, 1 L TBS.

- Blocking solution (5% non-fat dry milk in TTBS): 60 mL TTBS, 3 g non-fat dry milk.
- Transfer buffer (20% v/v methanol): 200 mL MeOH, 100 mL $10 \times$ Tris/Gly, 700 mL ddH₂O.

Cell pellets from section 8.4.2 were resuspended in 200 μ L of ddH₂O + 200 μ L of loading buffer + 0.1% β -mercaptoethanol and heated 2 times 10 min at 95 °C to allow the cells to resuspend properly.

The apparatus was set up as described in the instruction manual of the Criterion Blotter from Bio-Rad and the transfer was run at 100 V for 30 min in a cold room.

Samples (5 μ L) and protein ladder were loaded on SDS-PAGE 15% and the tank was filled up with buffer $1 \times$ Tris/Gly/SDS and run at 200 V for 1 h 15.

The membrane was rinsed with ddH₂O, stained with Ponceau S for 5 min under shaking and destained with ddH₂O. The membrane was then placed in a sealed bag with anti-L ferritin antibody solution (5 mL of anti-LF in blocking solution, dilution factor 1:200) and placed under shaking in a cold room for 30 min. The membrane was washed 4 times with ddH₂O and placed back in a sealed bag containing the secondary antibody anti-rabbit IgG (5 mL of goat anti-rabbit IgG:sc2004 in blocking solution, dilution factor 1:2,000) and placed under shaking in a cold room for 30 min.

The protein bands were finally visualized using a luminescent substrate. The membrane was equilibrated in 12 mL of 1:1 ratio luminol/enhancer and peroxide buffer for 5 min and placed in a plastic film for imaging.

References

- [1] Chalfie, M.; Tu, Y.; Euskirchen, G.; Ward, W. W. and Prasher, D. C., *Science* **1994**, *263*, 802-805.
- [2] Farinas, J.; Verkman, A. S., *J. Biol. Chem.* **1999**, *274*, 7603-7606.
- [3] Miyawaki, A.; Sawano, A.; Kogure, T., *Nat. Cell. Biol.* **2003**, S1-7.
- [4] Hainfeld, J. F. and Powell, R. D. and Hacker, G. W., *Nanobiotechnology*, Niemeyer, C. M. and Mirkin, C. A., Ed. Wiley-VCH: Weinheim, **2004**; pp 353-385.
- [5] <http://www.nanoprobes.com/GoldLip.html> (May **2008**).
- [6] Reed, M. A., *Sci. Am.* January, **1993**, pp 118-123.
- [7] Whitesides, G. M., *Nat. Biotechnol.* **2003**, *21*, 1161-1165.
- [8] Paull, R.; Wolfe, J.; Hébert, P.; Sinkula, M., *Nat. Biotechnol.* **2003**, *21*, 1144-1147.
- [9] Mazzola, L., *Nat. Biotechnol.* **2003**, *21*, 1137-1143.
- [10] Colvin, V. L., *Nat. Biotechnol.* **2003**, *21*, 1166-1170.
- [11] Hoet, P. H.; Bröske-Hohlfeld, I.; Salata, O. V., *J. Nanobiotechnol.* **2004**, *2*, 12.
- [12] Maysinger, D., *Org. Biomol. Chem.* **2007**, *5*, 2335-2342.
- [13] Alivisatos, A. P., *Science* **1996**, *271*, 933-937.
- [14] Alivisatos, A. P., *J. Phys. Chem.* **1996**, *100*, 13226-13239.

- [15] Alivisatos, A. P., *Endeavour* **1997**, *21*, 56-60.
- [16] Qu, L.; Peng, X., *J. Am. Chem. Soc.* **2002**, *124*, 2049-2055.
- [17] Rogach, A. L.; Talapin, D. V.; Weller, H., *Colloids and Colloid Assemblies*, Caruso, F., Ed. Wiley-VCH: Weinheim, **2003**; pp 52-95.
- [18] Michalet, X.; Pinaud, F. F.; Bentolila, L. A.; Tsay, J. M.; Doose, S.; Li, J. J.; Sundaresan, G.; Wu, A. M.; Gambhir, S. S.; Weiss, S., *Science* **2005**, *307*, 538-544.
- [19] Medintz, I. L.; Uyeda, H. T.; Goldman, E. R.; Mattoussi, H., *Nat. Mater.* **2005**, *4*, 435-446.
- [20] Schröck, E.; du Manoir, S.; Veldman, T.; Schoell, B.; Wienberg, J.; Ferguson-Smith, M. A.; Ning, Y.; Ledbetter, D. H.; Bar-Am, I.; Soenksen, D.; Garini, Y.; Ried, T., *Science* **1996**, *273*, 494-497.
- [21] Leevy, W. M.; Gammon, S. T.; Jiang, H.; Johnson, J. R.; Maxwell, D. J.; Jackson, E. N.; Marquez, M.; Piwnica-Worms, D.; Smith, B. D., *J. Am. Chem. Soc.* **2006**, *128*, 16476-16477.
- [22] Sutherland, A. J., *Curr. Opin. Sol. State and Mat. Sci.* **2002**, *6*, 365-370.
- [23] <http://www.qdots.com> (April **2008**).
- [24] <http://www.evidenttech.com> (April **2008**).
- [25] <http://www.invitrogen.com> (June **2008**).
- [26] <http://www.nanocotechnologies.com> (April **2008**).
- [27] Chan, W. C.; Maxwell, D. J.; Gao, X.; Bailey, R. E.; Han, M.; Nie, S., *Curr. Opin. Biotechnol.* **2002**, *13*, 40-46.
- [28] Gao, X.; Nie, S., *Nanobiotechnology*, Niemeyer, C. M.; Mirkin, C. A., Ed. Wiley-VCH: Weinheim, **2004**; pp 343-352.

- [29] Zhang, J.; Campbell, R. E.; Ting, A. Y.; Tsien, R. Y., *Nat. Rev. Mol. Cell. Biol.* **2002**, *3*, 906-918.
- [30] Ormö, M.; Cubitt, A. B.; Kallio, K.; Gross, L. A.; Tsien, R. Y.; Remington, S. J., *Science* **1996**, *273*, 1392-1395.
- [31] Yang, F.; Moss, L. G.; Phillips, G. N., Jr., *Nat. Biotechnol.* **1996**, *14*, 1246-1251.
- [32] Guzelian, A. A.; Banin, U.; Kadacanich, A. V.; Peng, X.; Alivisatos, A. P., *Appl. Phys. Lett.* **1996**, *69*, 1432-1434.
- [33] Bawendi, M. G., *Sol. Stat. Commun.* **1998**, *107*, 709.
- [34] Manna, L.; Scher, E. C.; Alivisatos, A. P., *J. Clus. Sci.* **2002**, *13*, 521-532.
- [35] Murray, C. B.; Norris, D. J.; Bawendi, M. G., *J. Am. Chem. Soc.* **1993**, *115*, 8706-8715.
- [36] Murray, C. B.; Kagan, C. R.; Bawendi, M. G., *Annu. Rev. Mater. Sci.* **2000**, *30*, 545-610.
- [37] Peng, Z. A.; Peng, X., *J. Am. Chem. Soc.* **2001**, *123*, 183-184.
- [38] Bailey, R. E.; Smith, A. M.; Nie, S., *Physica E* **2004**, *25*, 1-12.
- [39] Kortan, A. R.; Hull, R.; Opila, R. L.; Bawendi, M. G.; Steigerwald, M. L.; Carroll, P. J.; Brus, L. E., *J. Am. Chem. Soc.* **1990**, *112*, 1327-1332.
- [40] Hines, M. A.; Guyot-Sionnest, P., *J. Phys. Chem.* **1996**, *100*, 468-471.
- [41] Peng, X.; Wickham, J.; Alivisatos, A. P., *J. Am. Chem. Soc.* **1998**, *120*, 5343-5344.
- [42] Rajh, T.; Mićić, O. I.; Nozik, A. J., *J. Phys. Chem.* **1993**, *97*, 11999-12003.
- [43] Vossmeier, T.; Katsikas, L.; Giersig, M.; Popovic, I. G.; Diesner, K.; Chemseddine, A.; Eychmüller, A.; Weller, H., *J. Phys. Chem.* **1994**, *98*, 7665-7673.

- [44] Rogach, A. L.; Kornowski, A.; Gao, M.; Eychmüller, A.; Weller, H., *J. Phys. Chem. B* **1999**, *103*, 3065-3069.
- [45] Gaponik, N.; Talapin, D. V.; Rogach, A. L.; Hoppe, K.; Shevchenko, E. V.; Kornowski, A.; Eychmüller, A.; Weller, H., *J. Phys. Chem. B* **2002**, *106*, 7177-7185.
- [46] Rogach, A.; Kershaw, S.; Burt, M.; Harrison, M.; Kornowski, A.; Eychmüller, A.; Weller, H., *Adv. Mater.* **1999**, *11*, 552-554.
- [47] Michalet, X.; Pinaud, F.; Lacoste, T. D.; Dahan, M.; Bruchez, M. P.; Alivisatos, A. P.; Weiss, W., *Single Mol.* **2001**, *2*, 261-276.
- [48] Klarreich, E., *Nature* **2001**, *413*, 450-452.
- [49] Bentolila, L. A.; Weiss, S., *Physics World* **2003**, *16*, 23-24.
- [50] Gao, X.; Nie, S., *Trends Biotechnol.* **2003**, *21*, 371-373.
- [51] Seydel, C., *Science* **2003**, *300*, 80-81.
- [52] Baron, R.; Willner, B.; Willner, I., *Chem. Commun.* **2007**, 323-332.
- [53] Salata, O., *J. Nanobiotechnology* **2004**, *2*, 1-14.
- [54] Jain, K. K., *Clin. Chim. Acta* **2005**, *358*, 37-54.
- [55] Vashist, S. K.; Tewari, R.; Bajpai, R. P.; Bharadwaj, L. M.; Raiteri, R., *Online J. Nanotechnol.* **2006**, 1-14.
- [56] Chan, W. C.; Nie, S., *Science* **1998**, *281*, 2016-2018.
- [57] Weiss, S., *Science* **1999**, *283*, 1676-1683.
- [58] Härmä, H.; Soukka, T.; Lövgren, T., *Clin. Chem.* **2001**, *47*, 561-568.
- [59] Azzazy, H. M.; Mansour, M. M.; Kazmierczak, S. C., *Clin. Chem.* **2006**, *52*, 1238-1246.
- [60] Alivisatos, A. P., *Pure Appl. Chem.* **2000**, *72*, 3-9.

- [61] Niemeyer, C. M., *Science. Angew. Chem. Int. Ed. Engl.* **2001**, *40*, 4128-4158, *Angew. Chem.* **2001**, *113*, 4254-4287.
- [62] Dahan, M.; Laurence, T.; Pinaud, F.; Chemla, D. S.; Alivisatos, A. P.; Sauer, M.; Weiss, S., *Opt. Lett.* **2001**, *26*, 825-827.
- [63] Murphy, C. J., *Anal. Chem.* **2002**, *74*, 520A-526A.
- [64] Parak, W. J.; Gerion, D.; Pellegrino, T.; Zanchet, D.; Micheel, C.; Williams, S. C.; Boudreau, R.; Le Gros, M. A.; Larabell, C. A.; Alivisatos, A. P., *Nanotechnology* **2003**, *14*, R15-R27.
- [65] Penn, S. G.; He, L.; Natan, M. J., *Curr. Opin. Chem. Biol.* **2003**, *7*, 609-615.
- [66] Jaiswal, J. K.; Simon, S. M., *Trends Cell. Biol.* **2004**, *14*, 497-504.
- [67] Green, M., *Angew. Chem. Int. Ed. Engl.* **2004**, *43*, 4129-4131, *Angew. Chem.* **2004**, *116*, 4221-4223.
- [68] Smith, A. M.; Nie, S., *Analyst* **2004**, *129*, 672-677.
- [69] Gao, X.; Yang, L.; Petros, J. A.; Marshall, F. F.; Simons, J. W.; Nie, S., *Curr. Opin. Biotechnol.* **2005**, *16*, 63-72.
- [70] Pathak, S.; Cao, E.; Davidson, M. C.; Jin, S.; Silva, G. A., *J. Neurosci.* **2006**, *26*, 1893-1895.
- [71] Fortina, P.; Kricka, L. J.; Surrey, S.; Grodzinski, P., *Trends Biotechnol.* **2005**, *23*, 168-173.
- [72] Kim, S.; Lim, Y. T.; Soltesz, E. G.; De Grand, A. M.; Lee, J.; Nakayama, A.; Parker, J. A.; Mihaljevic, T.; Laurence, R. G.; Dor, D. M.; Cohn, L. H.; Bawendi, M. G.; Frangioni, J. V., *Nat. Biotechnol.* **2004**, *22*, 93-97.
- [73] Jiang, W.; Papa, E.; Fischer, H.; Mardyani, S.; Chan, W. C., *Trends Biotechnol.* **2004**, *22*, 607-609.

- [74] Uren, R. F., *Nat. Biotechnol.* **2004**, *22*, 38-39.
- [75] Sargent, E. H., *Adv. Mater.* **2005**, *17*, 515-522.
- [76] Arya, H.; Kaul, Z.; Wadhwa, R.; Taira, K.; Hirano, T.; Kaul, S. C., *Biochem. Biophys. Res. Commun.* **2005**, *329*, 1173-1177.
- [77] König, K., *J. Microsc.* **2000**, *200*, 83-104.
- [78] Taton, T. A., *Trends Biotechnol.* **2002**, *20*, 277-279.
- [79] Chan, W. C. W.; Gao, X.; Nie, S., *Colloids and Colloid Assemblies*, Caruso, F., Ed. Wiley-VCH: Weinheim, **2003**; pp 494-506.
- [80] Niemeyer, C. M., *Angew. Chem. Int. Ed. Engl.* **2003**, *42*, 5796-5800, *Angew. Chem.* **2003**, *115*, 5974-5978.
- [81] Alivisatos, P., *Nat. Biotechnol.* **2004**, *22*, 47-52.
- [82] Mattoussi, H.; Medintz, I. L.; Clapp, A. R.; Goldman, E. R.; Jaiswal, J. K.; Simon, S. M.; Mauro, J. M., *JALA* **2004**, *9*, 28-32.
- [83] Riegler, J.; Nann, T., *Anal. Bioanal. Chem.* **2004**, *379*, 913-919.
- [84] Katz, E.; Willner, I., *Angew. Chem. Int. Ed. Engl.* **2004**, *43*, 6042-6108, *Angew. Chem.* **2004**, *116*, 6166-6235.
- [85] Parak, W.; Pellegrino, T.; Plank, C., *Nanotechnology* **2005**, *16*, R9-R25.
- [86] Blum, A. S.; Carissa, M. S.; Wilson, C. D.; Whitley, J. L.; Moore, M. H.; Sapsford, K. E.; Lin, T.; Chatterji, A.; Johnson, J. E.; Ratna, B. R., *Nanotechnology* **2006**, *17*, 5073-5079.
- [87] Costa-Fernández, J. M.; R., P.; Sanz-Medel, A., *Trends Anal. Chem.* **2006**, *25*, 207-218.
- [88] Correa-Duarte, M. A.; Giersig, M.; Liz-Marzán, L. M., *Chem. Phys. Lett.* **1998**, *286*, 497-501.

- [89] Bruchez, M., Jr.; Moronne, M.; Gin, P.; Weiss, S.; Alivisatos, A. P., *Science* **1998**, *281*, 2013-2016.
- [90] Goldman, E. R.; Balighian, E. D.; Mattoussi, H.; Kuno, M. K.; Mauro, J. M.; Tran, P. T.; Anderson, G. P., *J. Am. Chem. Soc.* **2002**, *124*, 6378-6382.
- [91] Gerion, D.; Pinaud, F.; Williams, S. C.; Parak, W. J.; Zanchet, D.; Weiss, S.; Alivisatos, A. P., *J. Phys. Chem. B* **2001**, *105*, 8861-8871.
- [92] Parak, W. J.; Gerion, D.; Zanchet, D.; Woerz, A. S.; Pellegrino, T.; Micheel, C.; Williams, S. C.; Seitz, M.; Bruehl, R. E.; Bryant, Z.; Bustamante, C.; Bertozzi, C. R.; Alivisatos, A. P., *Chem. Mater.* **2002**, *14*, 2113-2119.
- [93] Gerion, D.; Parak, W. J.; Williams, S. C.; Zanchet, D.; Micheel, C. M.; Alivisatos, A. P., *J. Am. Chem. Soc.* **2002**, *124*, 7070-7074.
- [94] Chunyang, Z.; Hui, M.; Shuming, N.; Yao, D.; Lei, J.; Dieyan, C., *Analyst* **2000**, *125*, 1029-1031.
- [95] Winter, J. O.; Liu, T. Y.; Korgel, B. A.; Schmidt, C. E., *Adv. Mater.* **2001**, *13*, 1673-1677.
- [96] Voura, E. B.; Jaiswal, J. K.; Mattoussi, H.; Simon, S. M., *Nat. Med.* **2004**, *10*, 993-998.
- [97] Pathak, S.; Choi, S. K.; Arnheim, N.; Thompson, M. E., *J. Am. Chem. Soc.* **2001**, *123*, 4103-4104.
- [98] Hanaki, K.; Momo, A.; Oku, T.; Komoto, A.; Maenosono, S.; Yamaguchi, Y.; Yamamoto, K., *Biochem. Biophys. Res. Commun.* **2003**, *302*, 496-501.
- [99] Hoshino, A.; Hanaki, K.; Suzuki, K.; Yamamoto, K., *Biochem. Biophys. Res. Commun.* **2004**, *314*, 46-53.
- [100] Mitchell, G. P.; Mirkin, C. A.; Letsinger, R. L., *J. Am. Chem. Soc.* **1999**, *121*, 8122-8123.

- [101] Åkerman, M. E.; Chan, W. C.; Laakkonen, P.; Bhatia, S. N.; Ruoslahti, E., *Proc. Natl. Acad. Sci. U. S. A.* **2002**, *99*, 12617-12621.
- [102] Rosenthal, S. J.; Tomlinson, I.; Adkins, E. M.; Schroeter, S.; Adams, S.; Swafford, L.; McBride, J.; Wang, Y.; DeFelice, L. J.; Blakely, R. D., *J. Am. Chem. Soc.* **2002**, *124*, 4586-4594.
- [103] Pinaud, F.; King, D.; Moore, H. P.; Weiss, S., *J. Am. Chem. Soc.* **2004**, *126*, 6115-6123.
- [104] Sukhanova, A.; Devy, J.; Venteo, L.; Kaplan, H.; Artemyev, M.; Oleinikov, V.; Klinov, D.; Pluot, M.; Cohen, J. H.; Nabiev, I., *Anal. Biochem.* **2004**, *324*, 60-67.
- [105] Babu, P.; Sinha, S.; Surolia, A., *Bioconjug. Chem.* **2007**, *18*, 146-151.
- [106] Goldman, E. R.; Medintz, I. L.; Hayhurst, A.; Anderson, G. P.; Mauro, J. M.; Iverson, B. L.; Georgiou, G.; Mattoussi, H., *Anal. Chim. Acta* **2005**, *534*, 63-67.
- [107] Xie, M.; Liu, H. H.; Chen, P.; Zhang, Z. L.; Wang, X. H.; Xie, Z. X.; Du, Y. M.; Pan, B. Q.; Pang, D. W., *Chem. Commun.* **2005**, 5518-5520.
- [108] Alivisatos, A. P.; Johnsson, K. P.; Peng, X.; Wilson, T. E.; Loweth, C. J.; Bruchez, M. P., Jr.; Schultz, P. G., *Nature* **1996**, *382*, 609-611.
- [109] Lemon, B. I.; Crooks, R. M., *J. Am. Chem. Soc.* **2000**, *122*, 12886-12887.
- [110] Sondi, I.; Siiman, O.; Koester, S.; Matijević, E., *Langmuir* **2000**, *16*, 3107-3118.
- [111] Dubertret, B.; Skourides, P.; Norris, D. J.; Noireaux, V.; Brivanlou, A. H.; Libchaber, A., *Science* **2002**, *298*, 1759-1762.
- [112] Kim, S.; Bawendi, M. G., *J. Am. Chem. Soc.* **2003**, *125*, 14652-14653.
- [113] Larson, D. R.; Zipfel, W. R.; Williams, R. M.; Clark, S. W.; Bruchez, M. P.; Wise, F. W.; Webb, W. W., *Science* **2003**, *300*, 1434-1436.

- [114] Potapova, I.; Mruk, R.; Prehl, S.; Zentel, R.; Basche, T.; Mews, A., *J. Am. Chem. Soc.* **2003**, *125*, 320-321.
- [115] Pellegrino, T.; Manna, L.; Kudera, S.; Liedl, T.; Koktysh, D.; Rogach, A. L.; Keller, S.; Radler, J.; Natile, G.; Parak, W. J., *Nano Lett.* **2004**, *4*, 703-707.
- [116] Mattheakis, L. C.; Dias, J. M.; Choi, Y. J.; Gong, J.; Bruchez, M. P.; Liu, J.; Wang, E., *Anal. Biochem.* **2004**, *327*, 200-208.
- [117] Gao, X.; Cui, Y.; Levenson, R. M.; Chung, L. W.; Nie, S., *Nat. Biotechnol.* **2004**, *22*, 969-976.
- [118] Fan, H.; Leve, E. W.; Scullin, C.; Gabaldon, J.; Tallant, D.; Bunge, S.; Boyle, T.; Wilson, M. C.; Brinker, C. J., *Nano Lett.* **2005**, *5*, 645-648.
- [119] Wu, X.; Liu, H.; Liu, J.; Haley, K. N.; Treadway, J. A.; Larson, J. P.; Ge, N.; Peale, F.; Bruchez, M. P., *Nat. Biotechnol.* **2003**, *21*, 41-46.
- [120] Dahan, M.; Levi, S.; Luccardini, C.; Rostaing, P.; Riveau, B.; Triller, A., *Science* **2003**, *302*, 442-445.
- [121] Månsson, A.; Sundberg, M.; Balaz, M.; Bunk, R.; Nicholls, I. A.; Omling, P.; Tågerud, S.; Montelius, L., *Biochem. Biophys. Res. Commun.* **2004**, *314*, 529-534.
- [122] Lidke, D. S.; Nagy, P.; Heintzmann, R.; Arndt-Jovin, D. J.; Post, J. N.; Grecco, H. E.; Jares-Erijman, E. A.; Jovin, T. M., *Nat. Biotechnol.* **2004**, *22*, 198-203.
- [123] Xiao, Y.; Barker, P. E., *Nucl. Acids Res.* **2004**, *32*, e28.
- [124] Howarth, M.; Takao, K.; Hayashi, Y.; Ting, A. Y., *Proc. Natl. Acad. Sci. U. S. A.* **2005**, *102*, 7583-7588.
- [125] Edgar, R.; McKinsty, M.; Hwang, J.; Oppenheim, A. B.; Fekete, R. A.; Giulian, G.; Merril, C.; Nagashima, K.; Adhya, S., *Proc. Natl. Acad. Sci. U. S. A.* **2006**, *103*, 4841-4845.

- [126] Zhu, L.; Ang, S.; Liu, W. T., *Appl. Environ. Microbiol.* **2004**, *70*, 597-598.
- [127] Lagerholm, B. C.; Wang, M.; Ernst, L. A.; Ly, D. H.; Liu, H.; Bruchez, M. P.; Waggoner, A. S., *Nano Lett.* **2004**, *4*, 2019-2022.
- [128] Mattoussi, H.; Mauro, J. M.; Goldman, E. R.; Anderson, G. P.; Sundar, V. C.; Mikulec, F. V.; Bawendi, M. G., *J. Am. Chem. Soc.* **2000**, *122*, 12142-12150.
- [129] Mattoussi, H.; Mauro, J. M.; Goldman, E. R.; Green, T. M.; Anderson, G. P.; Sundar, V. C.; Bawendi, M. G., *Phys. Stat. Sol. B* **2001**, *224*, 277-283.
- [130] Goldman, E. R.; Balighian, E. D.; Kuno, M. K.; Labrenz, S.; Anderson, G. P.; Mauro, J. M.; Mattoussi, H., *Phys. Stat. Sol. B* **2002**, *229*, 407-414.
- [131] Lingerfelt, B. M.; Mattoussi, H.; Goldman, E. R.; Mauro, J. M.; Anderson, G. P., *Anal. Chem.* **2003**, *75*, 4043-4049.
- [132] Jaiswal, J. K.; Mattoussi, H.; Mauro, J. M.; Simon, S. M., *Nat. Biotechnol.* **2003**, *21*, 47-51.
- [133] Goldman, E. R.; Anderson, G. P.; Tran, P. T.; Mattoussi, H.; Charles, P. T.; Mauro, J. M., *Anal. Chem.* **2002**, *74*, 841-847.
- [134] Goldman, E. R.; Clapp, A. R.; Anderson, G. P.; Uyeda, H. T.; Mauro, J. M.; Medintz, I. L.; Mattoussi, H., *Anal. Chem.* **2004**, *76*, 684-688.
- [135] Wang, L. Y.; Wang, L.; Gao, F.; Yu, Z. Y.; Wu, Z. M., *Analyst* **2002**, *127*, 977-980.
- [136] Chen, Y.; Rosenzweig, Z., *Anal. Chem.* **2002**, *74*, 5132-5138.
- [137] Wang, Y. A.; Li, J. J.; Chen, H.; Peng, X., *J. Am. Chem. Soc.* **2002**, *124*, 2293-2298.
- [138] Parak, W. J.; Boudreau, R.; Le Gros, M.; Gerion, D.; Zanchet, D.; Micheel, C. M.; Williams, S. C.; Alivisatos, A. P.; Larabell, C., *Adv. Mater.* **2002**, *14*, 882-885.

- [139] Pellegrino, T.; Parak, W. J.; Boudreau, R.; Le Gros, M. A.; Gerion, D.; Alivisatos, A. P.; Larabell, C. A., *Differentiation* **2003**, *71*, 542-548.
- [140] Wang, J.; Liu, G.; Merkoci, A., *J. Am. Chem. Soc.* **2003**, *125*, 3214-3215.
- [141] Wang, J.; Liu, G.; Rivas, G., *Anal. Chem.* **2003**, *75*, 4667-4671.
- [142] Olivos, H. J.; Bachhawat-Sikder, K.; Kodadek, T., *ChemBioChem.* **2003**, *4*, 1242-1245.
- [143] West, J. L.; Halas, N. J., *Annu. Rev. Biomed. Eng.* **2003**, *5*, 285-292.
- [144] Sun, X. L.; Cui, W.; Haller, C.; Chaikof, E. L., *ChemBioChem.* **2004**, *5*, 1593-1596.
- [145] Liu, G.; Wang, J.; Kim, J.; Jan, M. R.; Collins, G. E., *Anal. Chem.* **2004**, *76*, 7126-7130.
- [146] Osaki, F.; Kanamori, T.; Sando, S.; Sera, T.; Aoyama, Y., *J. Am. Chem. Soc.* **2004**, *126*, 6520-6521.
- [147] Palaniappan, K.; Hackney, S. A.; Liu, J., *Chem. Commun.* **2004**, 2704-2705.
- [148] Ballou, B.; Lagerholm, B. C.; Ernst, L. A.; Bruchez, M. P.; Waggoner, A. S., *Bioconjug. Chem.* **2004**, *15*, 79-86.
- [149] Meziani, M. J.; Pathak, P.; Harruff, B. A.; Hurezeanu, R.; Sun, Y. P., *Langmuir* **2005**, *21*, 2008-2011.
- [150] Rozenzhak, S. M.; Kadakia, M. P.; Caserta, T. M.; Westbrook, T. R.; Stone, M. O.; Naik, R. R., *Chem. Commun.* **2005**, 2217-2219.
- [151] Sandros, M. G.; Gao, D.; Benson, D. E., *J. Am. Chem. Soc.* **2005**, *127*, 12198-12199.
- [152] Bakalova, R.; Zhelev, Z.; Ohba, H.; Baba, Y., *J. Am. Chem. Soc.* **2005**, *127*, 9328-9329.

- [153] Bentzen, E. L.; Tomlinson, I. D.; Mason, J.; Gresch, P.; Warnement, M. R.; Wright, D.; Sanders-Bush, E.; Blakely, R.; Rosenthal, S. J., *Bioconjug. Chem.* **2005**, *16*, 1488-1494.
- [154] Liu, G.; Lee, T. M.; Wang, J., *J. Am. Chem. Soc.* **2005**, *127*, 38-39.
- [155] Pellegrino, T.; Kudera, S.; Liedl, T.; Muñoz Javier, A.; Manna, L.; Parak, W. J., *Small* **2005**, *1*, 48-63.
- [156] Fu, A.; Gu, W.; Larabell, C.; Alivisatos, A. P., *Curr. Opin. Neurobiol.* **2005**, *15*, 568-575.
- [157] Aryal, B. P.; Benson, D. E., *J. Am. Chem. Soc.* **2006**, *128*, 15986-15987.
- [158] Lao, U. L.; Mulchandani, A.; Chen, W., *J. Am. Chem. Soc.* **2006**, *128*, 14756-14757.
- [159] Zhang, C. Y.; Johnson, L. W., *J. Am. Chem. Soc.* **2006**, *128*, 5324-5325.
- [160] Zimmer, J. P.; Kim, S. W.; Ohnishi, S.; Tanaka, E.; Frangioni, J. V.; Bawendi, M. G., *J. Am. Chem. Soc.* **2006**, *128*, 2526-2527.
- [161] Zhang, Y.; So, M. K.; Rao, J., *Nano Lett.* **2006**, *6*, 1988-1992.
- [162] Gill, R.; Freeman, R.; Xu, J. P.; Willner, I.; Winograd, S.; Shweky, I.; Banin, U., *J. Am. Chem. Soc.* **2006**, *128*, 15376-15377.
- [163] Klostranec, J. M.; Chan, W. C. W., *Adv. Mater.* **2006**, *18*, 1953-1964.
- [164] Zhou, M.; Nakatani, E.; Gronenberg, L. S.; Tokimoto, T.; Wirth, M. J.; Hruby, V. J.; Roberts, A.; Lynch, R. M.; Ghosh, I., *Bioconjug. Chem.* **2007**, *18*, 323-332.
- [165] Chalmers, N. I.; Palmer, R. J., Jr.; Du-Thumm, L.; Sullivan, R.; Shi, W.; Kolenbrander, P. E., *Appl. Environ. Microbiol.* **2007**, *73*, 630-636.
- [166] Dubach, J. M.; Harjes, D. I.; Clark, H. A., *J. Am. Chem. Soc.* **2007**, *129*, 8418-8419.

- [167] Lee, J. A.; Mardiyani, S.; Hung, A.; Rhee, A.; Klostranec, J.; Mu, Y.; Li, D.; Chan, W. C. W., *Adv. Mater.* **2007**, *19*, 3113-3118.
- [168] Willner, I.; Basnar, B.; Willner, B., *FEBS J.* **2007**, *274*, 302-309.
- [169] Douglas, T.; Young, M., *Nature* **1998**, *393*, 152-155.
- [170] Douglas, T.; Young, M., *Adv. Mater.* **1999**, *11*, 679-681.
- [171] Douglas, T.; Strable, E.; Willits, D.; Aitouchen, A.; Libera, M.; Young, M., *Adv. Mater.* **2002**, *14*, 415-418.
- [172] Lee, S. W.; Mao, C.; Flynn, C. E.; Belcher, A. M., *Science* **2002**, *296*, 892-895.
- [173] Flenniken, M. L.; Willits, D. A.; Brumfield, S.; Young, M. J.; Douglas, T., *Nano Lett.* **2003**, *3*, 1573-1576.
- [174] Ishii, D.; Kinbara, K.; Ishida, Y.; Ishii, N.; Okochi, M.; Yohda, M.; Aida, T., *Nature* **2003**, *423*, 628-632.
- [175] Vriezema, D. M.; Comellas Aragonès, M.; Elemans, J. A.; Cornelissen, J. J.; Rowan, A. E.; Nolte, R. J., *Chem. Rev.* **2005**, *105*, 1445-1489.
- [176] Granick, S., *Chem. Rev.* **1946**, *38*, 379-403.
- [177] Crichton, R. R., *FEBS Lett.* **1973**, *34*, 125-128.
- [178] Harrison, P.; Huehns, E. R., *Nature* **1979**, *279*, 476-477.
- [179] Crichton, R. R., *Struct. bonding*, Dunitz, J. D., Ed. Verlag-Springer: Berlin, Heidelberg, New York, **1973**; *17*, pp 67-134.
- [180] Clegg, G. A.; Fitton, J. E.; Harrison, P. M.; Treffry, A., *Prog. Biophys. Mol. Biol.* **1980**, *36*, 53-86.
- [181] Theil, E. C., *Annu. Rev. Biochem.* **1987**, *56*, 289-315.
- [182] Granick, S., *J. Biol. Chem.* **1943**, *149*, 157-167.

- [183] Harrison, P. M.; Andrews, S. C.; Artymiuk, P. J.; Ford, G. C.; Guest, J. R.; Hirzmann, J.; Lawson, D. M.; Livingstone, J. C.; Smith, J. M. A.; Treffry, A.; Yewdall, S. J., *Adv. Inorg. Chem.* **1991**, *36*, 449-486.
- [184] Harrison, P. M.; Hofmann, T., *J. Mol. Biol.* **1962**, *4*, 239-250.
- [185] Hofmann, T.; Harrison, P. M., *J. Mol. Biol.* **1963**, *6*, 256-267.
- [186] Crichton, R. R., *Biochem. J.* **1972**, *126*, 761-764.
- [187] Crichton, R. R., *Biochem. J.* **1970**, *119*, 40P.
- [188] Bryce, C. F.; Crichton, R. R., *J. Biol. Chem.* **1971**, *246*, 4198-4205.
- [189] Crichton, R. R., *N. Engl. J. Med.* **1971**, *284*, 1413-1422.
- [190] Björk, I.; Fish, W. F., *Biochemistry* **1971**, *10*, 2844-2848.
- [191] Crichton, R. R.; Eason, R.; Barclay, A.; Bryce, C. F., *Biochem. J.* **1973**, *131*, 855-857.
- [192] Hoare, R. J.; Harrison, P. M.; Hoy, T. G., *Nature* **1975**, *255*, 653-654.
- [193] Granick, S.; Michaelis, L., *J. Biol. Chem.* **1943**, *147*, 91-97.
- [194] Granick, S., *Physiol. Rev.* **1951**, *31*, 489-511.
- [195] Harrison, P. M.; Fischbach, F. A.; Hoy, T. G.; Haggis, G. H., *Nature* **1967**, *216*, 1188-1190.
- [196] Massover, W. H.; Cowley, J. M., *Proc. Natl. Acad. Sci. U. S. A.* **1973**, *70*, 3847-3851.
- [197] Crichton, R. R., *Angew. Chem. Int. Ed. Engl.* **1973**, *12*, 57-65, *Angew. Chem.* **1973**, *85*, 53-62.
- [198] Rothen, A., *J. Biol. Chem.* **1944**, *152*, 679-686.
- [199] Stefanini, S.; Chiancone, E.; Antonini, E., *FEBS Lett.* **1976**, *69*, 90-94.

- [200] Melino, G.; Stefanini, S.; Chiancone, E.; Antonini, E., *FEBS Lett.* **1978**, *86*, 136-138.
- [201] Aisen, P.; Listowsky, I., *Annu. Rev. Biochem.* **1980**, *49*, 375-393.
- [202] Treffry, A.; Harrison, P. M., *Biochem. J.* **1978**, *171*, 313-320.
- [203] Crichton, R. R.; Millar, J. A.; Cumming, R. L.; Bryce, C. F., *Biochem. J.* **1973**, *131*, 51-59.
- [204] Arosio, P.; Adelman, T. G.; Drysdale, J. W., *J. Biol. Chem.* **1978**, *253*, 4451-4458.
- [205] Crichton, R. R.; Millar, J. A.; Cumming, R. L., *Biochem. J.* **1970**, *117*, 35P.
- [206] Stefanini, S.; Chiancone, E.; Arosio, P.; Finazzi-Agrò, A.; Antonini, E., *Biochemistry* **1982**, *21*, 2293-2299.
- [207] Levi, S.; Yewdall, S. J.; Harrison, P. M.; Santambrogio, P.; Cozzi, A.; Rovida, E.; Albertini, A.; Arosio, P., *Biochem. J.* **1992**, *288*, 591-596.
- [208] Harrison, P. M.; Arosio, P., *Biochim. Biophys. Acta* **1996**, *1275*, 161-203.
- [209] Harrison, P. M.; Hofmann, T.; Mainwaring, W. I., *J. Mol. Biol.* **1962**, *4*, 251-256.
- [210] Heusterspreute, M.; Crichton, R. R., *FEBS Lett.* **1981**, *129*, 322-327.
- [211] Banyard, S. H.; Stammers, D. K.; Harrison, P. M., *Nature* **1978**, *271*, 282-284.
- [212] Granick, S., *J. Biol. Chem.* **1942**, *146*, 451-461.
- [213] Stefanini, S.; Cavallo, S.; Wang, C. Q.; Tataseo, P.; Vecchini, P.; Giartosio, A.; Chiancone, E., *Arch. Biochem. Biophys.* **1996**, *325*, 58-64.
- [214] Takahashi, T.; Kuyucak, S., *Biophys. J.* **2003**, *84*, 2256-2263.
- [215] Frey, R. F.; Donlin, M. J.; Bashkin, J. K. <http://www.chemistry.wustl.edu/edudev/LabTutorials/Ferritin/FerritinTutorial.html> (May **2008**).

-
- [216] Douglas, T.; Ripoll, D. R., *Protein Sci.* **1998**, *7*, 1083-1091.
- [217] Webb, B.; Frame, J.; Zhao, Z.; Lee, M. L.; Watt, G. D., *Arch. Biochem. Biophys.* **1994**, *309*, 178-183.
- [218] Yang, X.; Chasteen, N. D., *Biophys. J.* **1996**, *71*, 1587-1595.
- [219] Yang, X.; Arosio, P.; Chasteen, N. D., *Biophys. J.* **2000**, *78*, 2049-2059.
- [220] Fish, W. W., *J. Theor. Biol.* **1976**, *60*, 385-392.
- [221] Stuhmann, H. B.; Haas, J.; Ibel, K.; Koch, M. H.; Crichton, R. R., *J. Mol. Biol.* **1976**, *100*, 399-413.
- [222] Yang, D.; Nagayama, K., *Biochem. J.* **1995**, *307*, 253-256.
- [223] Listowsky, I.; Bethel, J. J.; Englard, S., *Biochemistry* **1967**, *6*, 1341-1348.
- [224] Listowsky, I.; Blauer, G.; Englard, S.; Bethel, J. J., *Biochemistry* **1972**, *11*, 2176-2182.
- [225] Harrison, P. M.; Gregory, D. W., *J. Mol. Biol.* **1965**, *14*, 626-629.
- [226] Drysdale, J. W.; Haggis, G. H.; Harrison, P. M., *Nature* **1968**, *219*, 1045-1046.
- [227] Harrison, P. M.; Gregory, D. W., *Nature* **1968**, *220*, 578-580.
- [228] Crichton, R. R.; Bryce, C. F., *Biochem. J.* **1973**, *133*, 289-299.
- [229] Imai, N.; Arata, Y.; Fujiwara, S., *Bull. Chem. Soc. Jpn.* **1981**, *54*, 1243-1244.
- [230] Gerl, M.; Jaenicke, R., *Biol. Chem. Hoppe Seyler* **1987**, *368*, 387-396.
- [231] Mann, S., *Nature* **1988**, *332*, 119-124.
- [232] Mann, S., *Biomimetic materials chemistry*, Mann, S., Ed. Wiley-VCH: Weinheim, **1996**; pp 1-40.
- [233] Mann, S., *Nature* **1993**, *365*, 499-505.

- [234] Douglas, T., *Biomimetic materials chemistry*, Mann, S., Ed. Wiley-VCH: New York **1996**; pp 91-115.
- [235] Mann, S.; Shenton, W.; Li, M.; Connolly, S.; Fitzmaurice, D., *Adv. Mater.* **2000**, *12*, 147-150.
- [236] Mann, S., *Chem. Commun.* **2004**, 1-4.
- [237] Pead, S.; Durrant, E.; Webb, B.; Larsen, C.; Heaton, D.; Johnson, J.; Watt, G. D., *J. Inorg. Biochem.* **1995**, *59*, 15-27.
- [238] Mann, S.; Meldrum, F. C., *Adv. Mater.* **1991**, *3*, 316-318.
- [239] Meldrum, F. C.; Wade, V. J.; Nimmo, D. L.; Heywood, B. R.; Mann, S., *Nature* **1991**, *349*, 684-687.
- [240] Harrison, P. M.; Hoy, T. G.; Macara, I. G.; Hoare, R. J., *Biochem. J.* **1974**, *143*, 445-451.
- [241] Douglas, T.; Dickson, D. P. E.; Betteridge, S.; Charnock, J.; Garner, C. D.; Mann, S., *Science* **1995**, *269*, 54-57.
- [242] Polanams, J.; Ray, A. D.; Watt, R. K., *Inorg. Chem.* **2005**, *44*, 3203-3209.
- [243] Meldrum, F. C.; Heywood, B. R.; Mann, S., *Science* **1992**, *257*, 522-523.
- [244] Bulte, J. W.; Douglas, T.; Mann, S.; Frankel, R. B.; Moskowitz, B. M.; Brooks, R. A.; Baumgarner, C. D.; Vymazal, J.; Strub, M. P.; Frank, J. A., *J. Magn. Reson. Imaging* **1994**, *4*, 497-505.
- [245] Wong, K. K. W.; Douglas, T.; Gider, S.; Awschalom, D. D.; Mann, S., *Chem. Mater.* **1998**, *10*, 279-285.
- [246] Meldrum, F. C.; Douglas, T.; Levi, S.; Arosio, P.; Mann, S., *J. Inorg. Biochem.* **1995**, *58*, 59-68.
- [247] Hainfeld, J. F., *Proc. Natl. Acad. Sci. U. S. A.* **1992**, *89*, 11064-11068.

- [248] Douglas, T.; Stark, V. T., *Inorg. Chem.* **2000**, *39*, 1828-1830.
- [249] Tsukamoto, R.; Iwahori, K.; Muraoka, M.; Yamashita, I., *Bull. Chem. Soc. Jpn* **2005**, *78*, 2075-2081.
- [250] Kim, J. W.; Choi, S. H.; Lillehei, P. T.; Chu, S. H.; King, G. C.; Watt, G. D., *Chem. Commun.* **2005**, 4101-4103.
- [251] Okuda, M.; Iwahori, K.; Yamashita, I.; Yoshimura, H., *Biotechnol. Bioeng.* **2003**, *84*, 187-194.
- [252] Yoshizawa, K.; Iwahori, K.; Sugimoto, K.; Yamashita, I., *Chem. Lett.* **2006**, *35*, 1192-1193.
- [253] Gálvez, N.; Sánchez, P.; Domínguez-Vera, J. M., *Dalton Trans.* **2005**, 2492-2494.
- [254] Gálvez, N.; Sánchez, P.; Domínguez-Vera, J. M.; Soriano-Portillo, A.; Clemente-León, M.; Coronado, E., *J. Mater. Chem.* **2006**, *16*, 2757-2761.
- [255] Warne, B.; Kasyutich, O. I.; Mayes, E. L.; Wiggins, J. A. L.; Wong, K. K. W., *IEEE Trans. Magn.* **2000**, *36*, 3009-3011.
- [256] Mayes, E. L.; Mann, S., *Nanobiotechnology. Concepts, Applications and Perspectives*, Niemeyer, C. M.; Mirkin, C. A., Ed. Wiley-VCH: Weinheim, **2004**; *18*, pp 278-287.
- [257] Ueno, T.; Suzuki, M.; Goto, T.; Matsumoto, T.; Nagayama, K.; Watanabe, Y., *Angew. Chem. Int. Ed. Engl.* **2004**, *43*, 2527-2530, *Angew. Chem.* **2004**, *116*, 2581-2584.
- [258] Clemente-León, M.; Coronado, E.; Soriano-Portillo, A.; Gálvez, N.; Domínguez-Vera, J. M., *J. Mater. Chem.* **2007**, *17*, 49-51.
- [259] Wong, K. K. W.; Mann, S., *Adv. Mater.* **1996**, *8*, 928-932.
- [260] May, M. E.; Fish, W. W., *Arch. Biochem. Biophys.* **1978**, *190*, 720-725.

- [261] Yamashita, I.; Hayashi, J.; Hara, M., *Chem. Lett.* **2004**, *33*, 1158-1159.
- [262] Iwahori, K.; Morioka, T.; Yamashita, I., *Phys. Stat. Sol. A* **2006**, *203*, 2658-2661.
- [263] Iwahori, K.; Yoshizawa, K.; Muraoka, M.; Yamashita, I., *Inorg. Chem.* **2005**, *44*, 6393-6400.
- [264] Iwahori, K.; Yamashita, I., *J. Phys.: Conf. Ser.* **2007**, *61*, 492-496.
- [265] Aime, S.; Frullano, L.; Geninatti Crich, S., *Angew. Chem. Int. Ed. Engl.* **2002**, *41*, 1017-1019, *Angew. Chem.* **2002**, *114*, 1059-1061.
- [266] Domínguez-Vera, J. M.; Colacio, E., *Inorg. Chem.* **2003**, *42*, 6983-6985.
- [267] Domínguez-Vera, J. M., *J. Inorg. Biochem.* **2004**, *98*, 469-472.
- [268] Simsek, E.; Kilic, M. A., *J. Mag. Mag. Mat.* **2005**, *293*, 509-513.
- [269] Liu, G.; Wang, J.; Wu, H.; Lin, Y., *Anal. Chem.* **2006**, *78*, 7417-7423.
- [270] Yang, Z.; Wang, X.; Diao, H.; Zhang, J.; Li, H.; Sun, H.; Guo, Z., *Chem. Commun.* **2007**, 3453-3455.
- [271] Zborowski, M.; Fuh, C. B.; Green, R.; Baldwin, N. J.; Reddy, S.; Douglas, T.; Mann, S.; Chalmers, J. J., *Cytometry* **1996**, *24*, 251-259.
- [272] Kim, I.; Hosein, H. A.; Strongin, D. R.; Douglas, T., *Chem. Mater.* **2002**, *14*, 4874-4879.
- [273] Ensign, D.; Young, M.; Douglas, T., *Inorg. Chem.* **2004**, *43*, 3441-3446.
- [274] Yamashita, I., *Thin Solid Films* **2001**, *393*, 12-18.
- [275] Hikono, T.; Uraoka, Y.; Fuyuki, T.; Yamashita, I., *Jpn. J. Appl. Phys.* **2003**, *42*, L398-L399.
- [276] Okuda, M.; Kobayashi, Y.; Suzuki, K.; Sonoda, K.; Kondoh, T.; Wagawa, A.; Kondo, A.; Yoshimura, H., *Nano Lett.* **2005**, *5*, 991-993.

- [277] Hikono, T.; Uraoka, Y.; Fuyuki, T.; Yoshii, S.; Yamashita, I.; Takeguchi, M., *Surf. Sci.* **2006**, *600*, 2817-2822.
- [278] Jeong, G. H.; Yamazaki, A.; Suzuki, S.; Yoshimura, H.; Kobayashi, Y.; Homma, Y., *J. Am. Chem. Soc.* **2005**, *127*, 8238-8239.
- [279] Iwahori, K.; Yamashita, I., *J. Clust. Sci.* **2007** *18*, 358-370.
- [280] Liu, G.; Wu, H.; Dohnalkova, A.; Lin, Y., *Anal. Chem.* **2007**, *79*, 5614-5619.
- [281] Li, M.; Wong, K. K. W.; Mann, S., *Chem. Mater.* **1999**, *11*, 23-26.
- [282] Liu, G.; Wang, J.; Lea, S. A.; Lin, Y., *ChemBioChem.* **2006**, *7*, 1315-1319.
- [283] Zeng, Q.; Li, T.; Cash, B.; Li, S.; Xie, F.; Wang, Q., *Chem. Commun.* **2007**, 1453-1455.
- [284] Weissleder, R., *Nat. Biotechnol.* **2001**, *19*, 316-317.
- [285] Olkhovets, A.; Hsu, R. C.; Lipovskii, A.; Wise, F. W., *Phys. Rev. Lett.* **1998**, *81*, 3539.
- [286] Levina, L.; Sukhovatkin, V.; Musikhin, S.; Cauchi, S.; Nisman, R.; Bazett-Jones, D. P.; Sargent, E. H., *Adv. Mater.* **2005**, *17*, 1854-1857.
- [287] Cademartiri, L.; Bertolotti, J.; Sapienza, R.; Wiersma, D. S.; von Freymann, G.; Ozin, G. A., *J. Phys. Chem. B* **2006**, *110*, 671-673.
- [288] Konstantatos, G.; Howard, I.; Fischer, A.; Hoogland, S.; Clifford, J.; Klem, E.; Levina, L.; Sargent, E. H., *Nature* **2006**, *442*, 180-183.
- [289] Nenadović, M. T.; Čomor, M. I.; Vasić, V.; Mićić, O. I., *J. Phys. Chem.* **1990**, *94*, 6390-6396.
- [290] Patel, A. A.; Wu, F.; Zhang, J. Z.; Torres-Martinez, C. L.; Mehra, R. K.; Yang, Y.; Risbud, S. H., *J. Phys. Chem. B* **2000**, *104*, 11598-11605.

- [291] Zhu, N.; Zhang, A.; Wang, Q.; He, P.; Fang, Y., *Electroanalysis* **2004**, *16*, 577-582.
- [292] Wu, S.; Zeng, H.; Schelly, Z. A., *Langmuir* **2005**, *21*, 686-691.
- [293] Hinds, S.; Taft, B. J.; Levina, L.; Sukhovatkin, V.; Dooley, C. J.; Roy, M. D.; MacNeil, D. D.; Sargent, E. H.; Kelley, S. O., *J. Am. Chem. Soc.* **2006**, *128*, 64-65.
- [294] Kowshik, M.; Vogel, W.; Urban, J.; Kulkarni, S. K.; Paknikar, K. M., *Adv. Mater.* **2002**, *14*, 815-818.
- [295] Choi, J. H.; Chen, K. H.; Strano, M. S., *J. Am. Chem. Soc.* **2006**, *128*, 15584-15585.
- [296] Hinds, S.; Myrskog, S.; Levina, L.; Koleilat, G.; Yang, J.; Kelley, S. O.; Sargent, E. H., *J. Am. Chem. Soc.* **2007**, *129*, 7218-7219.
- [297] Hyun, B. R.; Chen, H.; Rey, D. A.; Wise, F. W.; Batt, C. A., *J. Phys. Chem. B* **2007**, *111*, 5726-5730.
- [298] Zhao, X.; Gorelikov, I.; Musikhin, S.; Cauchi, S.; Sukhovatkin, V.; Sargent, E. H.; Kumacheva, E., *Langmuir* **2005**, *21*, 1086-1090.
- [299] Zhao, X.-S.; Xu, S.-Y.; Liang, L.-Y.; Li, T.; Cauchi, S., *J. Mater. Sci.* **2007**, *42*, 4265-4269.
- [300] Bakueva, L.; Musikhin, S.; Hines, M. A.; Chang, T. W. F.; Tzolov, M.; Scholes, G. D.; Sargent, E. H., *Appl. Phys. Lett.* **2003**, *82*, 2895-2897.
- [301] Bakueva, L.; Gorelikov, I.; Musikhin, S.; Zhao, X. S.; H. Sargent, E. H.; Kumacheva, E., *Adv. Mater.* **2004**, *16*, 926-929.
- [302] Turyanska, L.; Patanè, A.; Henini, M.; Hennequin, B.; Thomas, N. R., *Appl. Phys. Lett.* **2007**, *90*, 101913.
- [303] Peterson, J. J.; Krauss, T. D., *Nano Lett.* **2006**, *6*, 510-514.

- [304] Madelung, O., *Semiconductor: data handbook*, 3rd Ed. Springer: Berlin, **2004**; pp 691.
- [305] Fomin, V. M.; Gladilin, V. N.; Devreese, J. T.; Pokatilov, E. P.; Balaban, S. N.; Klimin, S. N., *Phys. Rev. B* **1998**, *57*, 2415-2425.
- [306] Bissiri, M.; Baldassarri Höger von Högersthal, G.; Bhatti, A. S.; Capizzi, M.; Frova, A.; Frigeri, P.; Franchi, S., *Phys. Rev. B* **2000**, *62*, 4642-4646.
- [307] Verzelen, O.; Ferreira, R.; Bastard, G., *Phys. Rev. Lett.* **2002**, *88*, 146803.
- [308] Sanguinetti, S.; Poliani, E.; Bonfanti, M.; Guzzi, M.; Grilli, E.; Gurioli, M.; Koguchi, N., *Phys. Rev. B* **2006**, *73*, 125342.
- [309] Uskov, A. V.; Jauho, A.-P.; Tromborg, B.; Mørk, J.; Lang, R., *Phys. Rev. Lett.* **2000**, *85*, 1516-1519.
- [310] Bayer, M.; Forchel, A., *Phys. Rev. B* **2002**, *65*, 041308.
- [311] Borri, P.; Langbein, W.; Woggon, U.; Stavarache, V.; Reuter, D.; Wieck, A. D., *Phys. Rev. B* **2005**, *71*, 115328.
- [312] Kang, I.; Wise, F. W., *J. Opt. Soc. Am. B* **1997**, *14*, 1632-1646.
- [313] Nomura, S.; Kobayashi, T., *Phys. Rev. B* **1992**, *45*, 1305-1316.
- [314] Krauss, T. D.; Wise, F. W., *Phys. Rev. B* **1997**, *55*, 9860-9865.
- [315] Scamarcio, G.; Spagnolo, V.; Ventruti, G.; Lugará, M.; Righini, G. C., *Phys. Rev. B* **1996**, *53*, R10489-R10492.
- [316] Pelekanos, N. T.; Haas, H.; Magnea, N.; Mariette, H.; Wasiela, A., *App. Phys. Lett.* **1992**, *61*, 3154-3156.
- [317] Shiang, J. J.; Risbud, S. H.; Alivisatos, A. P., *J. Chem. Phys.* **1993**, *98*, 8432-8442.
- [318] Mazur, A.; Baez, S.; Shorr, E., *J. Biol. Chem.* **1955**, *213*, 147-160.

-
- [319] Pape, L.; Multani, J. S.; Stitt, C.; Saltman, P., *Biochemistry* **1968**, *7*, 613-616.
- [320] Dognin, J.; Crichton, R. R., *FEBS Lett.* **1975**, *54*, 234-236.
- [321] Tufano, T. P.; Pecoraro, V. L.; Raymond, K. N., *Biochim. Biophys. Acta* **1981**, *668*, 420-428.
- [322] Tidmarsh, G. F.; Klebba, P. E.; Rosenberg, L. T., *J. Inorg. Biochem.* **1983**, *18*, 161-168.
- [323] Crichton, R. R.; Roman, F.; Roland, F., *J. Inorg. Biochem.* **1980**, *13*, 305-316.
- [324] Dognin, J.; Girardet, J. L.; Chapron, Y., *Biochim. Biophys. Acta* **1973** *297* 276-284.
- [325] Sirivech, S.; Frieden, E.; Osaki, S., *Biochem. J.* **1974**, *143*, 311-315.
- [326] Crichton, R. R.; Roman, F.; Wauters, M., *Biochem. Soc. Trans.* **1975**, *3*, 946-948.
- [327] Funk, F.; Lenders, J. P.; Crichton, R. R.; Schneider, W., *Eur. J. Biochem.* **1985**, *152*, 167-172.
- [328] Jones, T.; Spencer, R.; Walsh, C., *Biochemistry* **1978**, *17*, 4011-4017.
- [329] Brady, M. C.; Lilley, K. S.; Treffry, A.; Harrison, P. M.; Hider, R. C.; Taylor, P. D., *J. Inorg. Biochem.* **1989**, *35*, 9-22.
- [330] Linert, W.; Jameson, G. N. L., *J. Inorg. Biochem.* **2000**, *79*, 319-326.
- [331] Hoy, T. G.; Harrison, P. M.; Shabbir, M.; Macara, I. G., *Biochem J.* **1974**, *137*, 6770.
- [332] Gálvez, N.; Ruiz, B.; Cuesta, R.; Colacio, E.; Domínguez-Vera, J. M., *Inorg. Chem.* **2005**, *44*, 2706-2709.
- [333] Sanchez, P.; Gálvez, N.; Colacio, E.; Minones, E.; Domínguez-Vera, J. M., *Dalton Trans.* **2005**, 811-813.

- [334] Wong, K. K. W.; Whilton, N. T.; Cölfen, H.; Douglas, T.; Mann, S., *Chem. Commun.* **1998**, 1621-1622.
- [335] Wong, K. K.; Cölfen, H.; Whilton, N. T.; Douglas, T.; Mann, S., *J. Inorg. Biochem.* **1999**, *76*, 187-195.
- [336] Watt, G. D.; Frankel, R. B.; Papaefthymiou, G. C., *Proc. Natl. Acad. Sci. U. S. A.* **1985**, *82*, 3640-3643.
- [337] Watt, R. K.; Frankel, R. B.; Watt, G. D., *Biochemistry* **1992**, *31*, 9673-9679.
- [338] Kopp, R.; Vogt, A.; Maass, G., *Nature* **1963**, *198*, 892-893.
- [339] Price, D. J.; Joshi, J. G., *J. Biol. Chem.* **1983**, *258*, 10873-10880.
- [340] Matsuura, J.; Powers, M. E.; Manning, M. C.; Shefter, E., *J. Am. Chem. Soc.* **1993**, *115*, 1261-1264.
- [341] Paradkar, V. M.; Dordick, J. S., *Biotechnol. Bioeng.* **1994**, *43*, 529-540.
- [342] Hobbs, H. R.; Kirke, H. M.; Poliakoff, M.; Thomas, N. R., *Angew. Chem. Int. Ed. Engl.* **2007**, *46*, 7860-7863, *Angew. Chem.* **2007**, *119*, 8006-8009.
- [343] Danon, D.; Goldstein, L.; Marikovsky, Y.; Skutelsky, E., *J. Ultrastruct. Res.* **1972**, *38*, 500-510.
- [344] Righetti, P. G.; Righetti, A. B. B., *Isoelectric focusing*, Arbuthnott, J. P.; Beeley, J. A., Ed. Butterworths: London, **1975**; pp 114-131.
- [345] Habeeb, A. F., *Anal. Biochem.* **1966**, *14*, 328-336.
- [346] Hennequin, B.; Turyanska, L.; Ben, T.; Beltrán, A. M.; Molina, S. I.; Li, M.; Mann, S.; Patanè, A.; Thomas, N. R., *accepted in Adv. Mater.* **2008**, adma.200800530.
- [347] Hermanson, G. T., *Bioconjugate techniques*. 1st ed.; Academic Press: New York, **1996**.

- [348] Axford, D. N.; Davis, J. J., *Nanotechnology* **2007**, *18*, 145502.
- [349] Stephan, O.; Ajayan, P. M.; Colliex, C.; Redlich, P.; Lambert, J. M.; Bernier, P.; Lefin, P., *Science* **1994**, *266*, 1683-1685.
- [350] Suenaga, K.; Tencé, M.; Mory, C.; Colliex, C.; Kato, H.; Okazaki, T.; Shinohara, H.; Hirahara, K.; Bandow, S.; Iijima, S., *Science* **2000**, *290*, 2280-2282.
- [351] Bryce, C. F.; Crichton, R. R., *Biochem. J.* **1973**, *133*, 301-309.
- [352] Medintz, I. L.; Goldman, E. R.; Lassman, M. E.; Mauro, J. M., *Bioconjug. Chem.* **2003**, *14*, 909-918.
- [353] Lakowicz, J. R., *Principles of fluorescence spectroscopy*, 2nd Ed. Kluwer Academic: New York, **1999**; **13**, pp 367-394.
- [354] Miller, J. N., *Analyst* **2005**, *130*, 265-270.
- [355] Sapsford, K. E.; Berti, L.; Medintz, I. L., *Angew. Chem. Int. Ed. Engl.* **2006**, *45*, 4562-4589, *Angew. Chem.* **2006**, *118*, 4676-4704.
- [356] Clapp, A. R.; Medintz, I. L.; Mattoussi, H., *ChemPhysChem.* **2006**, *7*, 47-57.
- [357] Stryer, L.; Haugland, R. P., *Proc. Natl. Acad. Sci. U. S. A.* **1967**, *58*, 719-726.
- [358] Willard, D. M.; Van Orden, A., *Nat. Mater.* **2003**, *2*, 575-576.
- [359] Clapp, A. R.; Medintz, I. L.; Mauro, J. M.; Fisher, B. R.; Bawendi, M. G.; Mattoussi, H., *J. Am. Chem. Soc.* **2004**, *126*, 301-310.
- [360] Clapp, A. R.; Medintz, I. L.; Fisher, B. R.; Anderson, G. P.; Mattoussi, H., *J. Am. Chem. Soc.* **2005**, *127*, 1242-1250.
- [361] Raymo, F. M.; Yildiz, I., *Phys. Chem. Chem. Phys.* **2007**, *9*, 2036-2043.
- [362] Medintz, I. L.; Trammell, S. A.; Mattoussi, H.; Mauro, J. M., *J. Am. Chem. Soc.* **2004**, *126*, 30-31.

- [363] Medintz, I. L.; Clapp, A. R.; Mattoussi, H.; Goldman, E. R.; Fisher, B.; Mauro, J. M., *Nat. Mater.* **2003**, *2*, 630-638.
- [364] Medintz, I. L.; Clapp, A. R.; Melinger, J. S.; Deschamps, J. R.; Mattoussi, H., *Adv. Mater.* **2005**, *17*, 2450-2455.
- [365] Bakalova, R.; Zhelev, Z.; Ohba, H.; Baba, Y., *J. Am. Chem. Soc.* **2005**, *127*, 11328-11335.
- [366] Medintz, I. L.; Sapsford, K. E.; Clapp, A. R.; Pons, T.; Higashiya, S.; Welch, J. T.; Mattoussi, H., *J. Phys. Chem. B* **2006**, *110*, 10683-10690.
- [367] Shi, L.; De Paoli, V.; Rosenzweig, N.; Rosenzweig, Z., *J. Am. Chem. Soc.* **2006**, *128*, 10378-10379.
- [368] Tran, P. T.; Goldman, E. R.; Anderson, G. P.; Mauro, J. M.; Mattoussi, H., *Phys. Stat. Sol. B* **2002**, *229*, 427-432.
- [369] Levy, M.; Cater, S. F.; Ellington, A. D., *ChemBioChem.* **2005**, *6*, 2163-2166.
- [370] Snee, P. T.; Somers, R. C.; Nair, G.; Zimmer, J. P.; Bawendi, M. G.; Nocera, D. G., *J. Am. Chem. Soc.* **2006**, *128*, 13320-13321.
- [371] Kawahara, S.; Uchimara, T.; Murata, S., *Chem. Commun.* **1999**, 563-564.
- [372] Clapp, A. R.; Medintz, I. L.; Uyeda, H. T.; Fisher, B. R.; Goldman, E. R.; Bawendi, M. G.; Mattoussi, H., *J. Am. Chem. Soc.* **2005**, *127*, 18212-18221.
- [373] Wang, S.; Mamedova, N.; Kotov, N. A.; Chen, W.; Studer, J., *Nano Lett.* **2002**, *2*, 817-822.
- [374] Mamedova, N. N.; Kotov, N. A.; Rogach, A. L.; Studer, J., *Nano Lett.* **2001**, *1*, 281-286.
- [375] Oh, E.; Hong, M. Y.; Lee, D.; Nam, S. H.; Yoon, H. C.; Kim, H. S., *J. Am. Chem. Soc.* **2005**, *127*, 3270-3271.

- [376] Chang, E.; Miller, J. S.; Sun, J.; Yu, W. W.; Colvin, V. L.; Drezek, R.; West, J. L., *Biochem. Biophys. Res. Commun.* **2005**, *334*, 1317-1321.
- [377] Willard, D. M.; Carillo, L. L.; Jung, J.; Van Orden, A., *Nano Lett.* **2001**, *1*, 469-474.
- [378] Goldman, E. R.; Medintz, I. L.; Whitley, J. L.; Hayhurst, A.; Clapp, A. R.; Uyeda, H. T.; Deschamps, J. R.; Lassman, M. E.; Mattoussi, H., *J. Am. Chem. Soc.* **2005**, *127*, 6744-6751.
- [379] Patolsky, F.; Gill, R.; Weizmann, Y.; Mokari, T.; Banin, U.; Willner, I., *J. Am. Chem. Soc.* **2003**, *125*, 13918-13919.
- [380] Gill, R.; Willner, I.; Shweky, I.; Banin, U., *J. Phys. Chem. B* **2005**, *109*, 23715-23719.
- [381] Zhang, C. Y.; Yeh, H. C.; Kuroki, M. T.; Wang, T. H., *Nat. Mater.* **2005**, *4*, 826-831.
- [382] Medintz, I. L.; Clapp, A. R.; Brunel, F. M.; Tiefenbrunn, T.; Uyeda, H. T.; Chang, E. L.; Deschamps, J. R.; Dawson, P. E.; Mattoussi, H., *Nat. Mater.* **2006**, *5*, 581-589.
- [383] Shi, L.; Rosenzweig, N.; Rosenzweig, Z., *Anal. Chem.* **2007**, *79*, 208-214.
- [384] Ohmiya, Y., *Jpn. J. Appl. Phys.* **2005**, *44*, 6368-6379.
- [385] Frangioni, J. V., *Nat. Biotechnol.* **2006**, *24*, 326-328.
- [386] Seliger, H. H.; McElroy, W. D., *Proc. Natl. Acad. Sci. U. S. A.* **1964**, *52*, 75-81.
- [387] Zhang, Y.; So, M. K.; Loening, A. M.; Yao, H.; Gambhir, S. S.; Rao, J., *Angew. Chem. Int. Ed. Engl.* **2006**, *45*, 4936-4940, *Angew. Chem.* **2006**, *118*, 5058-5062.
- [388] Yao, H.; Zhang, Y.; Xiao, F.; Xia, Z.; Rao, J., *Angew. Chem. Int. Ed. Engl.* **2007**, *46*, 4346-4349, *Angew. Chem.* **2007**, *119*, 4424-4427.

- [389] Nakatsu, T.; Ichiyama, S.; Hiratake, J.; Saldanha, A.; Kobashi, N.; Sakata, K.; Kato, H., *Nature* **2006**, *440*, 372-376.
- [390] So, M. K.; Xu, C.; Loening, A. M.; Gambhir, S. S.; Rao, J., *Nat. Biotechnol.* **2006**, *24*, 339-343.
- [391] Evanko, D., *Nat. Methods* **2006**, *3*, 240-241.
- [392] Brunner, J., *Chem. Soc. Rev.* **1993**, *22*, 183-189.
- [393] Cornish, V. W.; Mendel, D.; Schultz, P. G., *Angew. Chem. Int. Ed. Engl.* **1995**, *34*, 621-633, *Angew. Chem.* **1995**, *31074*, 677-690.
- [394] Budisa, N., *Angew. Chem. Int. Ed. Engl.* **2004**, *43*, 6426-6463, *Angew. Chem.* **2004**, *116*, 6586-6624.
- [395] Hendrickson, T. L.; de Crécy-Lagard, V.; Schimmel, P., *Annu. Rev. Biochem.* **2004**, *73*, 147-176.
- [396] Wang, L.; Schultz, P. G., *Angew. Chem. Int. Ed. Engl.* **2005**, *44*, 34-66, *Angew. Chem. Int. Ed. Engl.* **2005**, *117*, 34-68.
- [397] Bain, J. D.; Glabe, C. G.; Dix, T. A.; Chamberlin, A. R., *J. Am. Chem. Soc.* **1989**, *111*, 8013-8014.
- [398] England, P. M., *Biochemistry* **2004**, *43*, 11623-11629.
- [399] Kothakota, S.; Mason, T. L.; Tirrell, D. A.; Fournier, M. J., *J. Am. Chem. Soc.* **1995**, *117*, 536-537.
- [400] van Hest, J. C.; Tirrell, D. A., *FEBS Lett.* **1998**, *428*, 68-70.
- [401] van Hest, J. C.; Kiick, K. L.; Tirrell, D. A., *J. Am. Chem. Soc.* **2000**, *122*, 1282-1288.
- [402] Jakubowski, H., *J. Biol. Chem.* **2000**, *275*, 21813-21816.

- [403] Kiick, K. L.; van Hest, J. C.; Tirrell, D. A., *Angew. Chem. Int. Ed. Engl.* **2000**, *39*, 2148-2152, *Angew. Chem.* **2000**, *112*, 2232-2236.
- [404] Kiick, K. L.; Tirrell, D. A., *Tetrahedron* **2000**, *56*, 9487-9493.
- [405] Kiick, K. L.; Weberskirch, R.; Tirrell, D. A., *FEBS Lett.* **2001**, *502*, 25-30.
- [406] Tang, Y.; Tirrell, D. A., *J. Am. Chem. Soc.* **2001**, *123*, 11089-11090.
- [407] Montclare, J. K.; Tirrell, D. A., *Angew. Chem. Int. Ed. Engl.* **2006**, *45*, 4518-4521, *Angew. Chem.* **2006**, *118*, 4630-4633.
- [408] Cowie, D. B.; Cohen, G. N., *Biochim. Biophys. Acta* **1957**, *26*, 252-261.
- [409] Grace, J. E., Jr.; Van Eden, M. E.; Aust, S. D., *Arch. Biochem. Biophys.* **2000**, *384*, 116-122.
- [410] Atkins, P. W.; de Paula, J., *Physical Chemistry*, 5th ed.; Oxford University Press: USA, Canada, 1994; pp 545-546.
- [411] Pirrung, M. C.; Pei, T., *J. Org. Chem.* **2000** *65*, 2229-2230.
- [412] Felix, A. L., *J. Org. Chem.* **1974**, *39*, 1427-1429.
- [413] Link, A. J.; Vink, M. K.; Tirrell, D. A., *J. Am. Chem. Soc.* **2004**, *126*, 10598-10602.
- [414] Gallagher, S.; Winston, S. E.; Fuller, S. A.; Hurrell, J. G. R., *Curr. Protoc. Mol. Biol.* **2004**, 10.8.1-10.8.24.
- [415] Beatty, K. E.; Xie, F.; Wang, Q.; Tirrell, D. A., *J. Am. Chem. Soc.* **2005**, *127*, 14150-14151.
- [416] Beatty, K. E.; Liu, J. C.; Xie, F.; Dieterich, D. C.; Schuman, E. M.; Wang, Q.; Tirrell, D. A., *Angew. Chem. Int. Ed. Engl.* **2006**, *45*, 7364-7347, *Angew. Chem.* **2006**, *118*, 7524-7527.
- [417] Link, A. J.; Tirrell, D. A., *J. Am. Chem. Soc.* **2003**, *125*, 11164-11165.

-
- [418] Kiick, K. L.; Saxon, E.; Tirrell, D. A.; Bertozzi, C. R., *Proc. Natl. Acad. Sci. U. S. A.* **2002**, *99*, 19-24.
- [419] Wang, Q.; Chan, T. R.; Hilgraf, R.; Fokin, V. V.; Sharpless, K. B.; Finn, M. G., *J. Am. Chem. Soc.* **2003**, *125*, 3192-3193.
- [420] Lemieux, G. A.; De Graffenried, C. L.; Bertozzi, C. R., *J. Am. Chem. Soc.* **2003**, *125*, 4708-4709.
- [421] Agard, N. J.; Prescher, J. A.; Bertozzi, C. R., *J. Am. Chem. Soc.* **2004**, *126*, 15046-15047.
- [422] Smith, P. K.; Krohn, R. I.; Hermanson, G. T.; Mallia, A. K.; Gartner, F. H.; Provenzano, M. D.; Fujimoto, E. K.; Goeke, N. M.; Olson, B. J.; Klenk, D. C., *Anal. Biochem.* **1985**, *150*, 76-85.
- [423] Lightowlers, E. C., *Growth and characterisation of semiconductors*, Stradling, R. A.; Klipstein, P. C., Ed. Adam Hilger: Bristol, **1990**; pp 135-163.
- [424] Binnig, G.; Quate, C. F.; Gerber, C., *Phys. Rev. Lett.* **1986**, *56*, 930-933.
- [425] Hillier, J.; Baker, R. F., *J. Appl. Phys.* **1944**, *15*, 663-675.
- [426] <http://mcb.berkeley.edu/barker/dnaseq> (April **2008**).